MALIGNANT HYPERTHERMIA

ALLELE SPECIFIC EXPRESSION AND MUTATION SCREENING OF THE RYANODINE RECEPTOR 1

A dissertation presented to Massey University in partial fulfilment of the requirements for the degree of Doctor of Philosophy in Biochemistry

Hilbert Grievink

2009

To be conscious that you are ignorant is a great step to knowledge

Benjamin Disraeli (1804-1881)

ACKNOWLEDGEMENTS

I would like to take this opportunity to first and foremost thank both my supervisors Assoc. Prof Max Scott and Assoc. Prof. Kathryn Stowell for their expertise, guidance and support during the last three years.

Kathryn, I will be forever grateful for the opportunities you have offered me and helped me realize. I sincerely thank you for presenting me with the possibility to do a PhD after my internship in your research group. You have always been enthusiastic, inspiring and supportive in your advice and guidance. Writing my thesis made me not only realize how much I have learned during these three years but also made me thankful for how much I enjoyed them.

Furthermore I would like to thank everybody in the Twilite Zone for the great times, elaborate pot-luck dinners and awesome lab outings. Will, thanks for all those great games of squash(ing). And Robyn, thank you for an awesome trip around Europe, the good times in the lab, and the much needed distraction (by Robert‟s emails) from the seemingly endless thesis writing.

I would also like to acknowledge Elaine Langton (Wellington Hospital) and Neil Pollock (Palmerston North Hospital) for supplying blood samples for genomic DNA extractions used for HRM. Thanks also goes to, Jo-Anne Stanton and Chris Mason from the Department of Anatomy and Structural Biology at University of Otago, for their contribution to the 454 data analysis. In addition, I am most grateful to Anthony Thrush and Paula Shields from Roche Diagnostics New Zealand, for their constant technical support over the last three years. Finally, this work would not have been possible without the financial support from the Royal Society of New Zealand Marsden Fund given to Assoc. Prof. Kathryn Stowell.

I am also greatly indebted to my family who have always shown me, love, support and understanding even when I decided to move to the other side of the world. I am looking

forward to being a bit closer to home again. Last but not least I would especially like to thank my wife Liat. Thank you for all your understanding, patience and encouragement over the last three years, all while undertaking your own PhD. I am really sorry for all those times I bored you with my far too detailed monologs of how cool or frustrating my results were. I wish I could promise you it won‟t happen again.

ABSTRACT

Malignant hyperthermia (MH) is a dominant skeletal muscle disorder caused by mutations in the ryanodine receptor skeletal muscle calcium release channel (RyR1). Allele-specific differences in RyR1 expression levels might provide insight into the observed incomplete penetrance and variations in MH phenotypes between individuals.

Firstly, an H4833Y allele-specific PCR (AS-PCR) assay was designed that allowed for the relative quantification of the two *RYR*1 mRNA alleles in heterozygous samples. In four MHS skeletal muscle samples and two lymphoblastoid cell lines (LCLs), the wild type allele was found to be expressed at higher levels than the mutant RyR1 allele. These differences were not caused by variations in *RYR*1 mRNA stabilities. Secondly, high-throughput amplicon sequencing was employed for the quantification of both the T4826I and H4833Y causative MH mutations in heterozygous MHS samples. With the exception of one, all detected H4833Y and T4826I mutation frequencies were about 50%. This included a control, which was constructed and proven to have a 3:1 ratio of the wild type (H4833) versus the mutant (Y4833) *RYR*1 allele. This suggested that that the high-throughput amplicon sequencing approach as used here, was not suitable for accurate quantification of the two RyR1 alleles in heterozygous H4833Y MHS samples.

To detect possible variations in RyR1 alleles at the protein level, the RyR1 was to be isolated from microsomes prepared from a H4833Y MHS frozen skeletal muscle tissue. Microsomes isolated from MHS skeletal muscle tissues lacked the immunoreactive band that was believed to be the full length RyR1. Poor muscle quality, due to long term storage was believed to be the main cause of RyR1 depletion.

Faster and less expensive screening methodologies are required for the identification of genetic variants in MH research. Thus, in an additional project inexpensive and high-throughput high-resolution melting (HRM) assays were developed to allow screening of the *RYR*1 gene, for mutations associated with MH and/or central core disease (CCD).

ABBREVIATIONS

ACTA1	Skeletal muscle α-actin
apoCaM	apo-calmodulin
AS1	Allele-specific primer 1
AS2	Allele-specific primer 2
AS-PCR	Allele-specific PCR
ATP	Adenosine triphosphate
AVA-CLI	Amplicon Variant Analyser Command Line Interface
CaM	Calmodulin
CCD	Central core disease
cDNA	Complementary DNA
CICR	Calcium-induced Ca^{2+} release channel
CLI	Command Line Interface
CSQ	Calsequestrin
Ct values	PCR crossing points
CV	Coefficient of variance
DEPC	Diethylpyrocarbonate
DHPR	Dihydropyridine receptor
DMSO	Dimethylsulfoxide
dNTP	Deoxyribonucleoside triphosphate
dsDNA	Double-stranded DNA
DTT	Dithiothreitol
E	Amplification efficiency
ECCE	Excitation-coupled Ca^{2+} entry
EC-coupling	Excitation-contraction coupling
EDTA	Ethylenediaminetetraacetic acid
eIF4E	Eukaryotic initiation factor 4E
EMHG	European Malignant Hyperthermia Group
emPCR	Emulsion PCR
ER	Endoplasmic reticulum
FKBP-12	12 kDa FK506 binding protein

FKBP12.6	12.6 kDa FK506 binding protein
gDNA	Genomic DNA
GUI	Graphical user interface
HPRT	Hypoxanthine-guanine-phosphoribosyltransferase
HRC	Histidine-rich calcium binding protein
HRM	High-resolution melting
IP_3R	Inositol 1,4,5-triphosphate receptors
IPTG	Isopropyl-beta-D-thiogalactopyranoside
IRE	Iron-responsive element
IRES	Internal ribosome entry sites
IVCT	*In vitro* contracture test
JFM	Junctional face membrane
KcsA	Bacterial K^+ channel
LCL	Lymphoblastoid cell line
m7G	7 methylguanosine
MALDI-TOF	Matrix-assisted laser desorption/ionization time-of-flight
MH	Malignant Hyperthermia
MHE	Malignant hyperthermia equivocal
MHN	Malignant hyperthermia negative
MHS	Malignant hyperthermia susceptible
MHS1 to 5	Malignant hyperthermia loci 1 to 5
miRNA	MicroRNA
MmD	Multi minicore disease
mRNA	Messenger RNA
MthK	*Methanobacterium autotrophicum* potassium channel
MYH7	Beta-myosin heavy chain
NAMHG	North American Malignant Hyperthermia Group
NTC	Non template control
ORF	Open reading frame
PABP	Poly(A)-binding protein
PMCA	Plasma membrane calcium ATPase
PPi	Pyrophosphate

RT-PCR	Reverse transcription-PCR
RyR1	Skeletal muscle ryanodine receptor 1 isoform
RyR2	Cardiac muscle ryanodine receptor 2 isoform
RyR3	Brain ryanodine receptor 3 isoform
SEPN1	Selenoprotein gene
SERCA	Sarco-Endoplasmic Reticulum Ca^{2+}-ATPase
SNP	Single nucleotide polymorphism
SOCE	Store-operated Ca^{2+} entry
SR	Sarcoplasmic reticulum
sstDNA	Single strand template DNA
T_m	Melting temperature
TRPC	Transient receptor potential channel
T-tubule	Transverse-tubule
UTR	Untranslated region
XALD	X-linked adrenoleukodystrophy
X-Gal	5-Bromo-4-Chloro-3-Indolyl-BD-Galactopyranoside

LIST OF FIGURES

LIST OF TABLES

TABLE OF CONTENTS

1. INTRODUCTION

1.1 Malignant Hyperthermia

1.1.1 History of Malignant Hyperthermia

MH (MIM no. 145600), first described by Denborough and Lovell in 1960 [1], is a dominantly inherited skeletal muscle disorder that predisposes susceptible individuals to a potentially fatal reaction during general anaesthesia [2]. Besides this toxic response to anaesthetics, in rare circumstances MH may also be triggered in susceptible individuals by severe exercise in hot conditions, infections, neuroleptic drugs, or overheating in infants. The syndrome became known as MH because hyperthermia, a steep and rapid rise in body temperature was a common accompaniment and malignant, because in earlier times the case-fatality rate was 70-80%. Today, the case-fatality rate is only 5-10% [3]. The reduction in MH mortality rates has been in part due to the introduction of an *in vitro* contracture test (IVCT), that allows the identification of susceptibility to MH (MHS) and the use of the drug dantrolene sodium, a specific high affinity inhibitor of the RyR1 [4]. The growing understanding of the mechanisms underlying MH, due to research, is another significant factor in the drastically reduced mortality rates. This is because, the generated research results can and are being translated into clinical practice and pre-symptomatic diagnosis of MH susceptibility [5]. MH has an extremely high incidence in the lower North Island of New Zealand due to the presence of a large MH susceptible Maori pedigree [6]. With 1 in every 120 patients undergoing surgery at Palmerston North possibly susceptible to MH, the local incidence greatly exceeds the reported MH susceptibility of 1 in 15,000 children and about 1 in 50,000 adults treated with anaesthetics worldwide [7]. These figures however, underestimate the true genetic predisposition of the condition, since many fulminant MH reactions occur for the first time in patients who have previously undergone uneventful anaesthesia [8]. So far there is no obvious explanation why age, gender differences and genotype/phenotype discordances occur in the incidence of MH [9]. One explanation for the predominance of MH reactions in men could involve sex differences in the expression of calcium regulating proteins or electrophysiology causing differences in the reactions of male and

female muscle during IVCT [10, 11]. In rat heart myocytes, differences between males and females in the expression of the proteins, for example RyR and DHPR, involved in calcium regulation have been found [12]. In addition it has been shown that the expression of the DHPR channels in mouse heart myocytes can be regulated via the oestrogen receptor [13]. The diagnostic limitations and variability of the IVCT itself can also have a significant effect on the clinical MH reaction observed (see 1.1.7). If one does assume that no sex differences occur in muscle physiology, another explanation for the sex differences with regard to MH susceptibility could lie in the genetics of MH. Modification of interacting genes or genes affecting the penetrance of the disorder could cause a relatively lower penetrance for women [10]. Another example of the complexity of MH is that in some MHS familes discordance between the IVCT phenotype and *RYR*1 genotype has been shown. Individuals carrying known *RYR*1 mutations test negative in the IVCT, and *vice versa* (see 1.1.7). [9]. One example of a gene that shows reduced penetrance in humans is brachydactyly (MIM no. 112500). Brachydactyly is an autosomal trait that causes shortened and malformed fingers and shows 50-80% penetrance (the frequency in the population with which a dominant or homozygous recessive allele manifests itself in the phenotype of an individual).

MH does not only occur in humans, but can also be detected in domestic animals such as swine, dogs, and horses. In particular swine have been a valuable resource for research. Even though swine are seldom exposed to anaesthesia, animals homozygous for the abnormality respond to stress in the same way as humans do to anaesthetics. The stress-induced death of such animals is called porcine stress syndrome and is but one aspect of economic loss due to the syndrome. On the other hand, abnormalities in the gene associated with MH may contribute to beneficial features such as leanness and heavy muscling in swine [8, 14].

1.1.2 Manifestations of Malignant Hyperthermia

In an MH reaction, MHS individuals respond to commonly used inhalation anaesthetics [15]. Among these are sevoflurane, desflurane, isoflurane, halothane, enfluarane and the depolarizing muscle relaxant succinylcholine. All other anaesthetic drugs do not trigger MH, including nitrous oxide, propofol, ketamine and non depolarizing muscle relaxants.

Besides the toxic response to anaesthetics, in rare circumstances MH may also be triggered in susceptible individuals by severe exercise in hot conditions, infections, neuroleptic drugs, and overheating in infants. In some but not all cases positive correlations with MH have been made [3]. In addition, patients with exercise-induced heat stroke have been reported as having responded to dantrolene [16]. The exact mechanisms of exercise-induced heat stroke are not yet understood. A recent study however, revealed that during exercise in mice and humans the RyR1 is progressively hyperphosphorylated by protein kinase A, S-nitrosylated, and depleted of the phosphodiesterase PDE4D3 and the stabilizing calstabin1 subunit. These modifications, which lead to remodelling of the RyR1, result in calcium leakage that was found to cause decreased exercise tolerance in mice [17].

1.1.3 Molecular genetics of Malignant Hyperthermia

The clinical signs of an MH reaction are highly variable and are caused by a hypermetabolic state with muscle rigidity, metabolic acidosis, rhabdomyolysis, tachycardia, and/or an increase in body temperature [18]. Initial studies underlying this pathology in humans and swine, indicated an abnormal regulation of the sarcoplasmic reticulum (SR; the specialized endoplasmic reticulum (ER) of striated muscle) Ca^{2+} release mechanism [19]. These results were substantiated by molecular genetic studies. The primary locus of MH (MHS1 locus) in humans is linked to chromosome 19q13.1, the position of the gene encoding the ryanodine receptor skeletal muscle calcium release channel (RyR1) [20, 21].

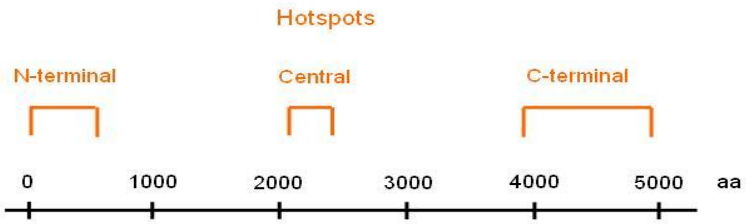

Figure 1.1: The mutation hotspots on the *RYR*1 gene.

Schematic representation of the *RYR*1 coding region. N-terminal amino acid positions: 35-614, central amino acid positions: 2129-2458, C-terminal region amino acid positions: 3916-4942.

About 50% of MH has been linked to the MHS1 locus, i.e. *RYR1* gene. This number was mainly derived from analysis of two reported „mutation hotspot regions" of the gene, the N-terminal and the central terminal regions, respectively [22]. However as the amount of sequencing data increases, the hotspot regions have steadily expanded, indicating that these initial numbers might have been the result of screening bias. Most mutations linked to MH appear to be clustered in the N-terminal and central *RYR*1 regions (Figure 1.1). A minor proportion of mutations linked to MH have been identified in the C-terminal region as well as between the identified „hotspots". However, many mutations linked to CCD (central core disease; see 1.1.4) are found in the C-terminal region [11]. In total, 242 missense RyR1 mutations have been described to date. Thirty four of those have been characterized by *in vitro* functional studies and shown to alter normal RyR1 function [5]. Almost all mutations occur in the heterozygous state. Nevertheless, homozygous missense mutations have been reported on rare occasions [23, 24]. Several other MH loci beside the RyR1 have been identified: MHS2 (MIM no. 154275) on chromosome 17q, MHS3 (MIM no. 154276) on 7q, MHS4 (MIM no. 600467) on 3q, and MHS6 (MIM no. 601888) on 5p. The MHS5 locus (MIM no. 601887) has been limited to a mutation in the *CACNL1A3* gene (MIM no. 114208) on 1q32. This gene encodes the pore forming α_1 subunit of the voltage-gated dihydropyridine receptor (DHPR), which is the voltage sensor for the SR calcium release channel [25]. Maintaining intracellular calcium homeostasis is a complex process and involves many proteins. This suggests the existence of other yet unidentified causative MH mutations in novel loci.

1.1.4 Associated myopathies

Besides MH, the *RYR1* gene is also linked to two congenital myopathies namely, central core disease (CCD, MIM no. 117000) and multi minicore disease (MmD, MIM no. 255320). CCD is a rare non-progressive myopathy, which is characterized pathologically by the presence of central core lesions extending the length of type I muscle fibers. The cores are regions of sarcomeric disorganization, which lack oxidative enzyme activity due to mitochondrial depletion [26]. CCD is usually inherited as an autosomal dominant disease but recessive forms of CCD have been described [27]. Presentation of dominantly inherited CCD is typical in infancy and affected individuals

are characterized by hypotonia and proximal muscle weakness [28]. Although CCD mutations have been reported in the N-terminal and central *RYR*1 regions, most CCD patients have mutations that cluster in the C-terminal pore forming region of the RyR1 [11]. Central cores in muscle biopsies have also been observed in patients with mutations in genes that are associated with hypertrophic cardiomyopathy (beta-myosin heavy chain; MYH7) and nemaline myopathy (skeletal muscle α-actin; ACTA1), indicating genetic heterogeneity. Patients with CCD are at high risk for MH and can be diagnosed as MHS by the IVCT. Nevertheless these results should be interpreted with caution since (i) any underlying muscular disorder can potentially influence the outcome of the IVCT and (ii) the caffeine and halothane IVCT thresholds (i.e. the lowest concentration of caffeine or halothane which produces a sustained increase of at least 0.2 g in baseline force from the lowest force reached. In addition the maximum contracture achieved at 2mM caffeine and 2% halothane are also reported) have been defined for individuals unaffected by neuromuscular disorders [28].

MmD is a non-progressive myopathy with an autosomal recessive mode of inheritance. The most common clinical presentations are neonatal hypotonia, delayed motor development, and generalized muscle weakness and amyotrophy, which may progress slowly or remain stable. Nevertheless, MmD is a clinically heterogeneous condition in which four subgroups have been distinguished. Histologically, the muscles are characterized by the presence of multiple small cores, which do not run the entire length of the muscle fibre and can be variable in size and number. Like in CCD, the cores lack or have limited mitochondrial function and exhibit disruption of the sarcomeric structure (sarcomeres give skeletal muscle its striated appearance). Although in some patients recessive RyR1 mutations have been found, the most common genetic defects found are mutations in the selenoprotein gene (SEPN1) [29].

1.1.5 Physiological basis of malignant hyperthermia

Calcium is a common second messenger that regulates many intracellular processes, such as metabolism, muscle contraction and gene expression. The resting intracellular calcium concentrations are maintained at very low levels (around 100 nM). Upon stimulation however, it can easily increase more than a 1000 fold in just a few

milliseconds [28]. During evolution cells have developed many refined and uniquely tailored systems that employ a series of pumps, channels, and organelles to maintain calcium homeostasis within the cell. The most specialized intracellular calcium storage organelle is the skeletal muscle SR. Calcium release from the SR is mediated by the depolarization of the transverse-tubule membrane (T-tubule) and is referred to as excitation. Depolarization induces conformational changes in the DHPR, which is located in the T-tubule, and leads to activation of the RyR channel, calcium release and subsequently muscle contraction (for more detail see chapter 1.3.3). The functional interaction between DHPR and RyRs is commonly referred to as excitation-contraction coupling (EC-coupling) [30]. These interactions are critical to the physiology of normal muscle as well as MH muscle. The (re)uptake of calcium into the SR from the cytoplasm is mediated by a very efficient P-type Ca^{2+}-ATPase, called the Sarco-Endoplasmic Reticulum Ca^{2+}-ATPase (SERCA). This process is mediated by two types of intracellular calcium channels, the 1,4,5-triphosphate receptors (IP_3R) and the RyRs, respectively. The slow, transient, calcium release through the IP_3R has been shown to regulate calcium-dependent gene expression [31, 32]. However, the focus here will be primarily on the fast transient calcium release generated by RyR1s during skeletal muscle EC-coupling.

A defect in skeletal muscle calcium homeostasis can account for all of the biochemical, physiological and clinical signs of MH. Muscle contraction, glycolysis and mitochondrial function are regulated by cytoplasmic Ca^{2+} concentrations. In a normal muscle relaxation-contraction cycle (Figure 1.2), SERCA pumps the calcium into the SR to initiate relaxation. Calcium is stored in the SR lumen and released through RyR1 to initiate contraction. Glycolytic and aerobic metabolism proceeds only rapidly enough to maintain the energy balance of the cell. RyR1 can be modulated by a variety of compounds but even when stimulated it has a relatively short opening time. In contrast, the MH muscle relaxation-contraction cycle employs a RyR1 which is more sensitive to stimuli. Thus, it releases calcium at enhanced rates and/or does not close readily. The abnormal channel floods the cell with calcium and overpowers the SERCA that ordinarily lowers cytoplasmic calcium. Sustained muscle contraction accounts for rigidity, while sustained glycolytic and aerobic metabolism account for the generation

of heat and acidosis. Tertiary imbalances of ion transport and damage to cell membrane account for the life-threatening systematic problems that appear during progression of an MH episode [8] .

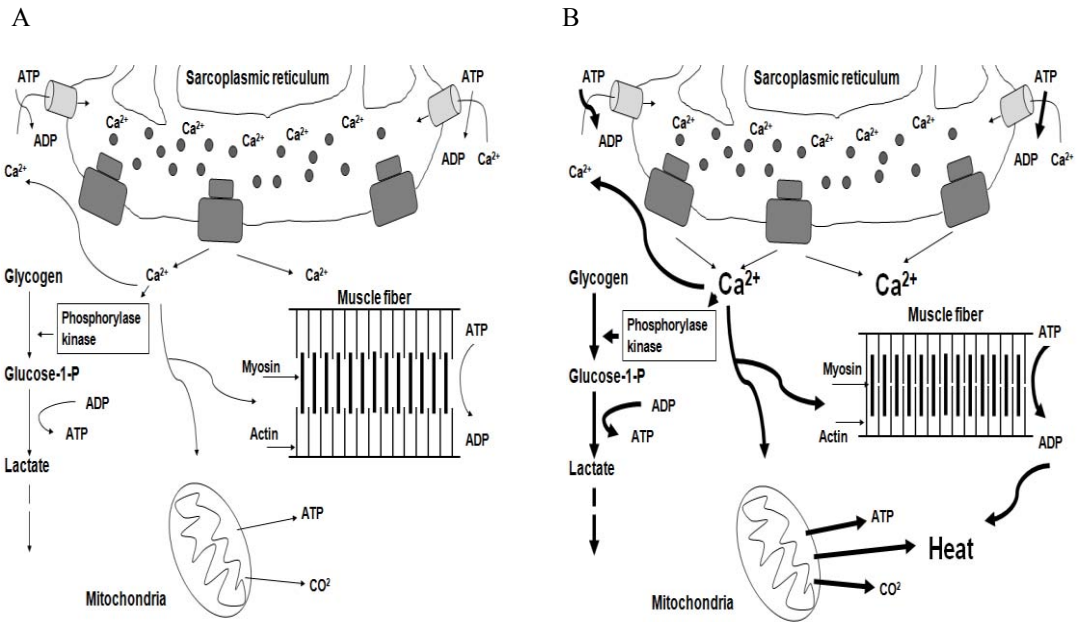

Figure 1.2: Proposed mechanism for induction of MH caused by abnormalities in the Ca^{2+} release channel of skeletal muscle sarcoplasmic reticulum.

A- Normal muscle contraction cycle. B- MH muscle contraction cycle. SERCAs are depicted light grey and RyR1s are depicted in dark grey. For clarity no other SR or junctional face membrane proteins are shown. Figure adapted from MacLennan (1992) [8].

1.1.6 Hypersensitivity of MHS RyR1 channels

Several mechanisms have been proposed to account for the hypersensitivity of MHS RyR1 channels. Kobayashi *et al*. (2005) proposed a domain switch model that assumes that the mode of interaction between the N-terminal and central RyR1 domains is involved in channel regulation, and also in MH pathogenesis [33]. Mutations in both the N-terminal and central RyR1 domains (see Figure 1.1) give rise predominantly to the MHS phenotype. The C-terminal domain is closely related to the classical CCD phenotype. In the resting state the N-terminal and central RyR1 domains make close contact at several subdomains in a zipped configuration. Stimulation of the RyR1 by depolarization or chemical agonist causes unzipping of the domain switch, leading to

Ca^{2+} channel opening. Partial unzipping/weakening of the domain switch may occur in response to MH mutation in the N-terminal and central RyR1 domains, making such channels hypersensitive to certain stimuli. Other studies, using dyspedic myotubes expressing mutant RyR1s and/or swine MHS muscle cells, revealed chronically elevated cytoplasmic [Ca^{2+}] and proposed that this could account for the detected channel hypersensitivities [34, 35]. Leakage of calcium from the internal stores could account for these higher cytoplasmic [Ca^{2+}]. The reason why intracellular [Ca^{2+}] is elevated is unclear but could be due to leakage from the SR stores mediated by a dysfunctional RYR1 channel, reduced uptake by SERCA pumps or increased influx though channels in the plasma membrane (e.g. DHPR) [5]. Depleted SR stores can lead to a decrease in the calcium released during EC-coupling and therefore to muscle weakness, which is the main symptom of patients affected with CCD. Quane *et al*. (1993) proposed another hypothesis termed EC-uncoupling, where the SR calcium store remains intact and the defect lies in the coupling between depolarization and calcium release. Thus, calcium transport would be impaired and less calcium would be available for muscle contraction and subsequently can lead to weak muscles (the main symptom of patients with CCD) [26]. Figure 1.3 depicts a cartoon explaining how the different mechanisms can lead to altered RyR1 channel regulation.

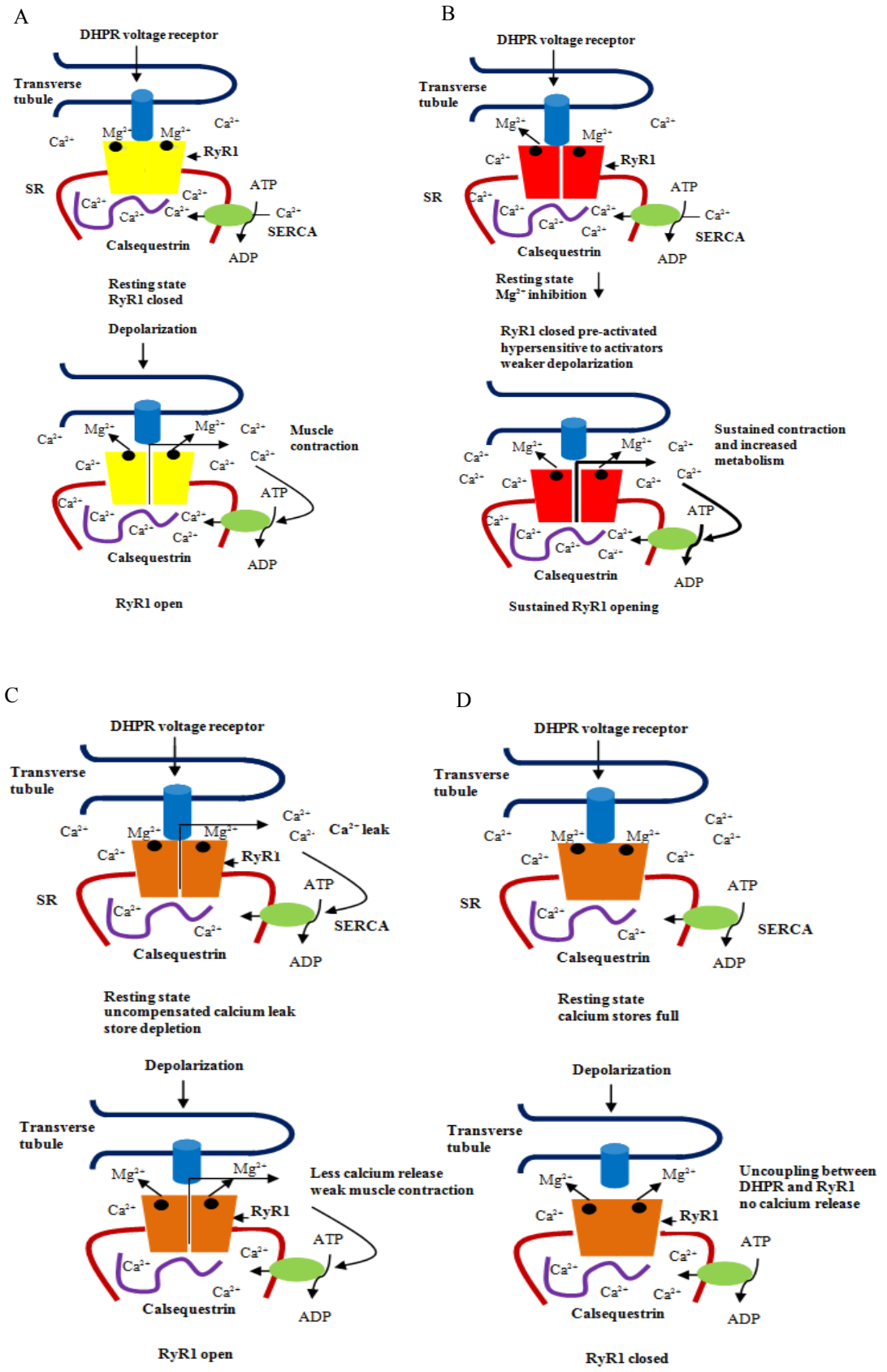
A
DHPR voltage receptor
Transverse tubule
RyR1
SR
ATP
SERCA
ADP
Calsequestrin
Resting state
RyR1 closed
Depolarization
Muscle contraction
RyR1 open
B
DHPR voltage receptor
Transverse tubule
RyR1
SR
ATP
SERCA
ADP
Calsequestrin
Resting state
Mg2+ inhibition
RyR1 closed pre-activated
hypersensitive to activators
weaker depolarization
Sustained contraction
and increased
metabolism
Sustained RyR1 opening
C
DHPR voltage receptor
Transverse tubule
Ca2+ leak
RyR1
SR
ATP
SERCA
ADP
Calsequestrin
Resting state
uncompensated calcium leak
store depletion
Depolarization
Transverse tubule
Less calcium release
weak muscle contraction
RyR1
ATP
ADP
Calsequestrin
RyR1 open
D
DHPR voltage receptor
Transverse tubule
RyR1
SR
ATP
SERCA
ADP
Calsequestrin
Resting state
calcium stores full
Depolarization
Transverse tubule
Uncoupling between
DHPR and RyR1
no calcium release
RyR1
ATP
ADP
Calsequestrin
RyR1 closed

Figure 1.3: Possible mechanisms of how RyR1 mutations can affect intracellular calcium concentrations.
A- A normal RyR1 Ca^{2+} channel under resting conditions (top) after depolarization-induced activation (bottom). Binding of Mg^{2+} to the inhibitory binding sites on the RyR1 keeps the channel in a closed inactive state. B- Mutations in the RyR1 can affect the inhibition of Mg^{2+}. Under resting conditions the channel is in a closed but pre-active state (top), such channels are hypersensitive to activators (bottom). C- The presence of a RyR1 mutation can cause the channel to be leaky and leads to depletion of the intracellular stores. D- The presence of RyR1 mutations can cause a defect in the coupling between depolarization and Ca^{2+} release, consequently less Ca^{2+} is released during activation. Figure adapted from Treves *et al*. (2005) [28].

1.1.7 Diagnostic testing

1.1.7.1 In vitro contracture test

A major goal of MH research has been to identify individuals susceptible to MH in advance of anaesthesia. Due to lack of clinical symptoms under normal conditions an MH IVCT was developed by the European and North American Malignant Hyperthermia Groups (EMHG & NAMHG, respectively) [36, 37]. This test requires a large fresh muscle biopsy and is therefore highly invasive in nature. It is based on the tendency of MH muscle to be abnormally sensitive to stimuli that induce SR calcium release. The resulting contracture upon stimulation is recorded, after which individuals are then classified according to their sensitivity. Three categories can result from each test according to the European protocol: An individual is considered MHS, when contractures occur under or at the threshold of both caffeine and halothane. An individual is considered negative for MH (MHN), when normal reactions to both agents are obtained. A third diagnosis, MH-equivocal (MHE) is obtained when only one of the two agents leads to an abnormal response. Using the NAMHG protocol, an individual is diagnosed as MHS when either of the halothane or caffeine tests is positive and an individual is diagnosed MHN when both tests are negative. The EMHG protocol may reduce the possibility of false positive and negative results when compared to the NAMHG but overall similar results are obtained [36].

1.1.7.2 Genetic testing

The identification of causative mutations for MH suggests the use of widespread relatively non-invasive DNA testing for MH. However, as mentioned previously, MH is known to be a heterogeneous genetic disorder with at least five other susceptibility loci being identified. Furthermore, there are several reports of discordance between phenotype and genotype [9, 38-40]. Both Deufel *et al*. (1995) [38] and Fortunato *et al*. (1999) [39] found that individuals who were classified as MHN according to the European IVCT carried an Arg614Cys mutation, which segregates with the MHS phenotype in their families. Deufel *et al*. (1995) suggested that their results may challenge the causative role of the Arg614Cys mutation. Nonetheless, also based on earlier observations, a person typed MHN who bears a possible causative mutation for MH should still be regarded as MHS for clinical purposes, since that individual does have a high risk familial haplotype. One must also realize that the IVCT is not 100% accurate. The NAMHG IVCT test results in an overall sensitivity of 97% and a specificity of 78%. The EMHG protocol test results in a sensitivity and specificity of 99 and 93.6%, respectively [36]. Additionally, Serfas *et al*. (1996) [40] found discrepancies between MHS IVCT and the absence of the Arg614Cys mutation, suggesting false-positive diagnosis by the IVCT. Although genetic data cannot replace the IVCT at the present time, the cases described above indicate that for MH status it can provide significant additional diagnostic information.

1.1.7.3 Functional assays

A number of functional tests have been successfully used to assess the role of RyR1 mutations in calcium release. These include the use of non-muscle expression systems, such as COS-7 [41] and HEK293 cells [42]. Tong *et al*. (1997) transfected HEK293 cells with the rabbit *RYR*1 complementary DNA (cDNA) carrying point mutations which were introduced by site-directed mutagenesis. 15 single amino acid mutations showed abnormal sensitivity in a calcium photometry assay [42]. The advantage of using heterologous expression systems such as these lies in the fact that an altered phenotype is likely to originate from mutations in the inserted gene. Ever since the discovery that human B-lymphocytes express not only the inositol 1,4,5-triphosphate

receptor, but also RyR1, LCLs established from MHS individuals, have also been used to assess the role of RyR1 mutations in calcium release [43-46]. No invasive muscle biopsy is necessary as a simple blood sample is all that is needed to establish LCL. The exact molecular mechanisms for calcium movement in non-excitable B-cells are not clearly understood. Wehner *et al*. (2002) used myotubes generated from muscle biopsy tissue to assess the role of RyR1 mutations in calcium release [47]. These authors found that the Thr2206Met mutation is causative for MH. Myotubes can be formed *in vitro* from satellite cells. Satellite cells are resting stem cells of mammalian skeletal muscle responsible *in vivo* for muscular growth or replacement after an injury. Yang *et al*. (2003) [48] extended the molecular and functional characterization of MH mutations to 1B5 dyspedic skeletal myotubes that express key proteins, such as skeletal triadin, calsequestrin (CSQ), 12 kDa FK506-binding proteins (FKBP-12), SERCA, and α1s-DHPR, but do not constitutively express any RyR protein isoform. Myotubes, since they differentiate from muscle cells, also contain larger and more efficiently filled SR stores then COS-7, HEK293 or LCL cells. It was found that myotubes transfected with mutated *RYR1* cDNA had significantly enhanced sensitivity to depolarisation agents.

1.2 Ryanodine receptor

The RyR is a calcium release channel of ER/SR as well as a bridging structure connecting the SR and T-tubule in skeletal muscle. The channel was identified and isolated through its high affinity binding of the modulator ryanodine, hence the name of the receptor. The RyRs are the largest known ion channels and are homotetrameric complexes of approximately 2260 kDa in size. Each individual subunit is about 560 kDa and is encoded by approximately 5,000 amino acids from 106 exons. Morphological studies and sequence analysis, using hydropathy plots have shown that the RyR1 consists of two main parts. A large cytoplasmic assembly (N-terminal), that is responsible for the characteristic square shape in cryo-images, and a smaller transmembrane assembly (C-terminal) (see Figure 1.4).

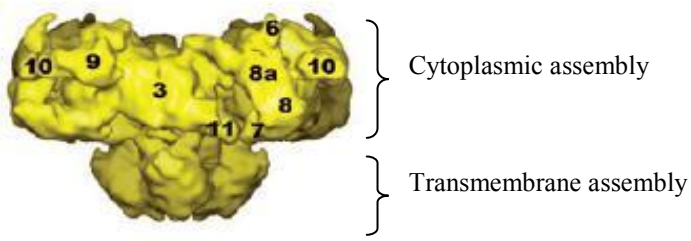

Figure 1.4: Side view of the three dimensional structure of RyR1.

The numbers indicate some of the different RyR1 domains (~10 Å resolution). Figure was adapted from Samso *et al*. (2005) [49].

Three different isoforms have been identified in mammals. Each is encoded by a different gene and named according to the tissue where they were first discovered. Although the RyRs can be found in a variety of tissues, they are most abundantly expressed in striated muscles. Three dimensional structures of all the three RyR isoforms are available, although so far it has not been possible to obtain X-ray crystallographic structures of the proteins. This is not only due to the fact that RyRs are structurally complex, but also because they are integral membrane proteins, which tend to be poor candidates for X-ray crystallography. Alternatively, cryo-electron microscopy has been used to create 3D models of the proteins. Until recently, only 3D models of the proteins with moderate resolutions of typically 30-40 Å were available [50-52].

The RyR1, which is the primary locus of MH, is the major isoform expressed in skeletal muscle. In addition it has also been found to be abundant in cerebellar Purkinje cells [53-55]. More recently RyR1 has also been found to be expressed in human B lymphocytes [43]. The cardiac RyR (RyR2) is the predominant form in cardiac muscle and is also the most widely distributed isoform throughout the brain [55, 56]. Despite its name the brain isoform, RyR3 was found to be expressed in only specific regions of the brain, such as corpus striatum, thalamus, and hippocampus [57]. However it can be found in a variety of other tissues, including skeletal muscle, but only in relatively low amounts [58, 59]. The three RyR isoforms show structural similarities, consistent with the approximately 70% overall sequence identity between the three (Figure 1.5) [57]. Some regions are highly conserved and other regions display more variability. The two

muscle isoforms, RyR1 and RyR2 diverge significantly in three regions, namely, D1 (RyR1 residues 4254-4631), D2 (RyR1 residues 1302-1406) and D3 (RyR1 residues 1864-1925) [60]. These three regions are thought to be responsible for the specific isoform characteristics and thus to be the binding sites for different modulators.

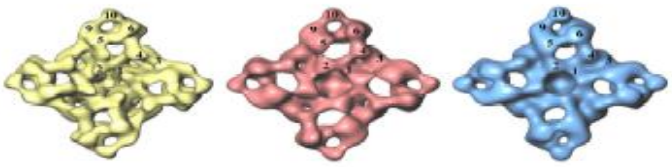

Figure 1.5: Solid body representations of the three isoforms of ryanodine receptor.
RyR1 (yellow), RyR2 (red), RyR3 (blue). The three receptors are shown as viewed from the cytoplasmic face. The domains are numbered (1-10) in one quarter of the tetramer molecule (25-30 Å resolution). Figure was adapted from Sharma and Wagenknecht (2004) [61].

Recently, three-dimensional reconstructions at ~10 Å resolution were obtained for the closed state RyR1 [49, 62]. Samso *et al.* (2005) proposed that the RyR1 ion pore has an architecture common with that of the bacterial K^+ channel KcsA, and revealed that it should have at least 6 transmembrane domains per subunit [49]. The exact number of transmembrane domains per subunit cannot yet be precisely established, however earlier research suggested that this number should lie between 4 and 12 [53, 54, 63]. Definition of the transmembrane domains will be essential for determining the RyR structure and mechanisms of modulation because they line the pore and constrain the structure of the entire molecule [64]. The higher resolution three-dimensional RyR1 model also indicated a more concave surface for the FKBP12 binding site. The approximate positions of the apo-calmodulin (apoCaM) and Ca^{2+}-CaM binding sites were also readily identified. A 9.6 Å resolution structure of RyR1 reported by Ludtke *et al.* (2005) allowed direct visualization of five α-helices in the membrane spanning region that suggest a pore structure more similar to the inward rectifier calcium gated potassium channel from *Methanobacterium autotrophicum* (MthK channel) [62]. Extended computational analysis of the 9.6 Å resolution RyR1 structure resolved 36 α-helices and 7 β-sheets in the cytoplasmic region of each RyR1 monomer. One β-sheet was identified close to the membrane-spanning region that resembles the cytoplasmic pore structures of inward rectifier K^+ channels like the MthK channels [65]. The observed similarities between the RyR and other ion channels will assist in the understanding and

design of future experiments that should provide more details concerning the mechanisms of cellular signalling in the process of muscle contraction.

1.3 Maintaining intracellular calcium homeostasis

The SR is one of the two membranes which make up the sarcotubular system. Together with T-tubules, which are openings of the sarcolemma (muscle cell plasma membrane) the SR regulates calcium concentrations [Ca^{2+}] within muscle cells, and thereby regulates muscle contraction and relaxation. The association of the T-tubules with the SR terminal cisternae is called the triad, and is the anatomical site of EC-coupling (see Figure 1.6). The proportion of terminal cisternae facing the T-tubules is referred to as the junctional face membrane (JFM) SR [66]. Calcium release is a finely regulated process that involves not only RyRs. The SR has developed an elaborate set of endogenous RyR1 modulators and JFM calcium-regulatory proteins that are involved in maintaining intracellular calcium concentration. Some of the key players are discussed below.

1.3.1 Endogenous RyR1 modulators

1.3.1.1 Calcium

Cytosolic calcium has a major importance in the regulation of RyR activity. The RyR channels are activated by micromolar Ca^{2+} but inhibited at millimolar concentrations [67]. Studies have been conducted to pinpoint the binding sites of these modulators. In many proteins calcium is bound with high affinity to EF hand calcium binding proteins. Nevertheless, no such sequence that fits the precise characteristics is present in the human *RYR1* gene. Based on the *RYR1* primary structure, Takeshima *et al*. 1989 identified three putative calcium binding sites at residues 4253-4264, 4407-4416, and 4489-4499 [53]. Chen *et al*. (1992) confirmed this by showing high affinity calcium binding to a RyR1 fragment containing residues 4478-4512 [68]. Zorzato *et al*. (1990) predicted a low-affinity Ca^{2+} binding site for a long acidic sequence in residues 1873-1923 (D3 region) of RyR1 [54]. Deletion of this region resulted in functional RyR1 channels that are more sensitive to activation by low [Ca^{2+}] and clearly more resistant to

inactivation by elevated [Ca^{2+}] and [Mg^{2+}] [69]. This strongly suggests the presence of an inhibitory domain in this region and also elucidates why different RyR isoforms differ in their calcium (and Mg^{2+}; see below) inhibition.

1.3.1.2 Magnesium

Magnesium is a potent inhibitor of RyRs in resting muscle. Its inhibition is believed to come about by two mechanisms. In type I inhibition, magnesium competitively displaces calcium from its high affinity binding site thus preventing opening of the channel. Type II inhibition is believed to result from binding of magnesium to the low affinity inhibition sites (see above), which do not discriminate between Ca^{2+} and magnesium [70].

1.3.1.3 Adenosine triphosphate

Adenine nucleotides including adenosine triphosphate (ATP) are strong activators of RyRs. Millimolar levels of ATP potently activate the skeletal muscle RyR in the virtual absence of cytoplasmic Ca^{2+}. The presence of both ATP and Ca^{2+} is needed for maximum opening of the channel [71]. The putative nucleotide binding site, GXGXXG, occurs twice in RyR1 and 2-4 times in RyR2 and RyR3, according to primary structure of the proteins [72].

1.3.2 Proteins involved in SR calcium storage

The efficacy of calcium release from the SR during EC-coupling depends strongly on the calcium binding capacity of the SR. The highly acidic protein CSQ (55 kDa) [73], with its low affinity and high Ca^{2+} binding capacity, plays an important role in SR calcium storage and buffering. While it has been suggested that CSQ interacts with RyR, its binding site still remains to be determined. Several reports have demonstrated the regulatory ability of CSQ on both native and purified RyRs [74, 75]. Beard *et al*. (2002) showed that at the physiological [Ca^{2+}] of 1 mM, CSQ associates with native RyR1 and so inhibits its activity. In contrast to native RyRs, purified channels (depleted of triadin and CSQ) were not inhibited by CSQ suggesting the importance of the

presence of at least one co-protein, probably triadin (95 kDa) and/or junctin (26 kDa), in the RyR complex [74]. Like triadin, the luminal structure of junctin binds both CSQ and RyR1, thus providing a physical link between CSQ and RyR. Raising luminal Ca^{2+} increases RyR activity in two phases. Firstly a fast phase, which was most likely due to direct calcium activation of the RyR (at cytoplasmic or luminal sites). Secondly, a slower phase which was likely due to CSQ dissociation (at luminal $[Ca^{2+}] \geq 4mM$) and hence removal of the CSQ inhibitory effect. In addition it was found that CSQ amplifies the response of native RyRs to changes in luminal $[Ca^{2+}]$ [75]. Recently, Paoline et al. (2007) generated and characterized the first murine model lacking the skeletal muscle CSQ isoform. The study revealed that mice lacking CSQ, preserved the ability to develop tension after electrical stimulation. Nevertheless, the reduced calcium release and the decreased cytosolic Ca^{2+} transient supported the view that the calcium storage capacity of the SR was impaired, whereas the prolongation of the contractile response was consistent with a defective calcium reuptake. The lack of skeletal muscle CSQ also causes significant ultrastructural changes [76]. Besides CSQ, two other less abundant skeletal muscle junctional face membrane calcium binding proteins have been identified. These include junctate (33 kDa) and histidine-rich calcium binding protein (HRC; 165 KDa) [77, 78]. Taken together, mounting evidence is clearly assigning important roles to calcium binding proteins like CSQ as luminal calcium sensors for the RyR.

1.3.3 Proteins involved in SR calcium release

1.3.3.1 Dihydropyridine receptor

The skeletal muscle DHPR consists of at least four different subunits (α_1, $\alpha_2\delta$, β and γ) and is an L-type calcium channel, with a long lasting current, sensitive to dihydropyridine. The pore forming α_1 subunit contains four homologous internal repeats (I-IV), each with six transmembrane segments (see Figure 1.6). Part of the α_1 subunit the DHPR II-III loop, has been shown to be of major importance for functional skeletal muscle EC-coupling [79]. Other regions of the α_1 and the other subunits have also been suggested but are less well defined and are reviewed elsewhere [30, 80].

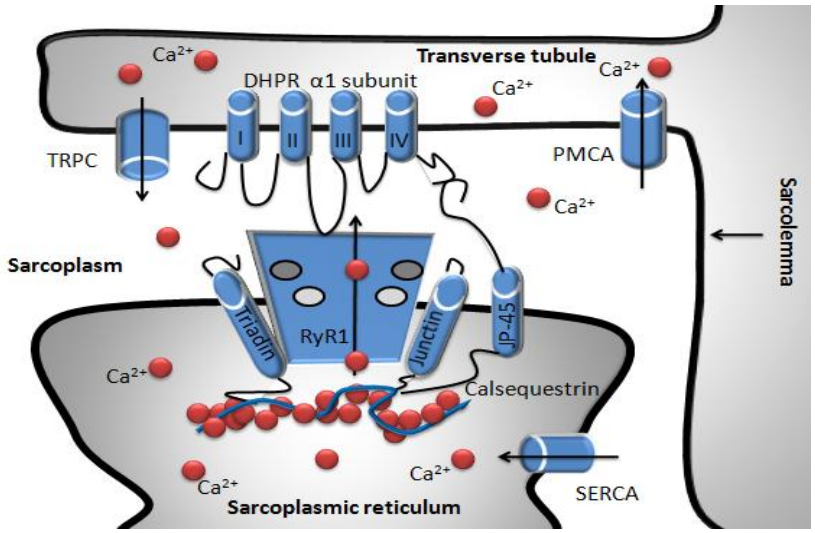

Figure 1.6: Schematic representation of the major components of the skeletal muscle triad.

The topologies and interactions of SR triad proteins calsequestrin, junctin, triadin, RyR1 and JP-45 are shown. Potential interactions between RyR1 and the DHPR α1 subunit are also depicted. Calcium (depicted in red) is pumped back into the stores by SERCA and out of the cell by the plasma membrane calcium ATPase (PMCA). FKBP12 and calmodulin are bound to the RyR1 and are depicted in dark and light grey, respectively. TRPC; transient receptor potential channels.

The interaction between DHPRs and RyRs is commonly referred to as EC-coupling. Depolarization of the T-tubule membrane (i.e. excitation) induces conformational changes in the DHPR that ultimately leads to activation of the RyR channel and subsequently muscle contraction. The molecular mechanism of EC coupling is fundamentally different in skeletal and cardiac muscle [30]. Only the RyR1 interacts physically with the DHPR to perform EC-coupling and subsequently calcium release, The RyR3 does not seem to be involved in EC-coupling in skeletal muscle, it most likely acts as a calcium-induced Ca^{2+} release channel (CICR) [58]. The main difference between the skeletal and cardiac isoforms RyR1 and RyR2, respectively, is the way the channel opens. In skeletal muscle the T-tubule contains tetrads of the DHPR. Every other RyR1 channel is associated with a DHPR tetrad. An action potential that travels down from the sarcolemma to the T-tubule activates the DHPR and triggers calcium release from the RyR1 (orthograde coupling) by a direct physical interaction. Calcium moves from the SR lumen to the cytosol (or sarcoplasm) where it in turn affects the open probability of the DHPRs (retrograde coupling). Thus in skeletal muscles no

calcium penetration through the DHPRs is required. At variance with RyR1, RyR2 functions as a CICR channel. In cardiac muscle there is about 1 DHPR for every 5-10 RyR2 channels. In addition, their alignments are less ordered. Upon activation of the DHPR by an action potential through the T-tubule, calcium influx occurs through the DHPR channels. This calcium influx subsequently activates the RyR2, which in turn releases the calcium that is stored inside the SR lumen.

1.3.3.2 Calmodulin

Calmodulin (CaM; 16 kDa) is another important RyR1 modulatory protein. Although many potential CaM binding sites have been identified, there is still some debate regarding the actual number of binding sites per RyR subunit [81]. Three dimensional structural determinations however suggest that each RyR1 subunit binds only one molecule of apoCaM or Ca^{2+}-CaM [82]. The nature of RyR regulation by CaM depends on its association with calcium. CaM activates the skeletal muscle Ca^{2+} release channel at low (nanomolar) Ca^{2+} concentrations whereas it inhibits the channel at micromolar to millimolar calcium concentrations [81]. Sencer *et.al.*(2001) showed that the regions adjacent to the CaM binding domain in the highly conserved carboxyl-terminal tail of the DHPR α_1 subunit interact with the RyR1 CaM binding peptide and that the addition of CaM blocks this interaction [83]. This suggests a possible role for CaM in the functional EC coupling between RyR and DHPR.

1.3.3.3 FK506-binding proteins

The approximately 12 kDa FK506-binding proteins (FKBP) are tightly associated with RyRs. Two FKBPs were identified and co-purified with RyR1 (FKBP12) and RyR2, (FKBP12.6), respectively. One FKBP12 molecule is bound to each RyR1 monomer [84]. Timmerman *et al*. (1993) showed that terminal cisternae vesicles treated with FK-506 have a reduced calcium uptake rate due to enhanced leak of calcium through the RyR1 [85]. In addition, the caffeine concentration required to stimulate caffeine-induced calcium release vesicles was reduced 2-fold in FKBP-deficient terminal cisternae. Additional studies conducted by Ahern *et al.* also revealed enhanced RyR1 channel sensitivity after depletion of FKBP12. [86]. It has also been proposed that the

FKBP12 plays a vital role in enabling the DHPRs to activate the calcium release channels [87]. Thus FKBP12 appears to stabilize the closed conformation of the skeletal muscle ryanodine receptor and may thereby be important in modulating the gating kinetics of the RyR1 during excitation-contraction coupling.

1.3.3.4 Other proteins involved

Two other proteins that have recently been suggested to aid in the regulation of intracellular calcium release are JP-45 and Homer. JP-45 is a novel integral membrane protein in skeletal muscle and interacts with both CSQ and the DHPR α_1 subunit [88]. Homer, a family of scaffolding proteins, was also found to be expressed in skeletal muscle. The protein was found to interact with and functionally modify the RyR1 [89].

A universal response to depletion of the intracellular calcium stores is to enhance calcium entry through the plasma membrane through a mechanism known as capacitative or store-operated Ca^{2+} entry (SOCE). After SOCE, intracellular calcium is pumped back into the stores by the SERCAs. A form of SOCE has recently been demonstrated to exist in skeletal muscle and was found to be activated by RyR1 in primary human muscle cells [90]. In addition to SOCE, skeletal myotubes also display a physiological mechanism termed excitation-coupled Ca^{2+} entry (ECCE). This pathway occurs in the absence of store depletion and is triggered by membrane polarization. It has been suggested that ECCE depends on the interactions of a Ca^{2+} entry channel with both RyR1 and DHPR. Possible candidates for ion channels which mediate these calcium entries are the transient receptor potential channels (TRPC) [91]. The dependence of both SOCE and ECCE on RyR1 activity, suggests the possibility of conformational signalling interactions between triad proteins, which control both calcium release during EC-coupling and activation of both capacitative and non-capacitative calcium entry pathways [73].

1.4 The role of gene expression in human disease

Different causative MH mutations have been found to differentially affect muscle contraction in IVCT and Ca^{2+} release in functional assays, respectively [92-94]. Girard *et al.* (2002) showed that halothane-induced changes in intracellular calcium concentrations of skeletal muscle cells, is not simply mutation specific. It was found to be specific for each individual [93]. This suggests that besides the specific mutation, a variety of other genetic and environmental factors, such as variations in gene expression might play a role as well.

Polymorphisms and variations in gene expression provide the genetic basis for variation in populations. Traditionally, most genetic studies suggest that alterations in protein structure and subsequently changes to its function and/or modulation are the major cause of hereditary diseases in populations. However, more recent studies show that a large proportion of inherited human phenotypic variation is influenced by changes in the quantity of the encoded protein rather than changes in its quality [95-99]. Ding *et al*. (2004) employed matrix-assisted laser desorption/ionization time-of-flight (MALDI-TOF) mass spectroscopy for allelic variation measurements on interleukin 6, *lex*A, and *ABCD*1 genes. The *ABCD*1 is involved in X-linked adrenoleukodystrophy (XALD). The manifestation of symptoms in XALD carriers has been associated with X-chromosome inactivation. This phenomenon might cause an individual to show symptoms similar to a homozygous mutant due to inactivation of the wild type *ABCD*1 gene. In concordance with this, one of the three investigated mutation carriers (S108W) showed predominant expression of the mutant allele [95]. Zhang *et al*. (2005) applied a method called SnaPshot (licensed by Applied Biosystems) that used fluorescently labelled ddNTPs to measure allelic expression imbalance of the A118G substitution in the human mu opioid receptor (OPRM1). This mutation has been implicated in predisposition to drug addiction and was found to cause significantly reduced yields of mRNA and receptor protein, indicating a loss of function [100]. Alternatively, Lo *et al*. (2006) conducted a large scale analysis of allele-specific gene expression of 1063 transcribed SNPs by using Affymetrix HuSNP oligo arrays. It was found that among the 602 genes that were heterozygous and expressed in kidney or liver tissues, 326 (54%) showed preferential expression of one allele in at least one individual and 170 of those

showed greater than fourfold difference between the two alleles. Some of these alleles were known to be imprinted however most were distributed throughout the genome. Thus variations in allelic expression can be the result of a variety of factors, such as X-chromosome inactivation and genomic imprinting or other mechanisms that, in contrast to the former, follow a Mendelian inheritance [99]. Allelic variations are the result of sequence alterations or variations in the level of expression of the encoded gene and are caused by either environmental or physiological conditions that can regulate gene expression (e.g. age, gender, nutrition) or by genetic polymorphisms acting in *cis* or *trans*. Polymorphisms in *cis*-acting sequences can have a direct effect on the affected gene. Firstly, these polymorphisms can lead to changes in the coding sequence of the protein, causing dramatic differences in structure, function or modulation. Secondly, *cis*-acting polymorphisms can have an effect on the RNA level by affecting transcription and translation efficiencies (due to polymorphisms in regulatory sites or regulatory elements), pre-mRNA processing (e.g. splicing), and mRNA stability. Polymorphisms in *trans*-acting sequences act by altering activity of downstream genes (polymorphisms in e.g. transcription factors). Although polymorphisms that alter amino acid coding are the most commonly studied polymorphisms it has been estimated that regulatory polymorphisms strongly outnumber those that alter protein sequence. Unfortunately the regulatory sequences are largely uncharacterized, since their location might be thousands of bases away from the transcription start site [96]. Alternatively, genomic structural variants (particularly copy number variants) have also been found to, at least in humans, account for a substantial amount of genetic variation and disease [101]. However, no association between copy number variants and the *RYR*1 gene or MH has been found as of yet.

Several studies have demonstrated reduced RyR1 expression levels, due to *RYR*1 mutations which are associated with core myopathies [102-104]. Zhou H *et al.* (2006) revealed the occurrence of tissue-specific monoallelic *RYR*1 expression in a group of CCD patients with recessive core myopathies. The transcribed allele carried a recessive mutation. In 6 of 11 patients studied (associated mutations: R109W, M402T, M2423K, R2939K, A4329D or T4709), it was found that the RyR1 was transcribed only from one allele in skeletal muscle, even though they were heterozygous at the genomic DNA

level. In four patients from whom parental gDNA samples were available the mutated allele was inherited from the father. The restoration of biallelic expression after treatment with the DNA methyltransferase inhibitor 5-azaC in one patient‟s primary myoblasts, suggested the association of DNA methylation with RyR1 silencing. However, bisulfite sequencing of the 5‟region which included three CpG islands did not reveal any differences in methylation between patients and controls. Additionally, analysis of normal fetal tissues indicated that *RYR*1 allele silencing was also tissue specific and polymorphic during early development and likely to be developmentally regulated, as monoallelic expression was absent in normal adult skeletal muscle. Thus, it was suggested that genomic imprinting due to long-term methylation effects could be responsible and possibly explain heterogeneity between MH phenotypes [105]. Further analysis of four (R109W, M402T, M2423K, and T4709) of the six *RYR*1 mutations also revealed dramatic reduction of RyR1 proteins levels in skeletal muscle tissues that were obtained from biopsies [103]. Subsequently, Robinson *et al*. (2009) recently investigated the possibility of epigenetic effects and variable penetrance of MH susceptibility. Firstly, the possibility of *RYR*1 silencing in MH was addressed using transmission data, because any bias in transmission of MHS status could indicate an unusual mode of inheritance. The numbers of sons and daughters (either affected; MHS/MHE or unaffected; MNH) born to affected parents were not significantly different. Thus, a bias in transmission of gender to offspring of affected parents was excluded. However, a significant parent-of-origin effect was detected. Out of 2113 transmissions, it was found that affected fathers had significantly fewer affected daughters (20%) than affected sons (25%) or unaffected daughters (27%). However, no discrepancies were observed between genotypes at the gDNA and cDNA level. Thus, the authors suggested that although epigenetic allele silencing may play a part in the inheritance of MH susceptibility, is unlikely to involve silencing of *RYR*1 [106]. Therefore the molecular mechanisms responsible for incomplete penetrance of MHS, and the wide variation of phenotype compared to genotype are unknown.

1.5 PhD project outline

In the main project of this PhD the aim was to determine if there are allelic-specific differences in RyR1 expression levels, in heterozygous MHS samples. Allele-specific differences in RyR1 expression levels might provide insight into the observed variable penetrance and variations in MH phenotypes between different individuals. The RyR1 is comprised of four identical subunits. Besides inter- and intra-subunit interactions, each RyR1 monomer also interacts with a variety of different modulators and only every other RyR1 tetramer is associated with a DHPR tetrad. In each tetramer, any of the individual RyR1 subunits can be defective and thus lead/contribute to the observed variations in MH phenotypes. The major hypothesis to be tested was that allele-specific differences occur in muscle samples from MHS patients.

Two different experimental strategies were designed to address possible allelic variation at the transcriptional level. In both strategies, causative MH mutations present in the coding region of the gene were employed as markers to distinguish between the two *RYR*1 alleles. Firstly, an allele-specific PCR assay was designed that allowed for the relative quantification of the two alleles in heterozygous samples. All samples contained the causative H4833Y MH mutation [45]. Plasmid constructs, representing the wild type and mutant 4833 *RYR*1 alleles, were used for assay validation. Four MHS skeletal muscle tissues (#470, #835, #116 and #145) were screened to determine if there were allele specific differences in mRNA expression levels between the wild type and mutant RyR1. Two LCLs (#1295 and #1333), derived from blood of MHS individuals, were used in mRNA stability assays to determine possible allelic-specific differences in RyR1 mRNA stabilities. Secondly, high-throughput amplicon sequencing was employed for the quantification of both the T4826I and H4833Y causative MH mutations in heterozygous MHS samples. A DNA bar coding system was designed and allowed multiplex analysis of multiple samples. Both T4826I (# 541, #289, #323, #255, #109, and #300) and H4833Y MHS skeletal muscle samples (#835, #470, #116, and #145) were screened simultaneously. As the four H4833Y samples used for high-throughput amplicon sequencing were analysed by the allele-specific PCR, assay comparisons between the two experimental strategies were made possible. Given that an

increase in mRNA levels does not necessarily mean an increase in protein levels this study also focussed on detecting possible variations in RyR1 alleles at the protein level. The identification of genetic variants is an important component of genetic research and therefore also MH research. Consequently, there is a constant search for more distinctive, faster and less expensive screening methodologies. Thus, in an additional project inexpensive and high-throughput HRM assays were developed and analysed using the LightCycler® 480 System to allow screening of the *RYR*1 gene, for mutations associated with MH and/or CCD. The SNPs investigated in this study, lead to the RyR1 amino acid substitutions T4826I, H4833Y (both linked to MH) or R4861H (linked to CCD). HRM analyses were conducted with both the LightCycler® 480 HRM Master and LCGreen PLUS.

2. MATERIALS AND METHODS

2.1 Materials

Only specialized reagents and kits used in this study are listed below, together with the name of the supplier. All general laboratory chemicals were of analytical grade or equivalent. See section 2.2 for more details.

- ABsolute™ QPCR SYBR® Green Capillary Mix was purchased from ABgene, Epson, Surrey, UK.
- Actinomycin D, Primary monoclonal anti-ryanodine receptor antibody (clone 34C, IgG1 isotype) and secondary anti-mouse IgG antibody were purchased from Sigma-Aldrich, Saint Louis, Missouri, USA.
- BM Chemiluminescence Blotting Substrate (POD), Complete™ Mini Protease Inhibitor Mix, FastStart *Taq* polymerase, LightCycler® 480 High Resolution Melting Master, LightCycler® 480 Probe Master Mix, MagNA Pure LC DNA Isolation Kit and MS2 RNA were purchased from Roche Diagnostics, Mannheim, Germany.
- Deoxyribonucleoside triphosphates, SuperScript™ III First strand Synthesis System for RT-PCR , TRizol® Reagent and the Quant-iT™ dsDNA HS Assay Kit were purchased from Invitrogen, Carlsbad, CA, USA.
- Diethylpyrocarbonate was purchased from AppliChem, Darmstadt, Germany.
- *Dpn*I and *Eco*RI were purchased from New England Bioabs Inc., Ipswich, MA, USA.
- Kodak Medical X-ray film was purchased from Carestream Health Inc., Rochester, NY, USA.
- LCGreen PLUS was purchased from IT Biochem, Salt Lake City, UT, USA.
- Oligonucleotides were purchased from Sigma-Aldrich, Castle Hill, NSW, Australia.

- Opti-MEM®I and penicillin/streptomycin were purchased from Gibco Carlsbad, CA, USA.
- PCR Cabinet (including airflow and a UV lamp) was purchased from Esco, Singapore.
- *Pfu*Turbo was purchased from Stratagene, La Jolla, CA, USA.
- PGEM®-T Easy Vector Systems Kit, Wizard® SV Gel and PCR Clean-Up System and the Wizard™ DNA extraction kit were purchased from Promega Corporation, Madison, WI, USA.
- Precision Plus Protein Dual Color Standard and the Quantum Prep® Plasmid Isolation Kit were purchased from BioRad, Hercules, CA, USA.
- TURBO DNA-*free*™ Kit was purchased from Ambion, Austin, TX, USA.

All genomic DNA samples, RNA samples, lymphoblastoid cell lines (LCL), and muscle tissues used in the studies were obtained with informed consent from participating subjects. All studies were carried out after ethical approval was obtained from the Whanganui-Manawatu human ethics committee.

2.2 Methods

2.2.1 Genomic DNA isolation

2.2.1.1 Previously isolated genomic DNA

Unless otherwise mentioned, human genomic DNA samples were already available and previously prepared from whole blood samples using the Wizard™ Genomic DNA Kit or the MagNa Pure LC DNA Isolation Kit I according to the manufacturer"s standard protocols. DNA concentrations were determined by A_{260} measurements, using a Nanodrop spectrophotometer (Nanodrop Technologies).

2.2.1.2 Genomic DNA isolation from lymphoblastoid cell lines

Genomic DNA was isolated from lymphoblastoid cell lines, using the Wizard™ Genomic DNA Kit protocol, following the instructions for tissue culture cells. 1-3 x 10^6

cells were harvested in 1.5 mL microcentifuge tubes, by centrifugation for 2 minutes at 13,000 x g. After removing the supernatant (leaving 10-50 µL residual liquid), cells were lysed by adding 600 µL Nuclei Lysis Solution. Clumps were removed by pipetting up and down. After adding 200 µL Protein Precipitating Solution, samples were mixed by vortexing vigorously (about 20 seconds). Proteins were then precipitated (can be seen as a white pellet) by centrifugation for 3 min at 13,000-16,000 x g. Supernatant (containing the DNA) was removed and placed into a clean 1.5 mL microcentrifuge tube. Genomic DNA was precipitated by adding 600 µL isopropanol and gentle mixing by inverting tubes. The DNA was pelleted by centrifugation for 1 minute at 13,000-16,000 x g. After removing the supernatant, the DNA was washed (by inverting tubes) with 600 µL 70% ethanol. The DNA was pelleted by centrifugation for 1 minute at 13,000-16,000 x g. The pellet was air-dried for 10-15 minutes at room temperature. The DNA was resuspended in 50 µL Rehydration Buffer by incubating at 65 ºC, or overnight at room temperature and stored in at -20 ºC until required. Nuclei Lysis Solution, Protein Precipitating Solution and Rehydration Buffer are proprietary reagents supplied in the Wizard™ Genomic DNA Kit.

2.2.2 Standard PCR protocol

PCR reaction conditions were conducted using the FastStart *Taq* polymerase reagents, and tailored for each primer set. However, the standard PCR protocol and cycle parameters are listed in Table 2.1 and 2.2, respectively.

Table 2.1: Reaction components of the standard PCR protocol

Component	Concentration	Volume (µL)
PCR buffer	10x	5
$MgCl_2$	25 mM	3
dNTPs	3 mM	5
Forward primer	100 ng/ µL	1
Reverse primer	100 ng/ µL	1
Template	-	*
GC-rich solution	5x	10
FastStart *Taq* Polymerase	5 U/µL	0.4
Sterile purified (MQ) water	-	To 50 µL

* Dependent on template quality and concentration.

Table 2.2: Cycle parameters of standard PCR

Temperature (ºC)	Time (mm:ss)	Cycles
95	05:00	1
95	00:30	30-45
59*	00:30	
72	01:00**	
72	07:00	1
4	Hold	1

*Dependent on the T_m of the primer.

**Dependent on length of the fragment. (~1 kb per minute)

The amplicons (10% of the reaction mixture) were analysed by agarose gel electrophoresis in 1x TAE buffer (980 mL purified water + 20 mL 50 x TAE (242 g Tris, 57.1 mL acetic acid, 100 mL 0.5 M EDTA, pH=8) to confirm size and product purity.

2.2.3 Cloning of PCR products

PCR products were cloned using the pGEM®-T Easy Vector Systems kit. The linear pGEM®-T Easy vectors are prepared by digestion with *Eco*RV and adding a 3´ terminal thymidine to both ends. These single 3´-T overhangs at the insertion site greatly improve the efficiency of ligation of a PCR product into the plasmids by preventing recircularization of the vector. Furthermore, it provides a compatible overhang for PCR products generated by *Taq* DNA polymerase. This enzyme adds a single deoxyadenosine, in a template-independent fashion, to the 3´-ends of the amplified fragments. The reaction mix for the ligations is listed in Table 2.3. Rapid ligation buffer and T4 DNA ligase were supplied in the pGEM®-T Easy Vector Systems kit.

Table 2.3: Reaction components of the pGEM®-T Easy cloning protocol

Component	Concentration	Volume (µL)
Rapid ligation buffer	2x	5
pGEM®-T easy vector	50 ng/ µL	1
PCR product	-	*
T4 DNA ligase	3U/ µL	1
MQ water	-	To 10 µL

*Dependent on insert:vector ratio.

For the ligations, 1:1, 2:1 and 1:3 insert:vector ratios were used. The reactions were incubated at room temperature for 1 hour and subsequently used to transform *Escherichia coli* XL1-blue cells.

2.2.4 Preparation of heat shock competent cells

An *Escherichia coli* XL1-blue strain was used for making competent cells using the following $CaCl_2$ method. A 5 mL overnight culture of the strain was grown at 37ºC in LB (+10 µg/mL tetracycline). Fresh medium, 200 mL LB + tetracycline, was inoculated with the overnight culture and grown to an OD_{600} ~ 0.5. The cells were harvested by centrifugation at 4º C for 10 minutes at 3000 x g. The pellet was resuspended in 1/2 culture volume of 100 mM cold $CaCl_2$ and incubated on ice for 20 minutes. Cells were

harvested as described above and the pellet was resuspended in 1/10 culture volume of 100 mM cold $CaCl_2$ and incubated on ice for 1 hour. Sterile glycerol was added to a final concentration of 15%. Quick-freeze was performed using liquid nitrogen and the cells were stored at -86 ºC.

2.2.5 Transformation

After thawing the competent cells on ice, 5 µL of the ligation reaction was added to 100 µL of cells and left on ice for 30 minutes. Heat shock was performed at 37 ºC for 5 minutes and the cells were placed back on ice for 10 minutes. After adding 1 mL of LB the cells were incubated 1 hour at 37 ºC. Subsequently the cells were harvested by centrifugation for 5 minutes at 5000 rpm (Biofuge Centrifuge, Heraeus Instrument). The supernatant was removed by decanting and the remaining LB was used to resuspend the cells. The resuspended *Escherichia coli* XL1-blue cells were plated on LB plates containing 10 µg/mL of tetracycline and 100 µg/mL of ampicillin, dependent on the plasmid used for transformation. To allow blue/white screening 50 µL of a 20 mg/mL 5-Bromo-4-Chloro-3-Indolyl-BD-Galactopyranoside (X-Gal) solution and 16.7 µL of a 24 mg/mL isopropyl-beta-D-thiogalactopyranoside (IPTG) solution were spread on the top of the agar plates.

2.2.6 Rapid boil plasmid preparation

In order to check whether or not the plasmids contained an insert of the correct size, an inexpensive plasmid isolation method was used, followed by an *Eco*RI digest. 5 mL overnight cultures of the transformants (white colonies) were grown in LB, containing 100 µg/mL of ampicillin, at 37 ºC. 1.5 mL of the overnight culture was pelleted by centrifugation at 12,000 x g for 1 minute. After removing the supernatant the pellet was resuspended 350 µL in STET (8% sucrose, 5% triton X-100, 50 mM Na_2EDTA pH 8, 50 mM Tris.HCl, pH 8, MQ water to 100 mL) by trituration with a pipette. After adding 25 µL of freshly made lysozyme (10 mg/mL) the samples were boiled for 40 seconds and centrifuged immediately for 10 minutes at 12,000 x g. The precipitate was removed and 375 µL of isopropanol was added to the supernatant. Subsequently the samples

were incubated for 30 minutes at -86 ºC. DNA was pelleted by centrifugation for 15 minutes at 4 ºC at a speed of 12,000 x g. The pellet was washed with 500 µL of 95% ethanol (-20 ºC) and centrifuged for 1 minute at 12,000 x g. Ethanol was poured off and the tubes were put in a speed vac (SC100, Savant) for 2 minutes to remove residual ethanol. The pellet was resuspended in 50 µL of TE (10 mM Tris, 1 mM EDTA, pH 8) and stored at -20 ºC.

The pGEM®-T Easy Vector cloning region is flanked by two *Eco*RI sites. Therefore, a single enzyme digestion with *Eco*RI will release the insert. The reaction mix for the digestion is depicted in Table 2.4..

Table 2.4: Reaction components of the *Eco*RI digestion protocol

Component	Concentration	Volume (µL)
DNA from rapid boil	-	3
NEB 1buffer	10x	3
*Eco*RI	10 U/µL	0.5
MQ water	-	To 30 µL

The reactions were incubated for 1.5-2 hours at 37 ºC and analysed by electrophoresis using a 1 % agarose gel in 1x TAE to check for appropriately sized inserts. Plasmids that contained inserts of the correct size were subsequently prepared for sequencing. Therefore, plasmid isolations were performed using 2 mL of the unused initial 5 mL overnight culture, using the Quantum Prep® Plasmid Isolation Kit. Subsequently, the plasmids were sent away for sequencing to confirm the presence of the correct insert (see 2.2.18).

2.2.7 Site-directed mutagenesis

Point mutations were introduced according to the QuikChange® Site-Directed Mutagenesis Kit (Stratagene, La Jolla, CA, USA). Figure 2.1 shows a schematic representation of the method. This mutagenesis method is performed using a DNA polymerase called *Pfu*Turbo that replicates both plasmid strands with high fidelity (6-

fold higher fidelity than *Taq* DNA polymerase) and without displacing the mutant oligonucleotide primers.

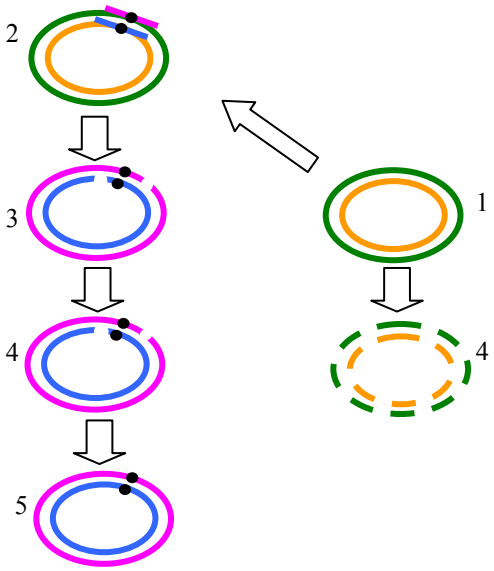

Figure 2.1: Schematic representation of the QuickChange® Site-Directed Mutagenesis procedure.

A double-stranded DNA construct was used as a template for mutagenesis (1). Two synthetic oligonucleotide primers containing the desired mutation bind to the vector (2). Incorporation of the oligonucleotide primers generated a mutated plasmid containing nicks (3). The generated plasmid construct was then treated with *Dpn*1. This resulted in the digestion of the methylated (non mutated) template DNA vector. After the digestion, the nicked DNA vector containing the desired mutation was used to transform XL1-blue competent cells. The XL-1 blue cells repair the nicks in the mutated plasmid (5).

The procedure utilizes a supercoiled double-stranded DNA construct (Figure 2.1 1) with an insert of interest and two synthetic oligonucleotide primers containing the desired mutation. The oligonucleotide primers, each complementary to opposite strands of the vector are extended by *Pfu*Turbo polymerase (Figure 2.1 2). Incorporation of the oligonucleotide primers generates a mutated plasmid containing staggered nicks (Figure 2.1 3). The site directed mutagenesis reaction protocol and cycle parameters are depicted in Tables 2.5 and 2.6, respectively. The mutagenic primers were designed manually according to the QuikChange® Site-Directed Mutagenesis Protocol.

Table 2.5: Reaction components of the site directed mutagenesis protocol

Component	Concentration	Volume (µL)
*Pfu*Turbo reaction buffer	10x	5
dsDNA template	15-50ng	1
Primer 1	125 ng/ µL	1
Primer 2	125 ng/ µL	1
dNTPs	3 mM	3
MQ water	-	To 50 µL
*Pfu*Turbo	2.5 U/µL	1

Table 2.6: Site directed mutagenesis cycle parameters

Temparature (ºC)	Time (mm:ss)	Cycles
95	00:30	1
95	00:30	12
55	01:00	
68	03:30	
68	05:00	1
4	Hold	1

Following the temperature cycling, the product was treated with 0.5 µL *Dpn*I (20 U/µL) and incubated for at least three hours at 37 ºC to digest the parental DNA template (i.e. the non-mutated supercoiled dsDNA; Figure 2.1 4). After the digestion, the nicked vector DNA containing the desired mutation was used to transform XL1-blue competent cells (see above). The XL-1 blue cells repair the nicks in the mutated plasmid (Figure 2.1 5). The introduction of the mutations was finally checked by DNA sequencing (see chapter 2.2.18). After confirmation of the presence of the desired mutation, glycerol stocks were made by adding 0.2 mL of sterile glycerol to 0.8 mL of overnight culture. Glycerol stocks were stored at -86 ºC for future use.

2.2.8 Isolation of RNA

RNA was isolated from both muscle tissue and LCLs. Muscle tissue was obtained with informed consent from patients undergoing a muscle biopsy. Muscle biopsies were carried out at Palmerston North Hospital and used for the IVCT, which allows diagnosis of MH. LCLs were grown to the desired cell densities in culture.

Approximately 100 mg muscle tissue was used for RNA isolation. For homogenisation the tissue was immersed in liquid nitrogen and crushed to a fine powder in a cooled steel mortar. After the addition of TRizol® Reagent (1 mL per 100 mg tissue) the tissue was further homogenised using a power homogenizer (Ultraturax). Lymphoblastoid cells on the other hand, were homogenized by resuspending the cells directly in TRizol® Reagent (1 mL 5-10 x 10^6 cells). Further steps in the isolation procedure are identical for tissue or cells.

The homogenized samples were incubated for 5 minutes at room temperature to permit complete dissociation of nucleoprotein complexes. For every 1 mL of TRizol® Reagent 0.2 mL chloroform was added and the samples were shaken vigorously by hand for 15 seconds and incubated at room temperature for 2 to 15 minutes. The samples were subsequently centrifuged, at no more than 12,000 x g for 15 minutes at 4 ºC. Following centrifugation, the mixture separates into a lower, red-coloured, phenol-chloroform phase, an interphase, and a colourless upper aqueous phase. RNA remains exclusively in the aqueous phase. The aqueous phase was transferred to a clean tube and the RNA was precipitated by mixing with 0.5 mL isopropyl alcohol per 1 mL TRizol® Reagent used for the initial homogenization. Samples were incubated at room temperature for 10 minutes and centrifuged at no more than 12,000 x g for 10 minutes at 4 ºC. The RNA precipitate formed a gel-like pellet on the side and bottom of the tube. After removing the supernatant the RNA was washed once with 75% ethanol (diluted from 99% ethanol in 0.01% Diethylpyrocarbonate; DEPC treated water), adding at least 1 mL of 75% ethanol per 1 mL of TRizol® Reagent used for the initial homogenization. Samples were mixed by vortexing and centrifuged at no more than 8900 x g for 5 minutes at 4ºC. At the end of the procedure the RNA pellet was air-dried for 5 to 10 minutes, dissolved in DEPC treated water and subsequently incubated for 10 minutes at 60 ºC. RNA

concentrations and purities were determined by absorbance ($A_{260/280}$ ratio need to be ~2) using a Nanodrop spectrophotometer (Nanodrop Technologies).

2.2.9 DNase treatment of the isolated RNA

Isolation of RNA using TRizol® Reagent separates the RNA from DNA and proteins. Nevertheless, an additional DNase treatment was performed to ensure that any remaining DNA does not cause problems in contamination sensitive downstream applications such as real-time PCR. This procedure was performed in the PCR cabinet.

The TURBO DNA-free Kit is designed to remove contaminating DNA using a novel method that does not require phenol/chloroform extraction, alcohol precipitation, heating or the addition of EDTA. The DNase digestion reagents are added to the RNA as depicted in Table 2.7. All reagents listed below were supplied with the TURBO DNA-free Kit.

Table 2.7: Reaction components of the TURBO DNase treatment protocol

Component	Concentration	Volume (µL)
Total RNA (up to 20 µg)	-	*
TURBO DNase buffer	10x	5
TURBO DNase	2U/µL	1
0.01% DEPC treated MQ	-	To 50 µL

*Dependent on the RNA concentration.

The mixture was incubated at 37 ºC for 30 minutes. Five µL DNase Inactivation Reagent (typically 0.1 volume) was added to the mix and the sample was incubated for 2 minutes at room temperature, with occasional mixing. The DNase enzyme plus divalent cations are subsequently removed from the solution by centrifugation at 10,000 x g for 1.5 minutes.

2.2.10 First-strand cDNA synthesis

SuperScript™ III First-Strand Synthesis System for Reverse Transcription-PCR (RT-PCR) was used for first-strand cDNA synthesis. SuperScript™ Reverse Transcriptase is a version of M-MLV Reverse Transcriptase that has been engineered to reduce RNase H activity and provide increased thermal stability. cDNA synthesis was performed in the first step using total RNA primed with oligo(dT). This procedure was performed in the PCR cabinet.

The following components were mixed, incubated at 65 ºC for 5 min and subsequently placed on ice for at least 1 minute (see Table 2.8). All reagents listed below were supplied in the SuperScript™ III First-Strand Synthesis System for RT-PCR.

Table 2.8: Reaction components for priming RNA with oligo(d)Ts

Component	Concentration	Volume (µL)
Total RNA (up to 2 µg)	-	*
Oligo(dT)$_{20}$	50 µM	1
dNTPs	10 mM	1
0.01% DEPC treated MQ	-	To 13 µL

*Dependent on the RNA concentration.

Seven µL of the following cDNA Synthesis Mix was added to each RNA/primer mixture (see Table 2.9). The samples were incubated for 60 minutes at 50 ºC. All reagents listed in Table 2.9 were supplied in the SuperScript™ III First-Strand Synthesis System for RT-PCR.

Table 2.9: Reaction components of the oligo(d)T primer extension protocol

Component	Concentration	Volume (µL)
First-strand buffer	5x	4
DTT	0.1 M	1
RNaseOUT™	40 U/ µL	1
SuperScript™ III RT	200 U/ µL	1

Reactions were terminated by incubating the samples for 15 minutes at 70 ºC. RNA was removed from the cDNA:RNA hybrid molecule by digestion with 1 µL RNase H (2 U/µL) for 20 minutes at 37 ºC. The resulting first-strand cDNA was directly amplified using real-time PCR or standard PCR.

2.2.11 High-Resolution Melting reaction conditions

Two commercially available high-resolution melting dyes were used and compared to develop assays that allow *RYR*1 mutation screening using the LightCycler® 480 System. This procedure was performed in the PCR cabinet.

The HRM reaction mixture for the LightCycler® 480 HRM Master is listed in Table 2.10. With the exception of primers and template and $MgCl_2$, this 2x mix contains all the components required for the amplification and detection of specific DNA sequences by HRM curve analysis. A separate 25 mM $MgCl_2$ stock solution is supplied with the LightCycler® 480 HRM Master to allow optimization of Mg^{2+} concentrations if necessary.

Table 2.10: Reaction components for the LightCycler® 480 HRM Master HRM protocol

Component	Concentration	Volume (µL)
Forward primer	2 or 3 µM	1
Reverse primer	2 or 3 µM	1
Template	(~10^4 plasmid copies or 5-150 ng/ µL gDNA	1
LightCycler® HRM Master	2x	5
$MgCl_2$	25 mM	1.2
MQ water	-	To 10 µL

The HRM reaction mixture for LCGreen PLUS included is listed in Table 2.11. LCGreen PLUS was supplied as a 10x solution in 10 mM Tris-HCl, pH 7.4, 0.1 mM EDTA. Thus, it was used together with the ready-to-use hot-start LightCycler® 480 Probe Master Mix.

Table 2.11: Reaction components for the LCGreen PLUS HRM protocol

Component	Concentration	Volume (µL)
Forward primer	2 or 3 µM	1
Reverse primer	2 or 3 µM	1
Template	~10^4 plasmid copies or 5-150 ng/ µL gDNA	1
LightCycler® Probe Master Mix	2x	5
LCGreen PPLUS	10	1
MQ water	-	To 10 µL

All HRM Assays were carried out in 96-well format and performed, using the same touchdown PCR cycling and HRM conditions listed in Table 2.12.

Table 2.12: PCR and HRM parameters

Target (ºC)	Acquisition mode	Hold (mm:ss)	Ramp Rate (ºC/s)	Acquisitions (per ºC)	Sec Target (ºC)	Step size (ºC)	Step delay (cycles)
Pre-incubation Cycles: 1 Analysis mode: None							
95	None	10:00	4.4	-	-	-	-
Amplification Cycles: 45 Analysis mode: Quantification							
95	None	00:10	4.4	-	-	-	-
62	None	00:10	2.2	-	56	0.5	-
72	Single	00:04	4.4	-	-	-	-
Melting Cycles: 1 Analysis mode: Melting curves							
95	None	00:05	4.4	-	-	-	-
40	None	01:00	1.5	-	-	-	-
72*	None	01:00	2.2	-	-	-	-
92	Continues		1.00	25	-	-	-
Cooling Cycles:1 Analysis mode: None							
40	None	0010	1.5	-	0	0	0

*For the 61 bp fragments the melting range was adjusted to 69-92 ˚C.

2.2.12 Allele-specific PCR reaction conditions

The ABsolute™ QPCR SYBR® Green Capillary Mix was used for quantitative real-time PCR assays. With the exception of primers and template, this 2x mix contains all the components required to perform a rapid, sensitive and reproducible QPCR reactions. Assays were carried out in 96-well format. The reaction setup was performed in the PCR cabinet. The allele specific PCR reaction setup and cycle parameters are listed in Tables 2.13 and 2.14, respectively.

Table 2.13: Reaction components for the allele specific PCR protocol

Component	Concentration	Volume (µL)
Forward primer	3 µM	1
Reverse primer	3 µM	1
cDNA (up to 2 µg)	-	1
SYBR® Green Capillary Mix	2x	5
MQ water	-	To 10 µL

Table 2.14: PCR parameters for allele specific PCR

Target (ºC)	Acquisition mode	Hold (mm:ss)	Ramp Rate (ºC/s)	Acquisitions (per ºC)	Sec Target (ºC)	Step size (ºC)	Step delay (cycles)
Pre-incubation Cycles: 1 Analysis mode: None							
95	None	15:00	4.4	-	-	-	-
Amplification Cycles: 45 Analysis mode: Quantification							
95	None	00:10	4.4	-	-	-	-
58	None	00:10	2.2	-	-	-	-
72	Single	00:06	4.4	-	-	-	-
Melting Cycles: 1 Analysis mode: Melting curves							
95	None	00:05	4.4	-	-	-	-
65	None	01:00	2.2	-	-	-	-
97	Continues		0.11	-	-	-	-
Cooling Cycles:1 Analysis mode: None							
40	None	0010	1.50	-	-	-	-

2.2.13 Tissue culture

B-lymphocytes had been previously transformed with Epstein-Barr virus to establish continuously dividing immortalized LCLs [107]. These cells were subsequently frozen and stored for later use.

2.2.13.1 Reactivation and culturing of lymphoblastoid cell lines

Frozen LCLs were reactivated from liquid nitrogen storage, by quickly defrosting the cells and resuspending them into at least 5 mL of medium (Opti-MEM®I; containing 2% FCS and 1x penicillin/streptomycin). The media was prepared according to the manufacturer‟s protocol. Subsequently, the cells were pelleted by centrifugation at 1000 rpm for 5 minutes (Labofuge 400, Heraeus Instruments). After carefully removing the supernatant the cells were resuspended in 2 mL of medium and dispensed into two vented T25 flasks each containing 3 mL of medium. The flasks were placed upright in 5% CO_2 at 37 ºC and checked daily. Once the cells start to clump together additional medium was added gradually up to a total of 10 mL. The media was easily replenished by carefully removing half of the spent medium and replacing it with fresh medium. This was done without disturbing the cells since the cell clumps tend to collect at the bottom of the flask. After the formation of large clumps, the two T25 flasks were pooled and passaged into one T75 flask. The cells were initially resuspended in 10 mL of medium, since they grow better at higher densities. Once the cell number increases, the cells were cultured in a maximum volume of 20 mL and can easily be grown up to a total of 1-3 x 10^7 cells per 20 mL. Cells at this density were now ready for total RNA isolation, mRNA stability assay or alternatively could be frozen for storage.

2.2.13.3 mRNA stability assay

An mRNA stability assay was designed and carried out using LCLs to assess possible differences in mRNA stabilities between the two RyR1 alleles in heterozygous samples. Actinomycin D was used as a transcription inhibitor, at a final concentration 5 µg/mL.

LCLs were cultured as described above to the desired cell densities in vented T75 flasks. When the desired number of cells was reached they were resuspended in about

half their original volume, counted (using a haemocytometer and trypan blue) and diluted to the desired cell densities. The cells were then aliquoted evenly over four wells in the absence or presence of actinomycin D for 0, 2, 7 or 24 hours, respectively. Stability assays were performed on two LCLs: #1295 and #1333. LCL #1295 was cultured in a total volume of 3 mL in a 12 well culture plate with ~ 3 x 10^6 cells/well. LCL #1333 was cultured in a total volume of 5 mL in a 6 well culture plate with ~ 5 x 10^6 cells/well. After the designated incubations the cells were counted as before, to assess viability. Subsequently, the cells were pelleted by centrifugation at 1000 rpm for 5 minutes (Labofuge 400, Heraeus Instruments). Subsequently, total RNA, and first-strand cDNA were generated each time from the same amount of total RNA, as described in sections 2.2.8 to 2.2.10, respectively.

2.2.13.3 Freezing cells for storage

Cells (~2 x 10^7) were frozen for long term storage by centrifugation at 1000 rpm for 5 minutes (Labofuge 400, Heraeus Instruments). They were then resuspended in 1.8 mL fetal calf serum plus 0.2 mL dimethylsulfoxide (DMSO). The cell suspensions were divided between two cryovials and slowly frozen overnight at -86 ºC, prior to long term storage in liquid nitrogen.

2.2.14 Measuring DNA concentrations using the Qubit fluometer

When low DNA concentrations needed to be determined accurately, the Qubit™ fluorometer was used together with the Quant-iT™ dsDNA HS Assay Kit, instead of UV absorbance readings. The Quant-iT™ kit provides a rapid, sensitive and specific method for dsDNA quantitation with minimal interference from RNA, protein, ssDNA (primers), or other common contaminants that effect UV absorbance. UV absorbance readings, especially at low concentrations, tend to result in overestimations of the actual DNA concentrations. Using between 1 and 20 µL of sample, the Quant-iT™ dsDNA HS assay can quantitate samples ranging from 10 pg/µL to 100 ng/µL. The Quant-iT™ kit provides concentrated assay reagent, dilution buffer, and pre-diluted DNA standards.

Each time a Quant-iT™ assay was conducted a new calibration was performed. Alternatively, it is possible to use values from a previous calibration. A Quant-iT™ working solution was made by diluting the Quant-iT™ dsDNA HS reagent 1:200 in Quant-iT™ HS buffer. Sufficient Quant-iT™ working solution needs to be prepared to accommodate all samples plus two standards. For 7 samples plus 2 standards the working solution was made by adding 9 µL Quant-iT™ dsDNA HS reagent to 1791 µL of Quant-iT™ HS buffer. The two standards were prepared by loading 190 µL Quant-iT™ working solution into acceptable tubes for fluorescence measurements. Subsequently 10 µL of each Quant-iT™ standard was added to the appropriate tube and mixed by vortexing for 2-3 seconds. Samples were prepared by loading 199 µL Quant-iT™ working solution into individual assay tubes. One µL of each of the samples was added and the contents were mixed by vortexing for 2-3 seconds. After incubating the tubes for 2 min at room temperature the DNA concentrations were measured using the Qubit™ fluorometer.

The Qubit™ fluorometer gives values for the Quant-iT™ dsDNA HS assay in ng/mL. This value corresponds to the concentration after samples were diluted into the assay tube. To calculate the concentration of the samples the value given by the Qubit™ needs to be multiplied by the dilution factor (here the dilution factor is 200/1).

2.2.15 Preparation of crude microsomes from skeletal muscle

Microsomes are small vesicles that can be derived from fragmented smooth ER produced when tissues, such as muscle or liver are mechanically broken (homogenized). Microsomes can then be concentrated and separated from other cellular organelles by centrifugation. Unbroken cells, nuclei and mitochondria sediment at 10,000 x g. At higher speeds of 100,000 x g, the ER sediments as a pellet leaving the soluble proteins in the supernatant. Frozen skeletal muscle biopsy samples were used for the preparation of crude microsomes. The muscle biopsies were carried out at Palmerston North Hospital and used for the *in vitro* contracture test.

This protocol was adapted from the method described by Saito *et* al. (1984) [108]. Approximately 500 mg of muscle tissue was immersed in liquid nitrogen and crushed to a fine powder in a cooled steel mortar. The tissue was further homogenized in 2 mL of buffer A (0.3 M sucrose, 5 mM imidazole pH 7.4, protease inhibitors; using 1 tablet of Complete™ Mini Protease Inhibitor Mix per 7 mL of buffer) using a power homogenizer (Ultraturax). The homogenate was centrifuged at 3000 x g for 10 minutes at 4 ºC. The pellet was stored (P1) at 86 ºC and the supernatant was collected and centrifuged at 15,000 x g for 15 minutes at 4 ºC. The supernatant was filtered though a gauze which was previously soaked in buffer A + EDTA pH 8. The filtrate was centrifuged at 100,000 x g for 90 minutes in a TLA-100.2 rotor (Beckman) at 4 ºC. The supernatant was stored at 86 ºC (S1). The pellet was resuspended in 150 µL buffer A. The crude microsomes obtained were also stored at 86 ºC.

2.2.16 Polyacrylamide gel electrophoresis

Proteins in the microsomes were analysed by polyacrylamide gel electrophoresis under denaturing conditions using the Mini PROTEAN® 3 System (BioRad, , Hercules, CA, USA). The gels were composed of a 4% stacking gel and a 7.5% resolving gel. The resolving gel was made by mixing 2.5 mL 1.5 M Tris-HCl (pH 8.8), 1.9 mL 40% acrylamide-bis ready to use solution (29.1:0.9), 100 µL 10 % SDS, 50 µL 10% ammonium persulfate, 5 µL TEMED and 5.5 mL purified water The stacking gel was made by mixing 1.25 mL 0.5 M Tris-HCl (pH 6.8), 500 µL 40% acrylamide solution, 50 µL 10 % SDS, 25 µL 10% ammonium persulfate, 5 µL TEMED and 3.15 mL purified water. Samples were mixed with 5x sample buffer (1.2 mL 0.5M Tris-HCl pH 6.8, 5 mL 50% glycerol 2 mL 10% SDS, 0.5 mL 2-mercaptoethanol, 0.01g bromophenol blue) and left at room temperature for 10 minutes. After loading the samples, gel electrophoresis was carried out at 20 mA for 1-1.5 hours in 1x protein running buffer diluted from a 10 x buffer containing 250 mM Tris, 1.9 M glycine, 1% SDS, purified water to 1 L.

After electrophoresis, gels were placed for 5 minutes in Coomassie-blue gel staining solution (0.5 g Coomassie blue R-250, 225 mL methanol, 225 mL purified water, 50

mL glacial acetic acid). Destaining was performed by soaking the gel in Coomassie gel destain solution (100 mL methanol, 100 mL glacial acetic acid, 800 mL purified water).

2.2.17 Western blot analysis

2.2.17.1 Transfer and labelling

Proteins in the samples were separated by SDS-PAGE as described above. Proteins were then transferred to a positively charged nylon membrane by electro blotting with 1x transfer buffer at 4 ºC for ~20 hours at 30V. 1x transfer buffer was diluted from a 10x buffer (156 M Tris, 1.2 M glycine, purified water to 1 L, pH ~8.2). After transfer, the gel was stained with Coomassie blue to determine the transfer efficiency. The membrane was soaked briefly in 1x TBST (10x TBS, Tween 20 1 mL (0.1%)) and blocked for 1 hour at room temperature with gentle shaking in 1% blocking solution (500 µL blocking reagent + 4.5 mL TBST). 1x TBST was diluted from a 10x TBS solution (500 mM Tris, 1.5 M NaCl, purified water to 800 mL, pH 7.5 with HCl). A 1/5000 dilution of primary monoclonal anti-ryanodine receptor antibody (clone 34C, IgG1 isotype) in 0.5% blocking solution was added to the membrane and incubated for 1 hour prior to washing 4 times with 1x TBST for 10 minutes each. The membrane was then incubated for 1 hour with a 1/5000 dilution of a peroxidase (POD) labelled secondary anti-mouse IgG antibody in 0.5% blocking solution prior to washing 4 times with 1x TBST for ten minutes each.

2.2.17.2 Detection

Detection of the membrane bound molecules was carried out in a dark room using BM Chemiluminescence Blotting Substrate (POD). The BM Chemiluminescence Blotting System is designed around peroxidase-labeled secondary reagents (i.e. antibodies) and the substrate luminol. In the presence of hydrogen peroxide (present in the detection solution; see below), peroxidase catalyzes the oxidation of the substrate luminol. An activated intermediate reaction product is formed, which decays to the ground state by emitting light which is detected on Kodak Medical X-ray film. Strong enhancement of the light emission is produced by 4-iodophenol. This acts as a radical transmitter

between the oxygen radical formed and luminol. The luminescence reaction is at its maximum after one to two minutes and is relatively constant for 20-30 minutes. After 1 hour the signal intensity decreases to about 60-70% of maximum.

The detection solution is made up by mixing luminescence substrate solution A (50 µL) and starting solution B (5 mL) in a ratio of 100:1. The membrane and the detection reagent were incubated for 1-2 minutes prior to exposing the membrane to the X-ray film. The exposure time is strongly dependent on the amount of membrane bound molecules and can vary from 5 seconds to 2 minutes. If the signal intensity was too high, a 10 minute wait was conducted before re-exposing.

2.2.18 DNA sequencing

DNA sequencing was performed by the Allan Wilson Centre Genome service [http://awcmee.massey.ac.nz]. All templates were diluted to the required concentrations, mixed with the appropriate primers, and submitted for sequencing. Sequence reactions were carried out using the BigDyeTM Terminator Version 3.1 Ready Reaction Cycle Sequencing Kit. Sequences were analysed using Chromas Version 1.45 (Conor McCarthy, Griffith University, Southport, QLD, Australia)

3. HIGH-RESOLUTION MELTING

3.1 Introduction

Genetic testing has an important role in many diagnostic laboratories and can provide dramatic prognostic and clinical benefits. Many genetic tests are available to detect and/or type SNPs. Most of these techniques however, require an additional separation step which makes them less favourable for high throughput assays. Examples of such methods are single-strand conformation polymorphism [109], denaturing gradient gel electrophoresis [110], restriction endonuclease analysis and DNA sequencing. Homogeneous, closed-tube methods for SNP detection/typing that do not require separation steps are available, and are based on either allele-specific PCR using SYBR Green I [111, 112] or expensive fluorescently labelled probes [113, 114] or primers [115]. SNP genotyping based on allele-specific PCR requires three primers, two of which need to be allele-specific. Thus, different mutations require different allele-specific primers. When using labelled probes for SNP detection/typing, only SNPs that lie under the probe can be detected. Consequently, multiple relatively costly probes are needed to cover all potential SNPs. In addition, the use of probes often requires extensive optimisation. These conditions limit the usefulness of these methods for screening purposes. If a PCR is performed with a 5‟-labelled primer as described by Grundy *et al.* (2003), high resolution amplicon melting allows genotyping and mutation scanning without probes. However, this method requires at least one expensive labelled oligonucleotide [115].

HRM was introduced as a homogeneous closed-tube system that allows mutation scanning and genotyping without the need of costly labelled oligonucleotides. It relies on a new generation of generic heteroduplex-detecting double-stranded DNA (dsDNA) binding dyes. Heteroduplex products are identified by the presence of a second, low-temperature melting transition [116]. The LightCycler® 480 High Resolution Melting Master is a recently introduced member of this new family. Unlike SYBR Green I, the generic heteroduplex-detecting dsDNA dyes can be used at saturating concentrations

without inhibiting or adversely affecting the PCR. The reason why this new family of dyes can detect heteroduplexes, whereas SYBR Green I does not is not entirely clear, but dye redistribution during melting is thought to be one reason (see Figure 3.1) [116].

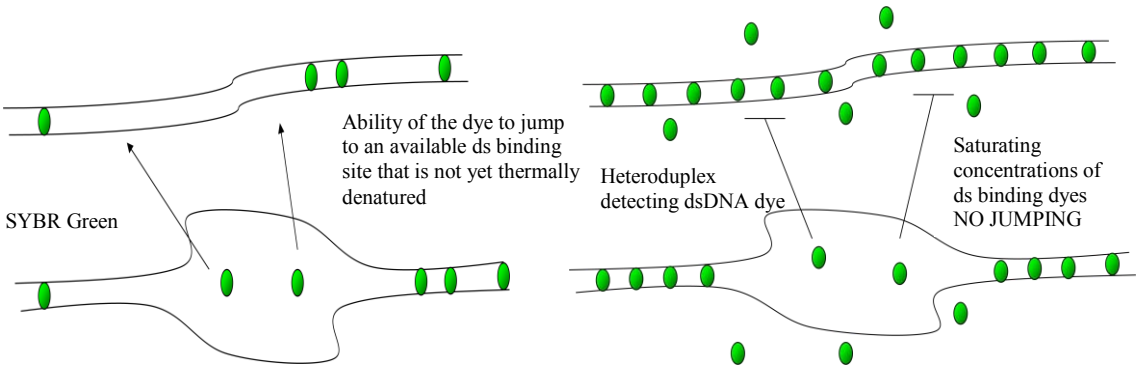

Figure 3.1: Dye redistribution during melting might interfere with heteroduplex detection.

SYBR Green released from low-temperature duplexes can redistribute during melting to preferred higher temperature melting duplexes as it cannot be used at saturating concentrations (left). No dye redistribution can occur during melting with saturating heteroduplex detecting dsDNA dyes since the potential binding sites are occupied (right).

The LightCycler480® System provides a unique format in which the entire experiment, including real-time and post-PCR analysis can be done on one instrument in 96-well and/or 384-well format, and completed within an hour. Different sequence variants can be identified based on differences in melting curves using the LightCycler® 480 Gene Scanning software. Heterozygous samples are best distinguished from homozygous samples by an altered shape in the melting curve. These differences are best visualised using difference plots because slight differences in curve shape and melting temperature (T_m) become obvious (see below) [116]. Different homozygous samples on the other hand are best distinguished by a change in T_m. Smaller amplicons have been found to improve discrimination between genotypes [115].

In this study inexpensive and high-throughput HRM assays were developed and analysed, using the LightCycler® 480 System, to allow screening of the *RYR*1 gene for mutations associated with MH and/or CCD.

Genomic DNA samples of known *RYR1* genotypes with either the wild-type sequence or a mutation associated with MH and/or CCD were used to validate the HRM assays. The SNPs investigated in this study, lead to the RyR1 amino acid substitutions T4826I, H4833Y (both linked to MH) or R4861H (linked to CCD). Almost all mutations associated with MH and/or CCD occur in the heterozygous state. Nevertheless, homozygous missense mutations have been reported on rare occasions [23, 24]. Therefore, four different homozygous *RYR1* genotypes were studied using engineered plasmids to show that even homozygous sequence variations can be identified using HRM on the LightCycler® 480 System. HRM analyses were conducted with both the LightCycler® 480 HRM Master and LCGreen PLUS.

3.2 Assay design

3.2.1 DNA samples used for assay validation

3.2.1.1 Genomic DNA samples

To validate the HRM assays, three homozygous wild-type and three heterozygous mutant genomic DNA samples of known genotypes were screened for the R4861H *RYR1* mutation. Ten homozygous wild-type and ten heterozygous genomic DNA samples of known genotypes were screened for each of the T4826I and H4833Y *RYR1* mutations. All genomic DNA samples used, were already available and previously prepared (see chapter 2.2.1.1).

3.2.1.2 Engineered plasmid constructs

Engineered plasmids constructs were created to address the possibility of discrimination between different types of homozygotes. Therefore, wild type gDNA was diluted 10x and amplified for 45 cycles (see chapter 2.2.2). The annealing temperature was adjusted to 58ºC and the extension time was set to 30 seconds. The sequences of the gDNA forward and reverse primers were 5‟-GTGGGTGGTGAAGGGATAAG-3‟ and 5‟-CTGGTTTCCAACTCCTGGAC-3‟, respectively. After amplification, 5 µL of the PCR products were visualized on 1% agarose gels stained with ethidium bromide (see Figure

3.3). A band of the expected size (485 bp) was excised from gel using the Wizard® SV Gel and PCR Clean-Up System. DNA concentrations were determined by A_{260} measurements using the Nanodrop spectrophotometer (Nanodrop Technologies).

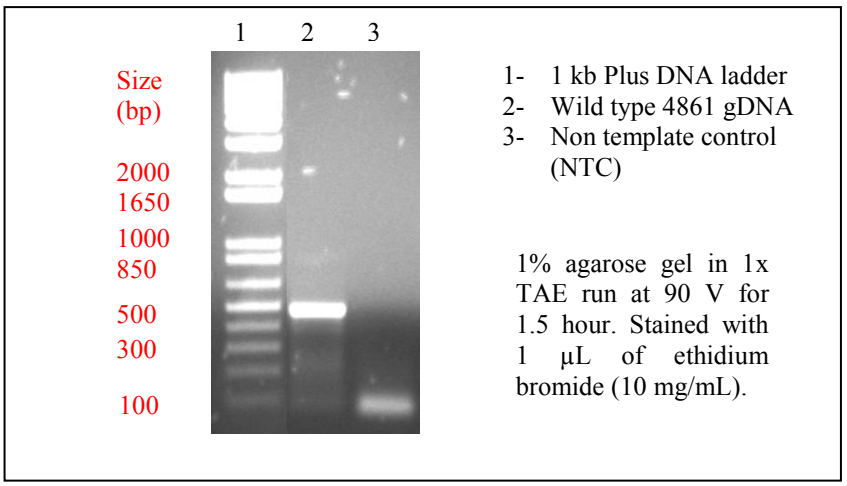

Figure 3.2: Visualizing of the amplified genomic DNA for cloning.

Cloning of the PCR product was performed using the pGEM®-T Easy Vector Systems kit (see chapter 2.2.3). For cloning of the PCR products into pGEM®-T Easy vector, three different insert:vector ratios were used; 1:1, 2:1 and 1:3, respectively. After incubation the ligation products were used to transform *Escherichia coli* XL1-blue cells to allow blue/white screening of the transformants. In order to check whether or not plasmids contained the right size insert, three transformants were grown overnight and subjected to a rapid boil plasmid isolation followed by an *Eco*R1 digest. Digestion with *Eco*RI should result in a ~500 bp insert fragment and a ~3000 bp fragment that corresponds to the full length pGEM®-T Easy Vector. Results of the digests are shown in Figure 3.3. Sequencing of one of the transformants was conducted to verify the presence of the correct insert (see appendix IIA).

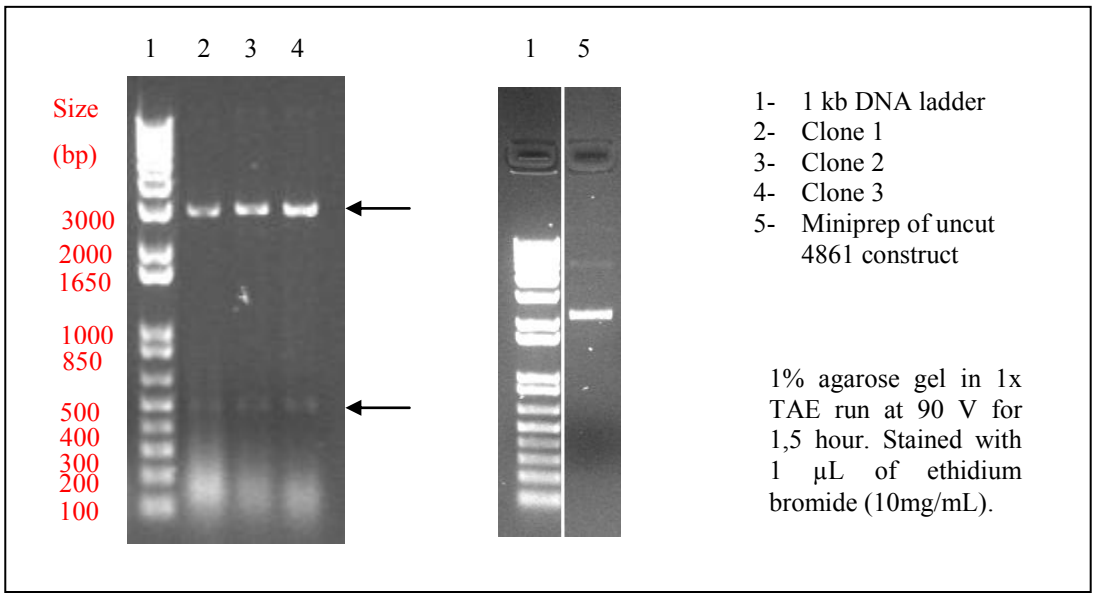

Figure 3.3: *Eco*R1 digests of 4861 transformants compared to untreated 4861 plasmid construct. Black arrows indicate the ~500 bp and ~3000 bp fragments that correspond to the sizes of the inserts and the linearized pGEM®-T Easy Vectors, respectively. For clarity purposes, additional irrelevant samples were removed from the picture, hence the white break.

The obtained wild type 4861 plasmid construct was used as a template for site-directed mutagenesis. SNPs representing A, C or T sequence variants at the defined position, were introduced using QuikChange® Site-Directed mutagenesis according to the manufacturer"s standard protocol (see chapter 2.2.7). The mutagenic primers were designed manually and are listed in Table 3.1. See Appendix III for the partial C-terminal RyR1 cDNA and amino acid sequences.

Table 3.1: Mutagenic primers for the 4861 amino acid

Variant	Orientation	Sequence (5'-> 3')
A	Fw.	GGCCTTCAACTTCTTC**C<u>A</u>C**AAGTTCTACAACAAG
	Rev.	CTTGTTGTAGAACTT**G<u>T</u>G**GAAGAAGTTGAAGGCC
C	Fw.	GGCCTTCAACTTCTTC**C<u>C</u>C**AAGTTCTACAACAAG
	Rev.	CTTGTTGTAGAACTT**G<u>G</u>G**GAAGAAGTTGAAGGCC
T	Fw.	GGCCTTCAACTTCTTC**C<u>T</u>C**AAGTTCTACAACAAG
	Rev.	CTTGTTGTAGAACTT**G<u>A</u>G**GAAGAAGTTGAAGGCC

The codon that encodes the 4861 amino acid is shown in bold. The introduced mutation is underlined in each of the mutagenic primers. The wild type codon is CGC.

After primer extension by *Pfu*Turbo, *Dpn*1 was added to digest the methylated template DNA. Thus after digestion, the product only contains the newly formed (unmethylated) mutated plasmid. Figure 3.4 shows the *Dpn*1 digested mutagenesis PCR products that were obtained after replacing the wild type guanine in the 4861 codon (CGC) by a thymidine (see Table 3.1). Both products contained plasmids of the expected ~3500 bp. This corresponds to the pGEM®-T Easy Vector (3018 bp) plus insert (485 bp). The nicked DNA vector, containing the desired mutation was next used to transform XL1-blue competent cells. The introduction of the mutations was finally checked by DNA sequencing (see chapter 2.2.18). The mutated 4861 sequences are listed in Appendix IIB-D.

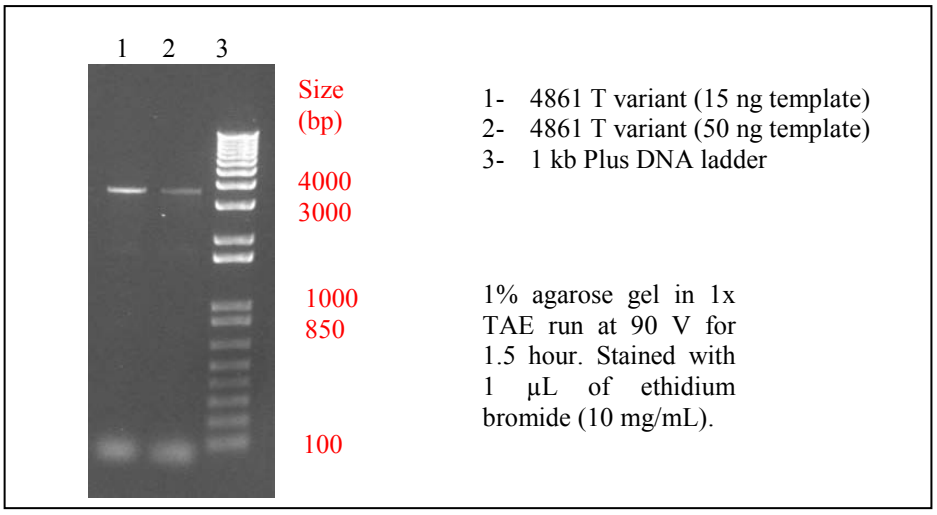

Figure 3.4: Representative results of the mutagenesis PCR products after *Dpn*1 digestion.

3.2.2 PCR and high resolution melting conditions

PCR primers were designed using the LightCycler Probe Design software 2.0. Primer sequences used in PCR are listed in Table 3.2. To prevent primer-dimer formation, the primers that were used to amplify the 61 bp 4861 target needed to be diluted to a lower concentration of 0.2 µM compared to the other samples. Amplicon lengths were kept relatively short (61-81 bp) to improve discrimination between genotypes. Real-time PCR cycling and HRM analysis of the engineered plasmids and genomic DNA samples were carried out on the LightCycler® 480 System (Roche). All assays described here could be conducted using identical PCR and high resolution melting conditions (see chapter 2.2.11). Experiments were conducted with both the LightCycler® 480 HRM Master and LCGreen PLUS.

Table 3.2: HRM primer sequences, primer concentrations and amplicon sizes

Target	Orientation	Sequence (5'-> 3')	Primer concentrations (µM)	Amplicon size
4826	Fw Rev.	ACTTCTTCTTTGCTGCC GGTGACAGAGGACAGGAT	0.3 0.3	77 bp
4833	Fw. Rev.	TCTCCTGGACATCGCC CACACCTGTTTCCCATTG	0.3 0.3	78 bp
4861	Fw. Rev.	CCGTGGTGGCCTTCAA GGTTCATCCTCATCCTCG	0.2 0.2	81 bp
4861	Fw. Rev.	GGTGGTCGTCTACCTGT GGTTCATCCTCATCCTCG	0.2 0.2	61 bp

3.2.3 Data analysis

Correct interpretation of the data depends to a large extent on the software algorithms used. The LightCycler® 480 Gene Scanning Software has been developed specifically to provide the most accurate analysis of HRM curves. The standard workflow consists of four basic steps. Figure 3.5 shows the data analysis conducted for identification of homozygous and heterozygous SNP variants at the 4861 position, using the 61 bp amplicons. First, the software automatically detects negative samples, i.e., samples with low fluorescence signals such as non-template controls. The second step in the analysis

is to normalize the raw melting curve data by setting the pre-melt (initial fluorescence) and post-melt (final fluorescence) signals of all samples to uniform values of 100% and 0%, respectively (see Figure 3.5A). The percentage of fluorescence between the two regions is calculated at each temperature as the distance to the experimental data compared with the distance between the extrapolated upper and lower lines. This results in normalized melting curves. Figure 3.2B depicts the derivative plots as generated by the LightCycler® 480 software. Note the second low-temperature melting transitions characteristic for heterozygous samples. Often homozygous samples can already be distinguished from heterozygous samples based on these secondary low melting transitions. Nevertheless, differences in melting transitions are best visualised using difference plots because slight differences in curve shape and T_m become most obvious. Thus the next step required for the generation of a difference plot is shifting the temperature axis of the normalized melting curves to the point where the entire double-stranded DNA is completely denaturated. For this the software automatically applies a default Temp Shift Threshold of 5% to all data (see Figure 3.5C). Each curve is superimposed over the given fluorescence interval. When the curves are shifted to superimpose their high-temperature, homoduplex transitions (low percentage of fluorescence), heteroduplexes can be identified by their early decrease in fluorescence at lower temperatures (Figure 3.5D). In some cases even homozygous SNPs may be distinguished from the wild type, by melting curve displacements. This is best visualized in the normalized non-temperature shifted data (see Figure 3.5C). Subtracting the melting curves from a reference curve (also called „base curve“) is the final step in the analysis This generates the difference plot (Figure 3.5E), and allows the clustering of samples into groups that have similar melting curves (i.e., those with the same genotype).

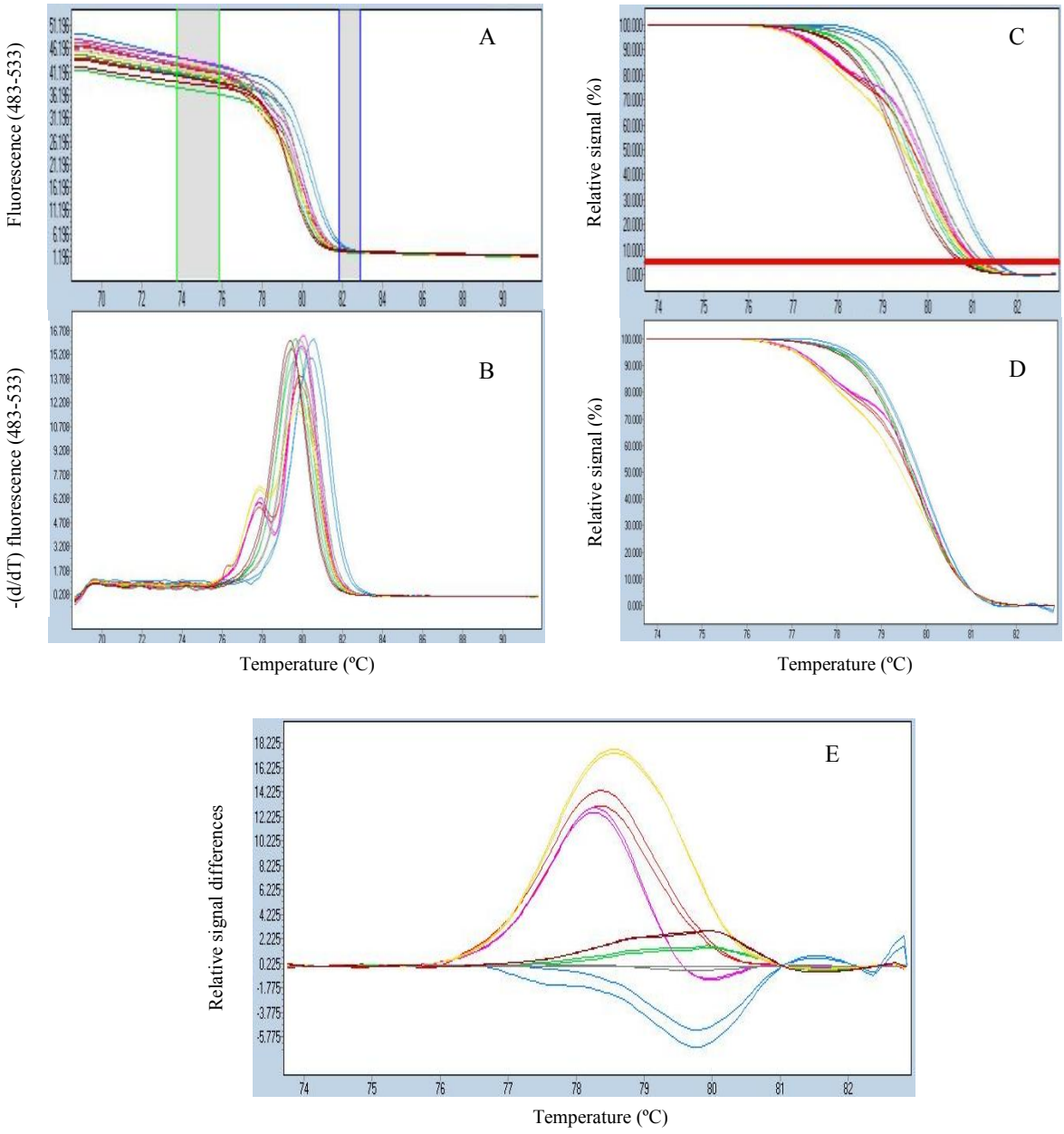

Figure 3.5: HRM data analysis of the 4861 61 bp amplicons, using the LightCycler® 480 Gene Scanning Software.

(A) Regions used for normalization are indicated by vertical bars on the unnormalized melting curves. (B) Derivative melting plots. (C) Normalized melting curves. (D) normalized, temperature-shifted melting curves. (E) Difference plot, heterozygotes: G/C(yellow), G/A (red), G/T (purple) and homozotes: T/T (brown), A/A (green), C/C (reference curve; grey),G/G blue.

3.3 Results

3.3.1 Genomic DNA samples

Amplicon melting analyses in the presence of the heteroduplex detecting dsDNA-binding dye LightCycler® 480 HRM Master or LCGreen PLUS were used to detect SNPs using the LightCycler® 480 System. Amplicons were 61 to 81 bp in length to allow definitive discrimination and identification of homozygous sequence variations. Figure 3.6 shows the difference plots produced by the HRM analysis, which followed the real-time PCR amplification of 81 bp amplicons from genomic DNA flanking the 4861 position, using either the LightCycler® 480 HRM Master or LCGreen PLUS. HRM analysis with either dye allows clear discrimination between the homozygous and heterozygous genomic DNA samples, based on differences in melting curve shapes. All samples were of known genotypes and were grouped correctly by the LightCycler® 480 Gene Scanning software.

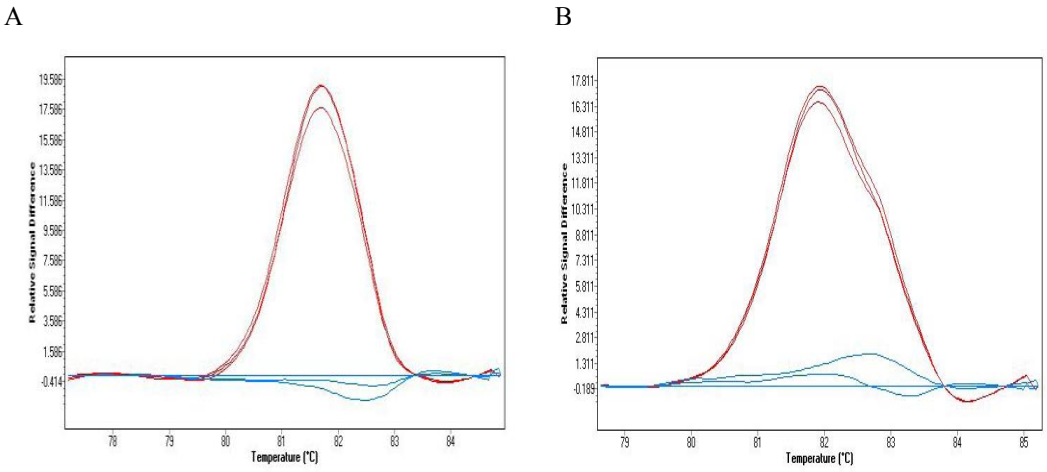

Figure 3.6: Difference plots of gDNA HRM analyses of the 4861 81 bp amplicons.

Three heterozygous samples (indicated in red) and three homozygous samples (indicated in blue) were analyzed using the LightCycler® 480 HRM dye (A) or LCGreen PLUS (B).

Two other HRM assays were designed and allowed screening of the *RYR1* gene for the T4826I or H4833Y *RYR1* mutations, respectively. Each of the assays was validated by screening ten homozygous wild-type and ten heterozygous genomic DNA samples of known genotypes for the SNPs causing the T4826I or H4833Y amino acid substitutions.

Unambiguous differences were visible in the shapes of the melting curves for heteroduplexes and homoduplexes. The difference plots shown in Figure 3.7 & 3.8 clearly separate homozygous from heterozygous genomic DNA samples for the 4826 and 4833 HRM assays, respectively. All samples were grouped correctly by the LightCycler® 480 Gene Scanning software with both LightCycler® 480 HRM Master and LCGreen PLUS. Both homozygous and heterozygous samples analysed for the 4833 SNP by HRM using LCGreen PLUS, show an increase in variability between melting curves (Figure 3.8B). The HRM assay performed with the LightCycler® 480 HRM Master shows no such variability (Figure 3.8A). The real-time PCR, which precedes the HRM analysis revealed that although the amplification curves of both assays look similar and up to standard, the crossing points of the reactions using the LC480 Probe Master Mix with LCGreen PLUS were delayed by at least three cycles compared to the LightCycler® 480 HRM Master. This trend could be detected in all experiments. In addition the LightCycler® 480 HRM Master generates a fluorescence signal which is at least eight times stronger than that with LCGreen PLUS.

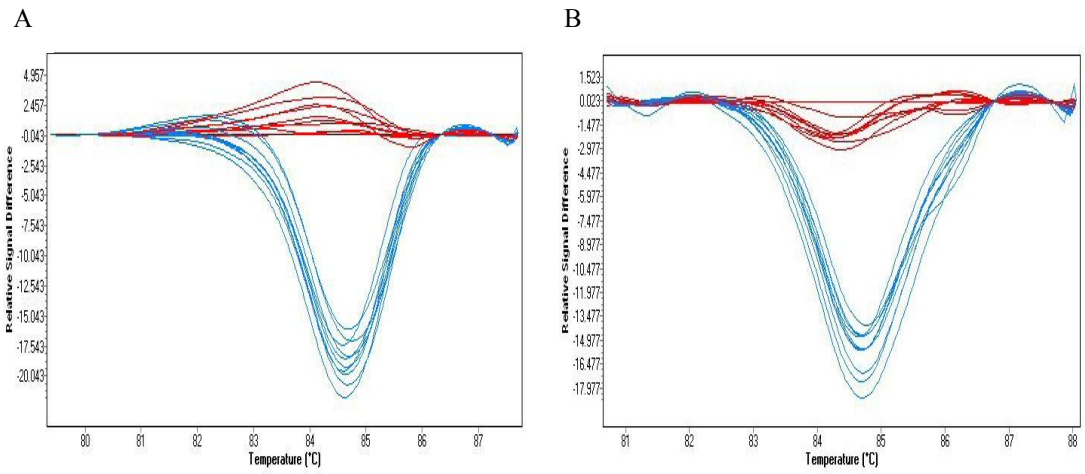

Figure 3.7: Difference plots of gDNA HRM analyses of the 4826 77 bp amplicons.

Ten heterozygous samples (indicated in red) and ten homozygous samples (indicated in blue) were analyzed using the LightCycler® 480 HRM Master (A) or LCGreen PLUS (B).

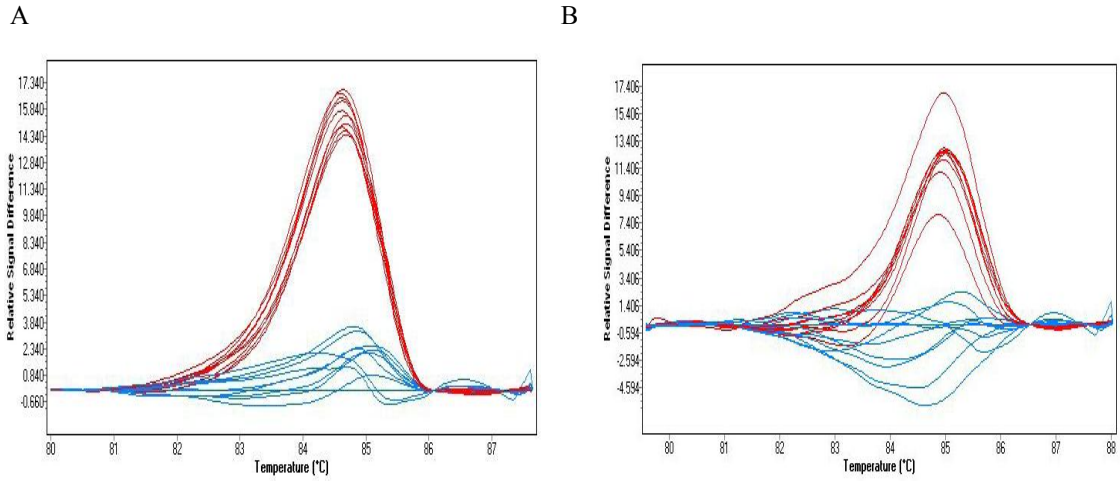

Figure 3.8: Difference plots of gDNA HRM analyses of the 4833 78 bp amplicons.

Ten heterozygous samples (indicated in red) and ten homozygous samples (indicated in blue) were analyzed using the LightCycler® 480 HRM Master (A) or LCGreen PLUS (B).

3.3.2 Engineered plasmid constructs

Engineered plasmids were used to study homozygote discrimination. Four plasmids (identical except for a G, C, T or A at the specified position) containing the sequence flanking the 4861 SNP, were used alone to simulate homozygous genotypes or in binary combinations to simulate heterozygous genotypes. HRM analyses of 81 bp and 61 bp amplicons were conducted to determine the effect of amplicon length on genotype differentiation. The difference plot of the HRM assay for the 81 bp amplicon causing the 4861 SNP, using the LC480 HRM Master, is shown in Figure 3.9A. Heterozygotes were easily distinguished from homozygotes based on shape of the melting curves. Difference plot analysis also allows discrimination between different heterozygotes. Homozygote discrimination is based on differences in T_m. These differences are best detected by normalized melting curves without temperature shifting and not by the temperature shifted difference curves [115]. Thus, for the detection of homozygote variants, amplicon melting data should always be analyzed both with and without temperature shifting. This is demonstrated by the homozygous C (C/C) genotype, which cannot be readily distinguished from the homozygous A (A/A) and T (T/T) genotypes in the difference plot (Figure 3.9A). Normalized melting curves on the other hand did allow clear differentiation between the homozygous C and from the homozygous A and

T (A/A, T/T) genotypes (Figure 3.9B). No differentiation is possible between homozygous A and T based on HRM analysis of the 81 bp amplicon. The T_m's of the homozygous A and T variants differ by only ~0.1˚C (Fig. 3.9B).

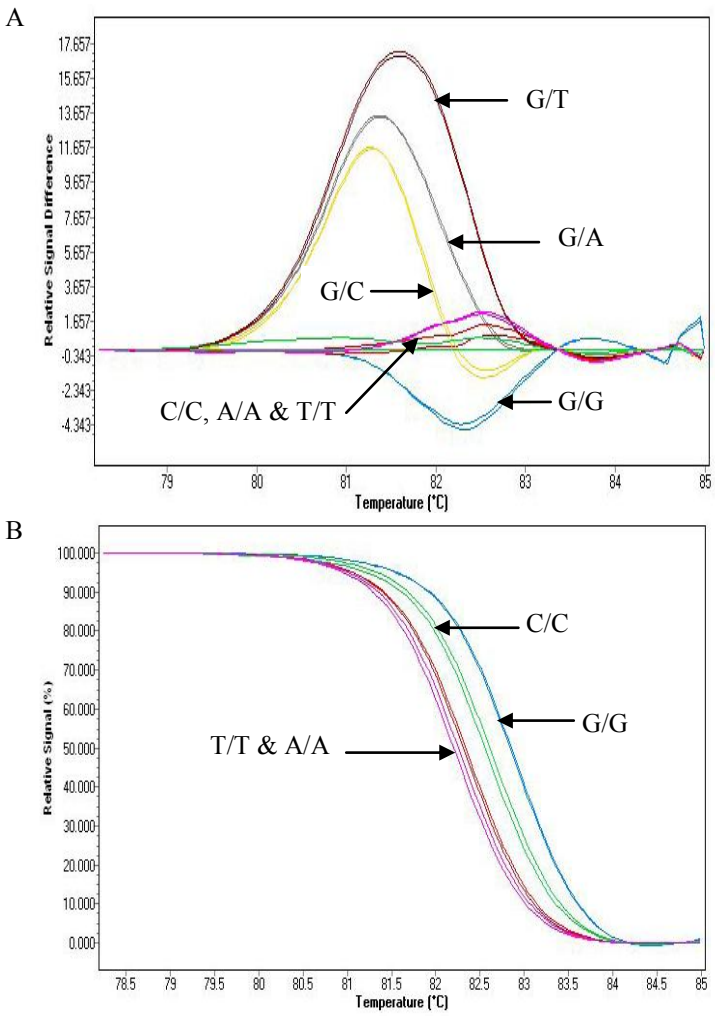

Figure 3.9: HRM analysis of possible SNP genotypes at the 4861 position, using the LightCycler® 480 HRM Master (81 bp amplicons).

Two samples of each genotype were analyzed and included four homozygotes (G/G, C/C, A/A & T/T) and three heterozygotes (G/T, G/A & G/C). (A) Difference plot of the HRM analyses. (B) Normalized HRM curves of the wild type samples. T_m's of homozygote variants: 82.96 & 82.94 ºC for G/G, 82.67 & 82.60 ºC for C/C, 82.22 & 82.28 ºC for T/T and 82.34 and 82.37 ºC for A/A.

Complete genotyping of all the 4861 SNPs in 81 bp amplicons with HRM was possible by adding exogenous wild-type DNA amplicons (in a 1:1 ratio) to unknown homozygous samples. If unknown samples are wild type their melting curves do not

change after the addition of exogenous wild-type DNA amplicons. If the unknown samples are homozygous mutants, heteroduplexes are produced and samples can be correctly identified as homozygous mutant. Figure 3.10 shows the result of adding 81 bp amplicons, containing the flanking wild type 4861 sequence to the homozygous samples. Heteroduplexes were formed when homozygous mutants were present. The shape of the melting curves that were generated by the addition of exogenous DNA to homozygous mutants correlated with those of the original heterozygotes and therefore allowed SNP genotyping.

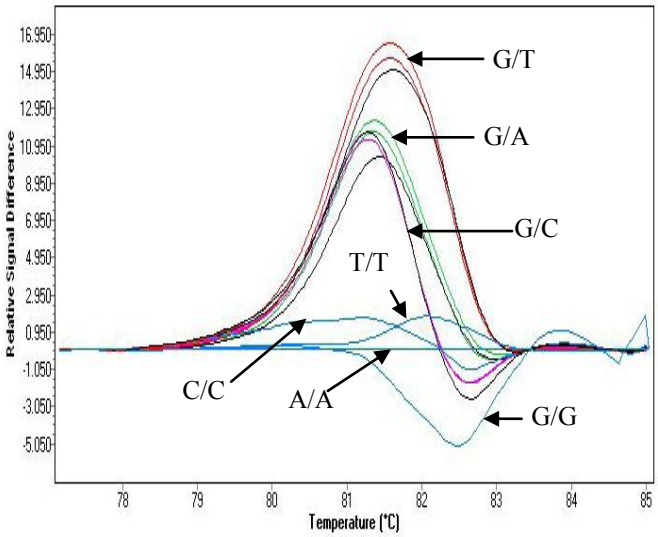

Figure 3.10: HRM analysis of possible SNP genotypes at the 4861 position by adding wild type DNA amplicons, using the LightCycler® 480 HRM Master (81 bp amplicons).

Unknown homozygous genotypes (indicated in blue) were mixed with wild type amplicons after PCR, creating heterozygotes (G/T, G/C & G/A; indicated in black) that have similar melting curves as the original heterozygotes (G/T; brown, G/A;green, G/C; purple).

HRM analyses using smaller 61 bp amplicons allowed discrimination between different heterozygous and different homozygous samples, without the addition of exogenous DNA. Heterozygous SNP variants were readily identified, using difference plots (Figure 3.11A). Homozygous SNP variants at the 4861 position were identified using non-temperature shifted normalization curves (Figure 3.11B). The T_m difference between the homozygous A and T variants was ~0.2˚C and proved to be sufficient for discrimination between the two. Occasionally homozygote SNP identification may also be possible by

using difference plots (Figure 3.11A). Since these smaller (61 bp) amplicons have a lower T_m, the melting range was adjusted to 69-92˚C.

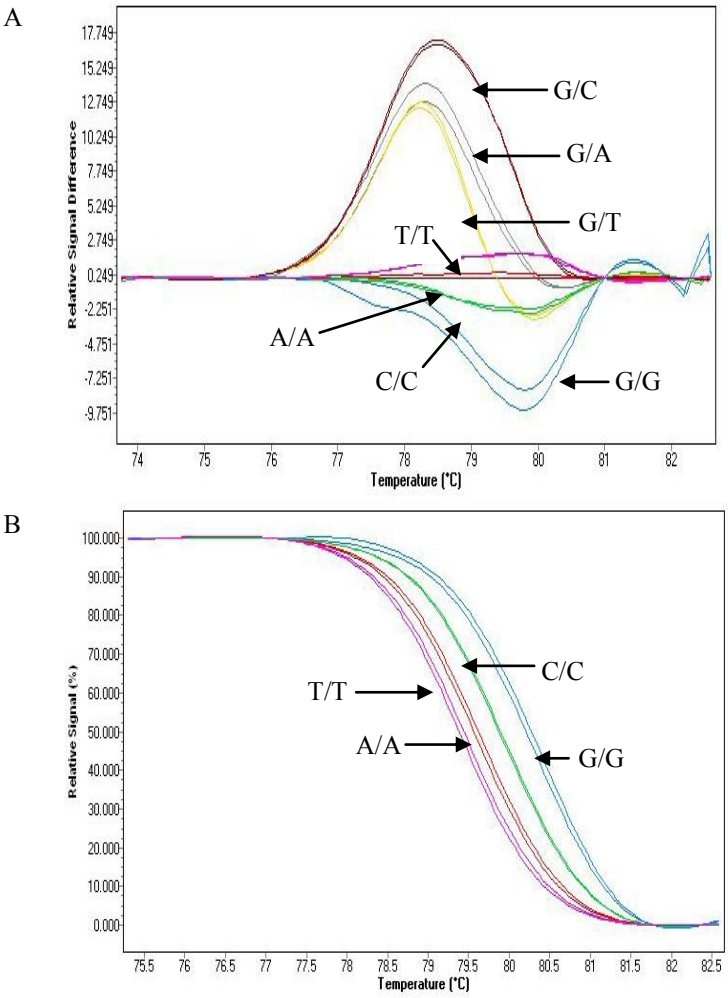

Figure 3.11: HRM analysis of possible SNP genotypes at the 4861 position, using the LightCycler® 480 HRM Master (61 bp amplicons).

Two samples of each genotype were analyzed and included four homozygotes (T/T, A/A, C/C & G/G) and three heterozygotes (G/C, G/A & G/T). (A) Difference plot of the HRM analyses. (B) Normalized HRM curves of the wild type samples. T_m"s of homozygote variants: 80.50 & 80.39 ºC for G/G, 79.97 & 79.95 ºC for C/C, 79.37 & 79.43 ºC for T/T and 79.58 and 79.64 ºC for A/A.

3.4 Discussion

HRM has been introduced as a homogenous closed-tube post-PCR method for genotyping and mutation scanning which does not need costly labelled oligonucleotides

[116]. Instead it relies on new generation generic heteroduplex-detecting dsDNA-binding dyes. Unlike other closed-tube genotyping methods that use melting analysis, HRM has the capacity to scan for unexpected as well as known variants within the whole amplicon [117]. Using HRM, SNPs have been genotyped in products as large as 544 bp [115]. HRM SNP detection and/or genotyping however, is strongly sequence dependent and often short amplicons and/or the use of unlabeled oligonucleotide probes are necessary or preferred [117-119]. This study focussed on using HRM analysis of relatively small amplicons for SNP detection and identification, without the use of labelled/unlabelled probes. By using only two standard unlabelled primers the robustness of the assay increases significantly, since optimisation is not normally needed. Only the primers that were used to amplify the 61 bp 4861 target needed to be diluted to a lower concentration to prevent primer-dimer formation. Hence, all assays described in this study could be conducted using identical PCR and high resolution melting conditions, making it ideal for high-throughput screening purposes. In addition the LightCycler480® System provides a unique format in which the entire experiment, including real-time PCR and post-PCR HRM analysis, can be done in 96-well and/or 384-well format and completed within the hour.

In this study HRM assays were developed and analysed, using the LightCycler® 480 System. The assays screened 61 to 81 bp RYR1 amplicons for mutations associated with MH (T4826I and H4833Y) or CCD (R4861H). HRM analyses were conducted using two different heteroduplex-detecting dsDNA-binding dyes, the LightCycler® 480 HRM Master and LCGreen PLUS, respectively.

When the purpose of the analysis is to scan for heterozygotes, normalized and temperature shifted difference plots is a convenient way of viewing HRM data because slight differences in curve shape become obvious. All assays that were developed in this study allowed unambiguous discrimination between heterozygous and homozygous samples. The use of the LightCycler® 480 HRM Master has some advantages over the use of the LC480 Probe Master Mix with LCGreen PLUS. The fluorescence signal generated by the LightCycler® 480 HRM Master is at least eight times as strong and PCR crossing points are lowered by at least three cycles. The latter of the two can be

crucial for accurate mutation scanning and/or genotyping, since it has been suggested that the validity of HRM analysis of samples with late or poor amplification is questionable [120]. The real-time PCR preceding the HRM analysis can therefore provide a useful quality control measure. Thus the late PCR crossing points are likely to be the cause of the increase in variability between the melting plots shown in Figure 3.8A and B.

Engineered plasmids, which contain the genomic DNA sequence flanking the 4861 SNP, were used to show that all four possible homozygous genotypes at one position could readily be distinguished from each other by HRM analysis. This is an important element for *RYR1* screening for possible MH and/or CCD mutations, since homozygous missense mutations have been reported on rare occasions [23, 24]. Differentiation between genotypes of 81 bp amplicons was made possible by spiking unknown samples with exogenous DNA after PCR (Figure 3.10). Spiking samples after PCR has the advantage that only homozygous samples need to be retested, since heterozygous samples can already be identified based on difference plot analysis. In addition, this technique eliminates strict monitoring of DNA concentrations and differences in amplification efficiencies between samples and spike, since exogenous DNA is added after the PCR. Secondly, SNP genotyping without the addition of exogenous DNA was possible by using 61 bp amplicons that maximize differences in T_m and therefore improve discrimination between genotypes (Figure 3.11). When looking at differences in T_m however, one should acknowledge the possible effects that ionic strength, product concentrations and differences in PCR amplifications can have on the T_m between different samples [115].

Studies with genomic DNA samples and engineered plasmids indicated that both SNP detection and genotyping, of all possible base combinations at one position by HRM analysis of relatively small amplicons (61-81 bp) is possible using the LightCycler® 480 System. Depending on the sequence that is studied, HRM assays on larger amplicons may need to be used in conjunction with a sequencing method to determine the precise mutation. Nevertheless, HRM is inexpensive, has the potential for high

throughput and can greatly benefit mutation screening and genotyping of clinical samples for many genetic disorders including MH and CCD.

4. ALLELE-SPECIFIC PCR

4.1 Introduction

The aim of the main project of this PhD was to determine if there are allelic-specific differences in RyR1 expression levels, in heterozygous MHS samples. Allelic variations in RyR1 expression levels might provide insight into the observed variable penetrance and variations in MH phenotypes between different individuals. The presence/absence of causative MH mutations in the RyR1 transcripts provides suitable markers that allow discrimination between the two alleles. While functional mutations present in the coding region may affect allele-specific expression, there might be other important *cis*- or *trans*-acting polymorphisms present. *Cis*-acting polymorphisms can have a direct effect on e.g. the function, stability or transcription levels of the affected gene. *Trans*-acting polymorphisms (e.g transcription factors) act by altering the action of downstream genes. Figure 4.1 shows a schematic view of the possible involvement of *cis*-acting mutations on variations in gene expression between different alleles in heterozygous samples.

In this study a relatively inexpensive and rapid assay was developed to determine the relative mRNA quantities of the two *RYR*1 alleles in heterozygous MHS samples. The causative MH mutations present in the coding region of the *RYR*1 gene were used as markers to allow discrimination between the two *RYR*1 transcripts. Measuring the expression of each of the two alleles simultaneously in the one target tissue is optimal for detecting *cis*-acting differences as each allele serves as an internal control for the other. Any *trans*-acting effects of environmental conditions that differentially influence gene expression among samples should not interfere [121].

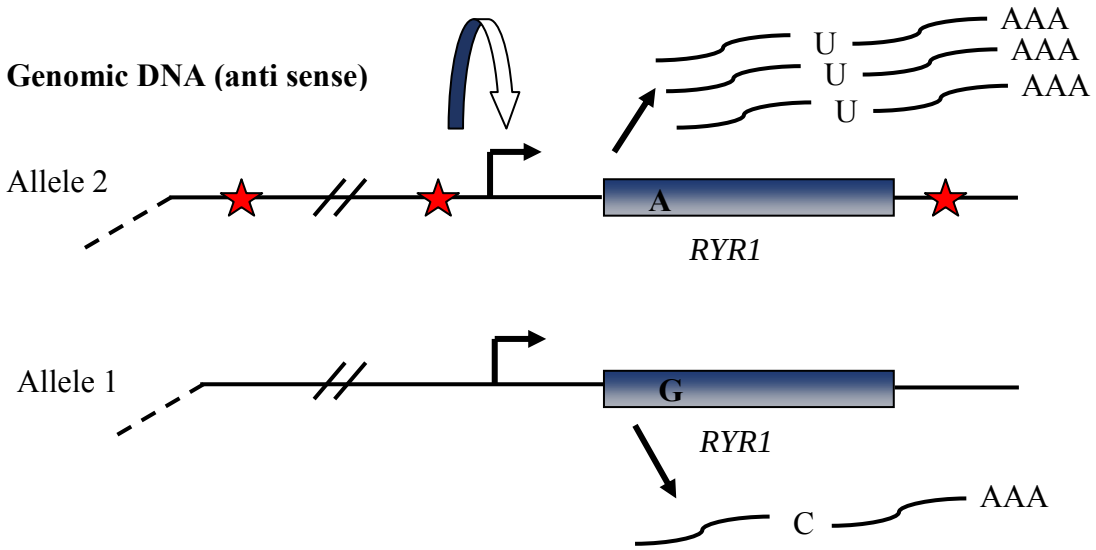

Figure 4.1: Allele specific differences in gene expression.

In this example allele 2 is the high producing genotype relative to allele 1. Although there is a functional mutation in the coding region, in this study it is being used as a marker. Other mutations/polymorphisms might be present on the high producing allele (depicted by red stars). One of which might be located in an important regulatory region (depicted by red star with arrow) that modulates gene expression.

The designed assay combined kinetic (real-time quantitative) PCR with allele-specific amplification. Unlike many other real-time PCR methods, allele-specific PCR (AS-PCR) does not need expensive fluorescently-labelled oligonucleotides. Instead SYBR Green can be used as an inexpensive fluorescent generic DNA-binding dye. In order to differentiate between the two alleles, two allele-specific primers were designed in the same orientation (AS1 & AS2, respectively). The sequence of the two primers was similar except for the base at the 3‟-end, which was allele specific. To ensure allele specificity, a mismatch was added to the two allele-specific primers, just two bases away from the 3‟-end [112]. If the primer has a mismatch at the 3‟ end then the additional mismatch 2 bases further along will destabilize the primer and prevent or significantly slow down the amplification. A third common primer in the opposite orientation was designed to be used with each of the AS-primers in separate reactions (Figure 4.2).

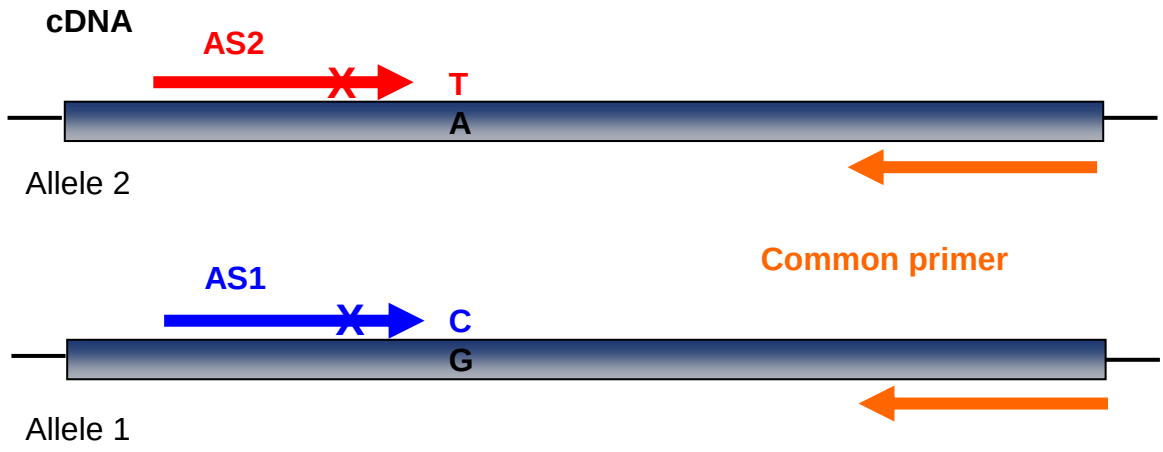

Figure 4.2: Principle of the AS-PCR of *RYR*1 cDNA.

Allele-specific primer 2 (AS2) is complementary to the mutant RyR1 allele. Allele-specific primer 1 (AS1) is complementary to the wild type RyR1 allele. X indicates the mismatches base 2 bases from the 3″ ends.

Plasmid constructs, representing the wild type and mutant 4833 *RYR*1 alleles, were used for assay validation. The H4833Y mutation co-segregates with the MH trait in a large NZ family. Variable penetrance has been observed within this family and three positive IVCTs have been reported without the presence of the H4833Y mutation. Four MHS muscle tissues, each containing the 4833Y MH mutation (#470, #835, #116 and # 145) were screened to determine if there were allele-specific differences in expression between the wild type and mutant RyR1. Two LCLs (#1295 and #1333), derived from blood of MHS individuals, were used in mRNA stability assays to determine possible allelic-specific differences in RyR1 mRNA stabilities.

4.2 Assay design

4.2.1 Primer design

An allele-specific PCR assay was designed for the causative RyR1 mutation located at amino acid residue 4833. The replacement of a thymine for a cytosine results in the replacement of the wild type histidine for a tyrosine in the mutated allele (H4833Y). PCR primers were designed using the LightCycler Probe Design software 2.0. The AS

primers were designed to have a melting temperature that was close to the annealing temperature used (58ºC) [122]. The common primer was chosen to have a melting temperature higher than the annealing temperature (65ºC). The AS PCR primers generate an amplicon of 142 bp in size and are listed in Table 4.1. The additional mismatches in each of the two AS PCR primers are underlined. Hypoxanthine-guanine-phosphoribosyltransferase (HPRT) was used as a reference (endogenous control) for real time PCR assays, since it is expressed at low levels as is RyR1. The primers generate an amplicon of 85 bp in size and are listed in Table 4.1. All the primer pairs listed below span an intron to prevent gDNA amplification. All *RYR*1 primers differ at several places (including their 3"ends) compared to the *RYR*2 and *RYR*3 transcripts. In addition RyR3 isoform is expressed at significantly lower levels than the RyR1 isoform in skeletal muscle. Consequently, no interference from the *RYR*2 and *RYR*3 isoforms is expected in the PCRs.

Table 4.1: Primers used in the allele-specific PCR assay

cDNA target	Orientation	Sequence (5'-> 3')
*RYR*1	Fw. (AS1)	CCATCCTGTCCTCTGTCA<u>T</u>CC
	Fw. (AS2)	CCATCCTGTCCTCTGTCA<u>T</u>CT
	Rev. (common)	GGTTCATCCTCATCCTCGCTCTTG
HPRT	Fw.	TCCAAAGATGGTCAAGGTCGC
	Rev.	TTCAAATCCAACAAAGTCTGGCT

The additional mismatches in the two AS PCR primers are underlined.

4.2.2 Testing allele specificity

4.2.1 Engineered plasmid constructs

Tests were performed to assess the specificity of AS1 and AS2 for the wild type and the mutant RyR1 allele, respectively. Plasmid constructs, containing a large C-terminal wild type or mutant 4833 *RYR1* cDNA sequence were prepared previously by Keisaku Sato. These constructs were used as templates for PCR to create plasmid constructs that were

smaller (insert of 409 bp) and easier to handle (see appendix III for the partial C-terminal RyR1 cDNA and amino acid sequences). Amplifications were carried out as described in section 2.2.2. The annealing temperature was adjusted to 53ºC and the extension time was set to 30 seconds. The sequences of the cDNA forward and reverse primers were 5‟-ACCTGGGCTGGTATATGGTG-3‟ and 5‟-TGACGATGACGAAGAAG -3‟, respectively. After amplification, 5 µL of the PCR products were visualized on 1% agarose gels stained with ethidium bromide. A single band of the expected size (409 bp) was visible (see Figure 4.3). PCR products were directly purified using the Wizard® SV Gel and PCR Clean-Up System. DNA concentrations were determined by A_{260} measurements using the Nanodrop spectrophotometer (Nanodrop Technologies).

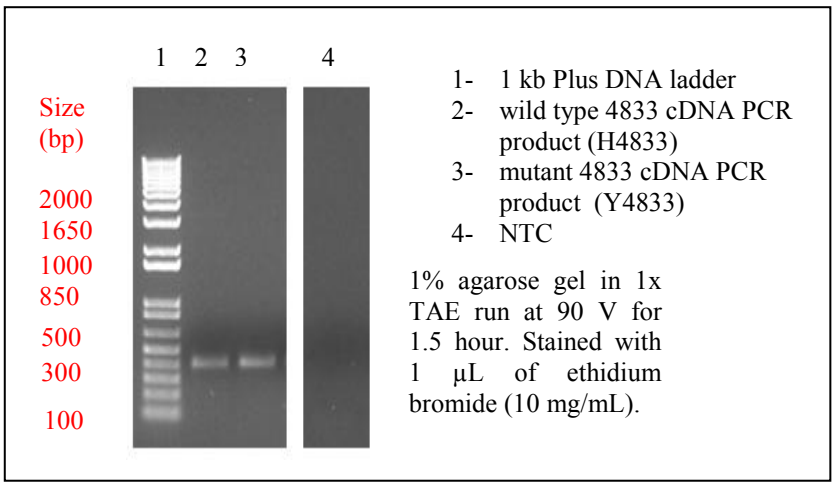

Figure 4.3: Visualizing the amplified cDNA fragments used for cloning.

For clarity purposes, additional irrelevant samples were removed from the picture, hence the white break.

Cloning of the PCR product was performed using the pGEM®-T Easy Vector Systems kit with two different insert:vector ratios; 1:1, 2:1, respectively (see chapter 2.2.3). After incubation the ligation products were used to transform *Escherichia coli* XL1-blue cells to allow blue/white screening of the transformants. In order to check whether or not plasmids contained the right size insert, two transformants of each clone were grown overnight and subjected to a rapid boil plasmid isolation followed by an *Eco*R1 digest. Digestion with *Eco*RI should result in a ~400 bp insert fragment and a ~3000 bp fragment that corresponds to the full length pGEM®-T Easy Vector. Figure 4.4 shows the results of the digests of two of the clones. Weak bands of the correct sizes were

visible for both the wild type and the mutant 4833 clones. Sequencing of one of the transformants was conducted to verify the presence of the correct insert (see appendix IVA & B).

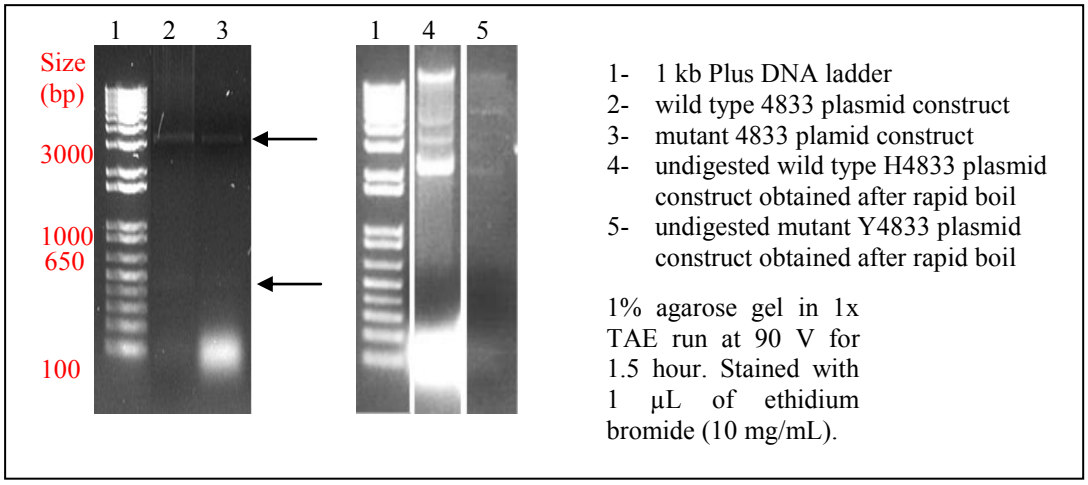

Figure 4.4 Transformants before and after digest with *Eco*R1.
Black arrows indicate the ~400 bp and ~3000 bp fragments that correspond to the sizes of the inserts and the linearized pGEM®-T Easy Vectors, respectively. For clarity purposes, additional irrelevant samples were removed from the picture, hence the white breaks.

4.2.2 Allele-specific PCR

Both wild type and mutant plasmids were amplified with both AS1 and AS2 according to the conditions described in chapter 2.2.12. Plasmid concentrations were estimated using a Nanodrop spectrophotometer (Nanodrop Technologies) and diluted empirically. The amplification curves had identical steep sigmoid curve shapes, and reached plateaus as the reactions reached their saturation points. No amplification occurred in the NTC, indicating that the results were not due to contamination issues. Derivative melting curves generated only a single peak (Tm ~ 88 ºC), indicating that no non-specific products or primer-dimers were present (see Figure 4.5). As expected the amplification of the mismatches (i.e. wild type sequence by AS2 and amplification of the mutant sequence by the AS1) was delayed by at least 10 cycles. Crossing points and melting temperatures are listed below Figure 4.5. After real-time PCR, 5 µL of the PCR products were analysed on 4% agarose gels stained with ethidium bromide. Single bands of the expected size (142 bp) were visible and confirmed the absence of non-specific products and primer-dimer formation (see Figure 4.6). Note that the

amplification of the products visualized in lanes 3 and 5 (Figure 4.6) were significant delayed due to primer mismatches (see Figure 4.5).

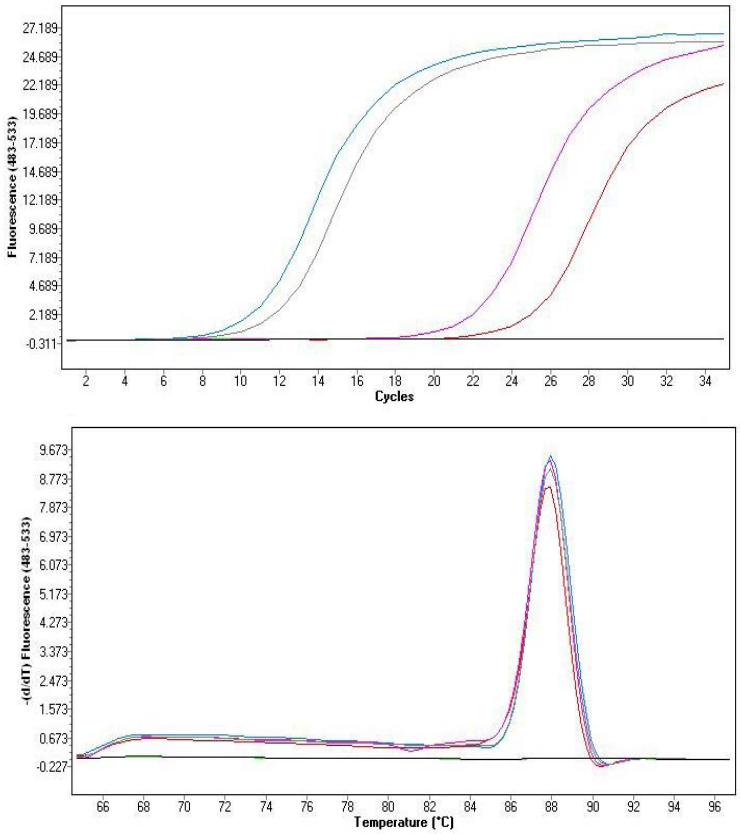

Figure 4.5: Testing allele-specific PCR primer specificities using plasmid constructs.

Amplification curves are displayed in the top graph. Melting peaks are displayed in the bottom graph. Blue is AS1 + wild type plasmid construct (Ct= 10.53, Tm= 87.98), grey is AS2 + mutant plasmid construct (Ct= 11.68, Tm= 87.96), purple is AS1+ mutant plasmid construct (Ct= 24.87, Tm=87.82), red is AS2 + wild type plasmid construct (Ct= 21.98, Tm= 87.89), green is AS1 +water, black; AS2 + water.

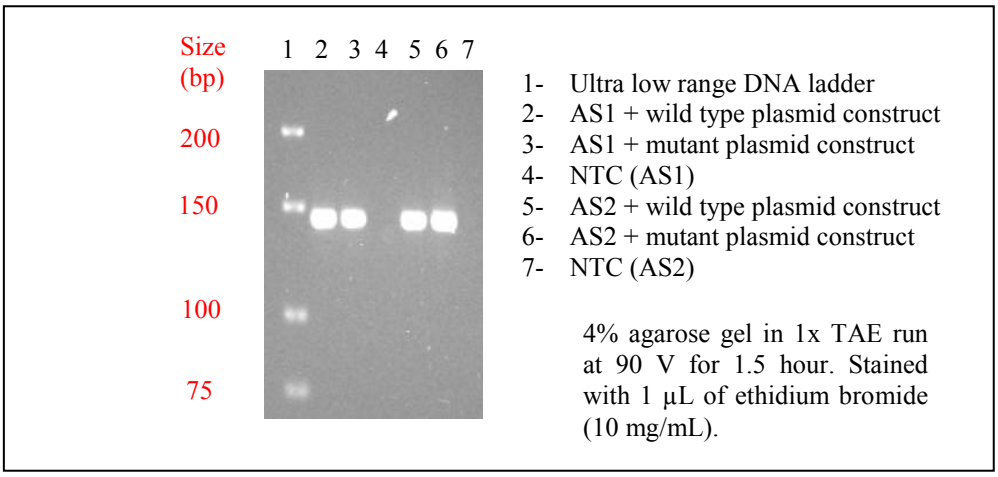

Figure 4.6: Visualizing the AS-PCR products.

4.2.3 Validation of allele-specific PCR assay using engineered plasmid constructs

To test the possibility of using the designed AS PCR protocol for relative quantification, different ratios of the engineered wild type and mutant plasmid constructs were mixed together in order to simulate heterozygotes. Plasmid concentrations were estimated using the Nanodrop spectrophotometer (Nanodrop Technologies) and diluted empirically so their PCR crossing points (Ct values) were similar to the expected Ct values of the MHS samples that were tested. When real-time PCR was performed, all amplification curves showed reliable steep sigmoidal curves. The derivative melting curves generated single peaks, indicating there was no primer-dimer formation. Table 4.2 shows representative results as generated by a relative quantification experiment using plasmid constructs that contained either the wild type or mutant *RYR*1 sequences. Each sample was amplified in triplicate. Note the depicted ratios are relative. Accurate determinations of the concentrations of the two plasmid construct were not conducted as they can be corrected for using the 1:1 ratio. The average of the three Ct values was used to calculate the allele frequencies of that allele by using Equation 4.1 [123].

Table 4.2: Relative allele frequencies using engineered plasmid constructs

Ratio (WT:MT)		Ct values							Percentage (%)	
		1	**2**	**3**	**Av.**	**Std.**	**ΔCt**	**[b]ΔΔCt**	**Theor.**	**Obs.**
4:1	**AS1**	18.35	18.28	18.14	18.26	0.09	-3.35	-2.10	80.00	81.09
	AS2	21.73	21.57	21.52	21.61	0.09	3.35	2.10	20.00	18.91
3:1	**AS1**	18.44	18.58	18.47	18.50	0.06	-2.72	-1.47	75.00	73.43
	AS2	21.14	21.18	21.32	21.21	0.08	2.72	1.47	25.00	26.57
1:2	**AS1**	19.45	19.60	19.61	19.55	0.07	-0.21	1.04	33.33	32.67
	AS2	19.75	19.81	19.72	19.76	0.04	0.21	-1.04	66.67	67.33
1:1	**AS1**	19.13	18.65	19.06	18.95	0.21	[a] -1.25	0.00	-	-
	AS2	20.30	20.17	20.12	20.20	0.08	[a] 1.25	0.00	-	-

Std.= Standard deviation, Av= average, Theor.= theoretical values, Obs.= experimentally observes values. [a] The ΔCt value for the 1:1 ratio should be equal to zero. Any deviation indicates differences in amplification efficiencies or DNA concentrations of the added plasmid constructs. Therefore the 1:1 ΔCt values were subtracted from the ΔCt values leading to [b]ΔΔCt. This value was used in the equation 1 to calculate the relative allele frequencies.

Equation 4.1

$$\text{Frequency of allele}_1 = 1 / (2^{\Delta\Delta Ct} + 1)$$

$$\Delta Ct = (Ct \text{ of allele}_1 \text{ specific PCR} - Ct \text{ of allele}_2 \text{ specific PCR})$$
$$\Delta\Delta Ct = (Ct \text{ of allele}_1 \text{ specific PCR} - Ct \text{ of allele}_2 \text{ specific PCR}) - (\Delta Ct \text{ 1:1 ratio})$$

The "2" in the denominator originates from "1 + the initial replication efficiency" [123]. Optimally, the amplification efficiency in PCR is 2, due to the doubling of the products in each PCR cycle. For a PCR to achieve maximum efficiency, every single factor affecting the process (e.g., sample preparation, nucleic acid purification, primer specificity) must occur optimally. Not surprisingly, most PCRs run at efficiency slightly different than 2 and thus the amplification efficiencies need to be determined. In order to correct for potential differences in amplification efficiencies and plasmid concentrations the 1:1 ΔCt value was subtracted from the 4:1, 3:1 and 2:1 ΔCt values. The resulting $2^{\Delta\Delta Ct}$ was used in equation 4.1. to calculate the relative allele frequencies. As depicted in Table 4.1., the observed ratios match the theoretical ratios with a maximum error of <2%. Thus, indicating the applicability and sensitivity of the assay.

4.2.4 Relative quantification of RyR1 cDNA

Amplification efficiencies of each primer pair used in the assay must be determined before assessing the relative quantities of the two RyR1 cDNA transcripts. This is essential as they need to be corrected for. In chapter 4.2.3 amplification efficiency corrections were carried out using plasmid constructs that were mixed together in a 1:1 ratio. This however is not possible using sample cDNA. Therefore, amplification efficiency determinations were conducted by making so called relative standards. These standards are serial dilutions of the template (e.g., undiluted, 1:5, 1:25, etc.) and their concentrations are expressed as relative units (e.g., 1, 0.2, 0.04, etc.). By using such dilutions one avoids the time-consuming preparation of cloned standards using plasmid constructs. In addition, the relative standards are more likely to have PCR efficiencies identical to the unknown samples as they are made from actual sample material. In

contrast, absolute quantification experiments employ artificial or cloned standards for the determination of the amplification efficiencies.

An appropriate dilution series for relative standards should cover a minimum of 4 dilution steps in the range of the samples to be analysed and at least 3 replicates to ensure statistically valid results. Four MHS muscle tissues (#470, #835, #116 and #145) were screened to determine if there were allele specific-differences in expression between the wild type and mutant *RYR*1. Two LCLs (#1295 and #1333), derived from blood of MHS individuals, were screened to assess allelic variations in expression and mRNA stabilities.

4.2.4.1 Linearity of the reverse transcription

The reverse transcription is a crucial step in quantitative analysis, since it converts the mRNA population into the cDNA library that is further analyzed by real-time PCR. To ensure that varying RNA amounts or RNA dilutions did not affect the reverse transcription reaction the linearity of the reverse transcription reaction was checked. This was done for all three targets (wild type transcript *RYR*1; AS1, mutant *RYR*1 transcript; AS2 and *HPRT* transcript) for each individual sample. This is imperative if large differences in mRNA levels are detected between the two *RYR*1 alleles. In addition, different amounts of RNA are expected when cells are incubated for different lengths of time with the transcription inhibitor actinomycin D.

Total RNA was DNase treated and serially diluted four or five times in 1:5 or 1:3 steps, respectively. Due to the low RyR1 mRNA expression levels, dilutions included MS2 RNA (Roche; final concentration 10 ng/ µL). This RNA from bacteriophage MS2 was used alongside siliconized tubes to prevent binding to the sides of the tubes and thus improve reproducibility. Equal volumes of the serially diluted RNA were then subjected to cDNA synthesis and amplified in triplicate, as described in chapter 2.2.13. A NO-RT control was performed to rule out amplification of any contaminating cDNA or gDNA. The NO-RT control was treated as any other sample but instead of adding 1 µL SuperScript™ III RT (200 U/µL), 1 µL of 0.01% DEPC treated MQ water was added.

Figure 4.7 depicts the real-time PCR results from a typical experiment performed for the determination of the linearity of the reverse transcription of the wild type *RYR*1 allele using AS1. The amplification curves showed identical and steep sigmoidal curves, even at lower template concentrations. No amplification occurred in the non template control or the NO-RT control. All derivative melting curves generated only a single peak of the expected Tm ~88 ºC.

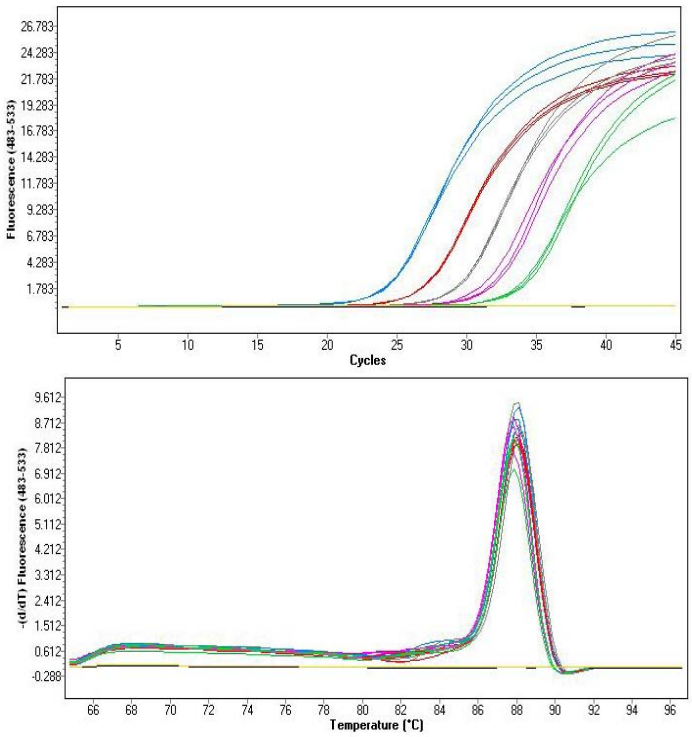

Figure 4.7: Real-time PCR results for the determination of reverse transcription linearity.

Amplification curves (top) and melting curves (bottom) as generated by the amplification of wild type *RYR*1 cDNA, using AS1. The five 1:5 dilutions are depicted as a result of declining initial RNA concentrations in blue, red, grey, purple and green, respectively. The NO-RT and NTC are shown in yellow and black, respectively.

4.2.4.2 PCR amplification efficiency determination

PCR amplification efficiencies of all three primers pairs (AS1, AS2 and HPRT) were determined by making a four or five times cDNA serial dilution in 1:5 or 1:3 steps, respectively. The dilutions were made with MS2 RNA (Roche; final concentration 10 ng/ µL) in siliconized tubes to prevent binding to the sides of the tubes and thus

improve reproducibility. The serially diluted cDNAs were amplified in triplicate as described in chapter 2.2.13. Figure 4.8 depicts real-time PCR results from a typical experiment performed for the determination of the amplification efficiency for the mutant RyR1 transcript using AS2. Derivative melting curves (data not shown) generate a single peak of the expected Tm.

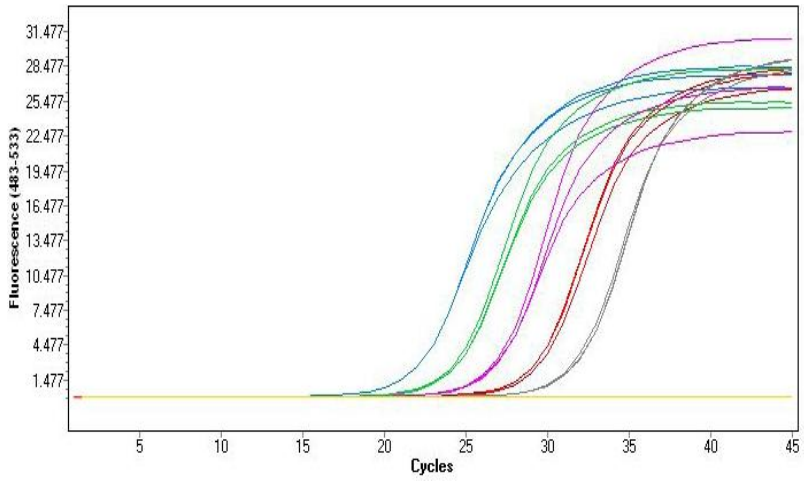

Figure 4.8: Determination of the PCR amplification efficiency of mutant *RYR*1 cDNA.

Amplification curves as generated by the amplification of mutant *RYR*1 cDNA, using AS2. The five 1:5 dilutions are depicted as a result of declining initial RNA concentrations in blue, green, purple, red and grey, respectively. The NTC is depicted in yellow.

4.3 Results

4.3.1 Screening muscle tissues

A total of four MHS muscle tissues (#470, #835, #116 and # 145) were screened to assess possible allele-specific differences in expression between the wild type and mutant RyR1 transcripts.

4.3.1.1 Linearity of the reverse transcription

For each sample the linearity of reverse transcription was determined, for all three targets, by plotting the log concentration against the mean of the PCR crossing points. Figure 4.9 shows the results for #470. The slopes of the generated standard curves are

used to calculate the amplification efficiencies (E), using Equation 4.2. These values are an indication of the linearity of the reverse transcription and should not deviate too much from the "perfect" amplification efficiency of 2. Table 4.3 summarizes the results of testing all four MHS samples for reverse transcription linearity.

Equation 4.2

$$E = 10^{-1/slope}$$

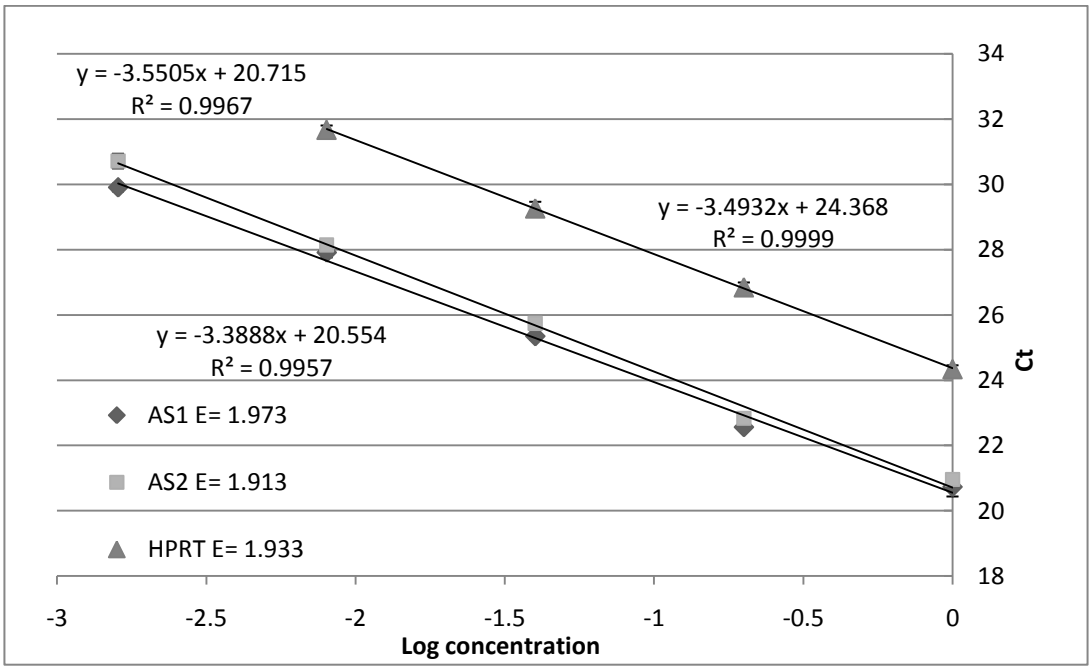

Figure 4.9: Linear relationship of cDNA synthesis as a function of RNA content.

Serially diluted 1:5 RNA extract from the #470 MHS muscle biopsy, was used for cDNA synthesis. Each standard curve was generated by triplicate amplifications of the housekeeping gene; HPRT (triangles), wild type *RYR*1; AS1 (diamonds) and mutant *RYR*1; AS2 (squares). The error bars show the standard deviation. The regression coefficient was ≥ 0.99 in all cases.

Table 4.3: Summary of the linearity of the reverse transcription reactions

Muscle sample #	Amplification efficiencies and coefficient of correlation (E/R^2)		
	AS1	**AS2**	**HPRT**
470	1.973/0.9957	1.913/0.9967	1.933/0.9990
835	2.074/0.9955	2.075/0.9956	2.032/0.9945
116	1.988/0.9986	1.873/0.9990	1.995/0.9923
145	1.976/0.9950	2.005/0.9908	2.107/0.9981

The results described above reveal that the reverse transcription reactions of all RNA extracts were linear over the range used in this study. Thus, the cDNA library generated can be expected to be a fair representation of the mRNA populations in the samples. Amplification efficiency determinations by serially diluting the isolated RNA, and subsequently making cDNA, is more laborious and results in larger intra- and inter assay variations. Therefore, in this study the amplification efficiencies used in the calculations were generated by making serial dilutions of the cDNA instead (= PCR amplification efficiencies; see below).

4.3.1.2 PCR amplification efficiency determination

PCR amplification efficiencies were calculated and used for the determination of the relative RyR1 allele frequencies. In order to correct for between-assay-variability, PCR amplification efficiencies were determined by constructing standard curves from the data of four individual experiments. Figure 4.10 shows the constructed standard curves for wild type *RYR*1 (AS1), mutant *RYR*1 (AS2) and *HPRT*. As the error bars indicate, assay variability was low. The "coefficient of variance" (CV) of the Ct values, between triplicates (intra-assay variation) and between assays (inter-assay variation) was between 0.12% and 3% in all cases. As expected, the higher CVs were generally associated with the more dilute samples.

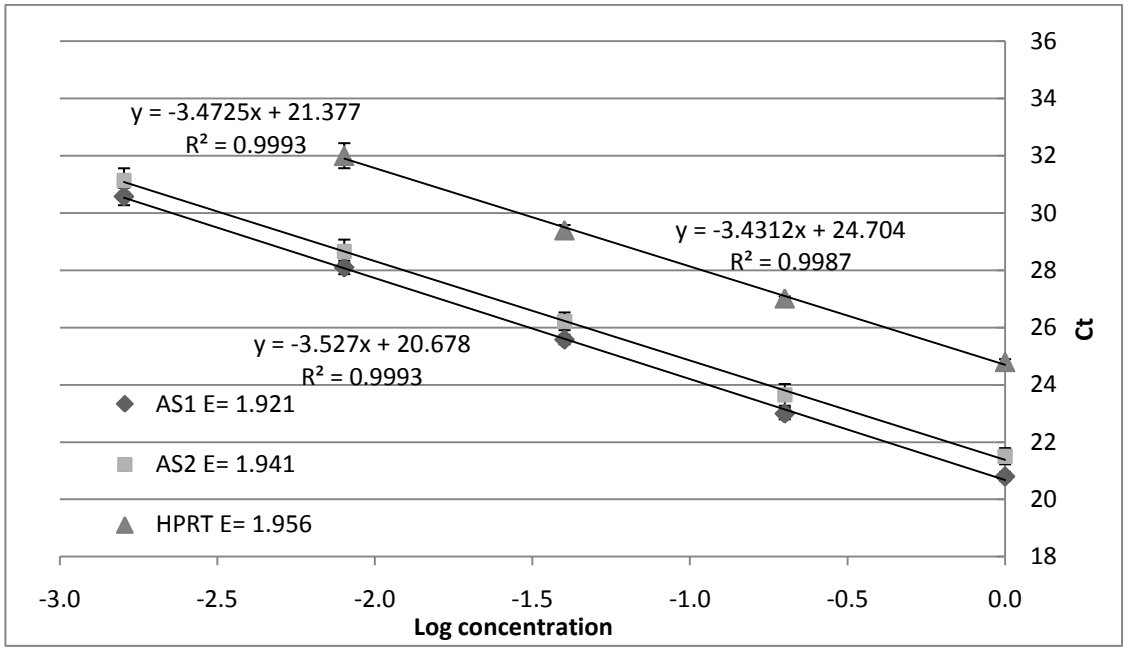

Figure 4.10: Constructed standard curves for the determination of the PCR amplification efficiencies.

Serially diluted 1:5 cDNA dilutions from the #470 MHS muscle biopsy. Each standard curve represents the pooled results of four individual experiments. Amplifications in each individual experiment were conducted in triplicate. Housekeeping gene; HRPT (triangles), wild type *RYR*1; AS1 (diamonds) and mutant *RYR*1; AS2 (squares). The error bars show the standard deviation. The regression coefficient was ≥0.99 in all cases.

Only standard curves with slopes between -3.1 to -3.6 and regression coefficients >0.99 were considered to be reliable. These slopes correspond to amplification efficiencies between 2.1 to 1.9, respectively. All three targets that were screened in the four samples fulfilled these requirements (see Table 4.4). Due to differences in muscle samples and/or muscle sample quality, the mRNA levels of the three targets were found to vary between samples. This was not a problem for the purpose of the assay, since the targets were measured simultaneously in the target tissue and only compared to targets from the same and not other tissues. The dilution series for each of the four samples were chosen according to their detected mRNA levels and the previously determined range of reverse transcription linearity. PCR amplification efficiencies of samples, in which fewer transcripts were detected, were determined by making 5 dilutions of 1:3 dilution steps instead 4 or 5 dilutions of 1:5 dilution steps. This was done to eliminate elevated inter-

and intra assay variations, due to high Ct values. Ct values higher over 35 were found to result in significantly higher variation between and within assays.

Table 4.4: Mean PCR amplification efficiencies (n=4)

Muscle sample #	Amplification efficiencies and coefficient of correlation (E/R^2)		
	AS1	**AS2**	**HPRT**
470	1.921/0.9993	1.941/0.9993	1.956/0.9987
835	2.068/0.9989	2.104/0.9995	1.999/0.9995
116	2.030/0.9989	2.045/0.9996	2.028/0.9988
145	2.011/0.9986	2.079/0.9993	1.976/0.9895

Dilutions series used for the determination of the PCR amplification efficiencies for each of the four MHS muscle tissues: 470; 1:5 dilution steps, 835; 1:3 dilution steps, 116; 1:3 dilution steps, 145; 1:3 dilution steps.

4.3.1.3 Determining the relative allele frequencies

After assessing the linearity of the reverse transcription reactions and determining the PCR amplification efficiencies, the samples were screened to determine the relative quantities of the two RyR1 alleles in each of the four samples. To confirm accuracy and reproducibility, the allele frequencies were determined by performing three independent experiments. Targets were amplified in triplicate within each experiment. Intra- and inter assay variabilities as obtained by screening sample #470 are shown in Table 4.5 and 4.6, respectively. As the results show, both intra- and inter assay variations are low.

Table 4.5: Intra-assay variability of real-time PCR when screening #470 (n=3)

Experimental run #	AS1			AS2			HPRT		
	Mean Ct	Stdev.	CV%	Mean Ct	Stdev.	CV%	Mean Ct	Stdev.	CV%
1	23.66	0.13	0.54	24.08	0.10	0.40	27.21	0.12	0.42
2	23.65	0.06	0.06	24.13	0.02	0.09	27.16	0.05	0.19
3	23.53	0.27	1.14	24.08	0.11	0.11	27.09	0.12	0.43

Stdev.= Standard deviation, CV%= coefficient of variance.

Table 4.6: Inter-assay variability of real-time PCR when screening #470

Target	Mean Ct (n=3)	Stdev.	CV%
AS1	23.61	0.07	0.31
AS2	24.10	0.03	0.14
HPRT	27.15	0.06	0.22

Stdev.= Standard deviation, CV%= coefficient of variance.

Several mathematical models are available for relative quantification during real-time PCR [124]. There are some small differences between the individual models. Nevertheless, all relative quantification analyses are based on the assumption that the concentration of the template (e.g. cDNA) at a sample‟s crossing point is the same for every sample containing the same target cDNA. The model used in this study, is a rearranged version of the efficiency calibrated mathematical method (see Equation 4.3) [124]. In this model, calculations are based on E and the Ct values of an unknown "sample" versus a "calibrator". The "target" is the nucleic acid of interest, while the "reference" is a nucleic acid that is found at constant copy number in all samples and serves as an endogenous control. The "calibrator" is typically a sample with a stable ratio of target-to-reference and can be used to normalize all samples within a run, but in addition provides a constant calibration point between several runs.

Equation 4:3

$$\text{Normalized ratio} = \frac{(E_{\text{ref}})^{Ct_{\text{sample}}}}{(E_{\text{target}})^{Ct_{\text{sample}}}} \div \frac{(E_{\text{ref}})^{Ct_{\text{calibrator}}}}{(E_{\text{target}})^{Ct_{\text{calibrator}}}}$$

In this study the relative expression levels of all targets were measured simultaneously in one target tissue. When the two *RYR*1 alleles have identical mRNA expression levels it is assumed that their HPRT:AS1 and HPRT:AS2 ratios will also be identical. Therefore, the two can be compared as long as the amplification efficiencies are corrected for. This eliminates the need for a calibrator, and if preferred also the reference. Here, the reference was still used as an endogenous control. As a result, the above equation was rearranged to Equation 4.4 and used for the calculations.

Equation 4:4

$$\text{Normalized ratio} = \frac{(E_{\text{HPRT}})^{Ct_{\text{HPRT}}}}{(E_{\text{AS1}})^{Ct_{\text{AS1}}}} \div \frac{(E_{\text{HPRT}})^{Ct_{\text{HPRT}}}}{(E_{\text{AS2}})^{Ct_{\text{AS2}}}}$$

Table 4.7 summarizes the results from the screens of the four muscle samples, using the H4833Y causative MH mutation as a marker. In all samples, the wild type *RYR*1 transcript (AS1) was found to be more abundant than the mutant *RYR*1 transcript (AS2). When these values are compared with the data from the IVCT (see Table 4.8), no clear correlation between transcript ratio and maximum muscle contraction was detected.

Table 4.7: **Relative *RYR*1 transcript abundance ratios in muscle tissue (n=3)**

Normalized ratios	**Muscle sample (gender)**			
Mean ± stdev.	**#470 (male)**	**#835 (male)**	**#116 (female)**	**#145 (male)**
Wt RyR1 (CV%)	1.76± 0.08 (4.35%)	1.72±0.27 (15.49%)	1.44±0.14 (9.86%)	2.44±0.40 (16.50%)
Mt RyR1	1.00	1.00	1.00	1.00

Stdev.= Standard deviation, CV%= coefficient of variance. # 470, #836 and #145 are related. The family history of #116 to the others is unknown.

Table 4.8: Data from the *in vitro* contracture test

IVCT data	**Muscle sample (gender)**			
	#470 (male)	**#835 (male)**	**#116 (female)**	**#145 (male)**
Max. caffeine tension (g)	3.8	2.0	1.9	2.9
Max.h alothane tension (g)	3.2	6.6	2.6	7.0

Maximum caffeine and halothane tensions were measured at 2mM caffeine and 2% halothane, respectively. # 470, #836 and #145 are related. The family history of #116 to the others is unknown.

4.3.2 mRNA stability assays

Allele-specific differences in mRNA expression levels can have various causes (e.g. variations in mRNA transcription, maturation or stability). No myoblasts containing the H4833Y mutation were available, thus immortalized LCLs that were derived from blood of MHS (H4833Y) individuals were used to assess the possibility that the detected allelic variations could be caused by allele-specific differences in *RYR*1 mRNA stabilities. In order to do so, LCLs were incubated for different times with the transcription inhibitor actinomycin D. Subsequently, the initial mRNA levels of the two *RYR*1 alleles and a housekeeping gene were measured in real-time PCR, by employing the designed AS PCR assay.

4.3.2.1 Clonal evolution in lymphoblastoid cell lines after prolonged culturing

Initial mRNA stability experiments, were conducted on LCL #1051. This cell line had been previously cultured, frozen, and reactivated from liquid nitrogen for an unknown number of times. In this study, the LCL #1051 was reactivated from storage and used for initial optimizations. During optimizations, the cells were kept growing continuously in T75 flasks by replenishing the media daily and/or by diluting the cells to more manageable concentrations.

At several random points in time, RNA was isolated from the cells. The generated cDNA was analysed by real-time PCR. After a period of 8 weeks (since reactivation of the cells from storage) the AS1 Ct values seemed to drop, indicating an increase in initial mRNA levels. The opposite was seen for the AS2 Ct values, suggesting a decrease in initial mRNA values. The HPRT Ct values did not seem to change. After another two weeks of culturing this drift became even more apparent. Table 4.9 depicts the real-time PCR results for all three targets after prolonged culturing of the LCL #1051. Each target was measured in triplicate. Note that at week 10 the Ct values of AS1 and AS2 are approaching a difference of 10 cycles. This was the proven to be the number of cycles by which the mismatched PCRs were delayed (see 4.2.2). Thus, the products being amplified by AS2 at week 10 will be a mix of both H4833 and Y4833 transcripts.

Table 4.9: Real-time PCR results for the after prolonged culturing of LCL #1051

Culture time (weeks)	AS1			AS2			HPRT		
	Mean Ct	Stdev.	CV%	Mean Ct	Stdev.	CV%	Mean Ct	Stdev.	CV%
4	27.72	0.07	0.24	27.6	0.37	1.33	19.74	0.06	0.31
8	26.95	0.13	0.48	30.26	0.18	0.60	19.61	0.03	0.18
10	25.06	0.03	0.13	32.53	0.52	1.60	19.27	0.26	1.36

Stdev.= Standard deviation, CV%= coefficient of variance.

The ratios between the wild type and the mutant *RYR*1 transcripts were determined using Equation 4.4 and are depicted in Table 4.10. As already indicated by the Ct values listed above, the LCL #1051 seems to lose its heterozygosity due to loss of expression of the mutant *RYR*1 allele.

Table 4.10: Relative *RYR*1 transcript abundance ratios after prolonged culturing of LCL #1051

Normalized ratios	**Culture time (weeks)**		
	4	**8**	**10**
Wt RyR1	1.01	11.63	222.19
Mt RyR1	1.00	1.00	1.00

As amplification efficiencies for LCL #1295 were used for the calculations (see Table 4.12).

Genomic DNA was isolated from the LCL (see chapter 2.2.1.2) in order to examine if the detected loss of heterozygozity after 10 weeks of culturing, is the result of transcriptional silencing or has its origin at the genomic DNA level. The 4833 HRM assay (see chapter 3) was carried out to quickly verify the loss of heterozygosity. Genomic DNA samples and plasmid constructs of known genotypes were included in the assay to validate the results. Figure 4.11 shows the HRM difference plot as generated by the LightCycler® 480 Gene Scanning Software. The genomic DNA isolated from the prolonged cultured LCL#1051 was grouped as a homozygous sample. Note that genomic DNA isolated from #1051 blood was heterozygous. The absence of the 4833 mutation was subsequently confirmed by sequencing of the genomic DNA.

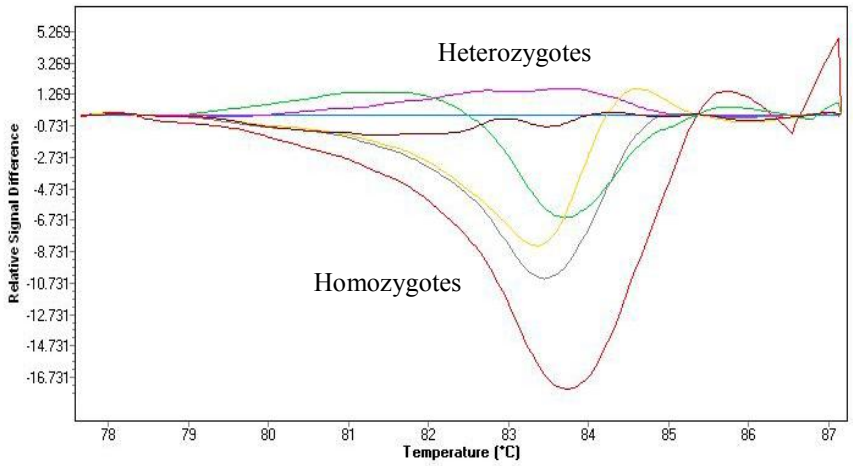

Figure 4.11: Difference plot generated by HRM analysis of the 4833 78 bp amplicons.

Heterozygous samples were distinguished from homozygous samples by the LightCycler® 480 Gene Scanning Software. The heterozygous samples are depicted in blue; known heterozygous gDNA sample, brown; mix of wild type and mutant RyR1plasmid constructs, purple; previously isolated gDNA sample from blood of #1051 sample. The homozygous samples are depicted in: yellow; plasmid construct representing a homozygous mutant, green; gDNA isolated from LCL#1051 after prolonged culturing, grey; plasmid construct representing a homozygous wild type, red; known wild type gDNA sample.

4.3.2.2 Linearity of the reverse transcription

As a result of the detected loss of heterozygosity after prolonged culturing of LCL #1051, two newly and never before used immortalized LCL (#1295 and #1333) were employed for the mRNA stability assays. Experiments using these two LCLs were conducted with short culture times in order to eliminate the effects of clonal evolution.

As for the muscle tissues, the linearity of the reverse transcription was determined for all three targets, by plotting the log concentration against the mean of the PCR crossing points. Due to the lower RyR1 expression in LCLs both the #1295 and #1333 LCLs amplification efficiencies were determined using 5 dilutions of 1:3 dilution steps. Table 4.11 summarizes the results of the reverse transcription linearity determination. As before, the results revealed that the reverse transcription reactions of all RNA extracts were linear over the range used in this study.

Table 4.11: Summary of the linearity of the reverse transcription determinations

LCL #	Amplification efficiencies and coefficient of correlation (E/R^2)		
	AS1	**AS2**	**HPRT**
1295	1.882/0.9954	1.988/0.9953	2.059/0.9972
1333	2.051/0.9965	2.007/0.9998	2.034/0.9994

4.3.2.3 PCR amplification efficiency determination

Figure 4.12 shows the constructed standard curves for wild type *RYR*1 (AS1), mutant *RYR*1 (AS2) and *HPRT* as generated when using LCL #1295. PCR amplification efficiencies were determined from the data of four assays, and used for the determination of the relative RyR1 allele frequencies. All standard curves fulfilled the requirements mentioned in chapter 4.3.1.2. Due to the lower *RYR*1 mRNA expression levels in lymphocytes, the PCR amplification efficiencies were determined using 5 dilutions of 1:3 dilution steps. Note that the HPRT expression levels are higher in the growing LCLs, compared to those in the muscle tissues. As can be expected, the higher Ct values resulted in higher assay variability compared to the variability seen for the muscle samples. Nevertheless, both intra and inter-assay variations were still acceptable with CV values remaining <3%. Table 4.12 shows the PCR amplification efficiencies of all three targets for both LCLs.

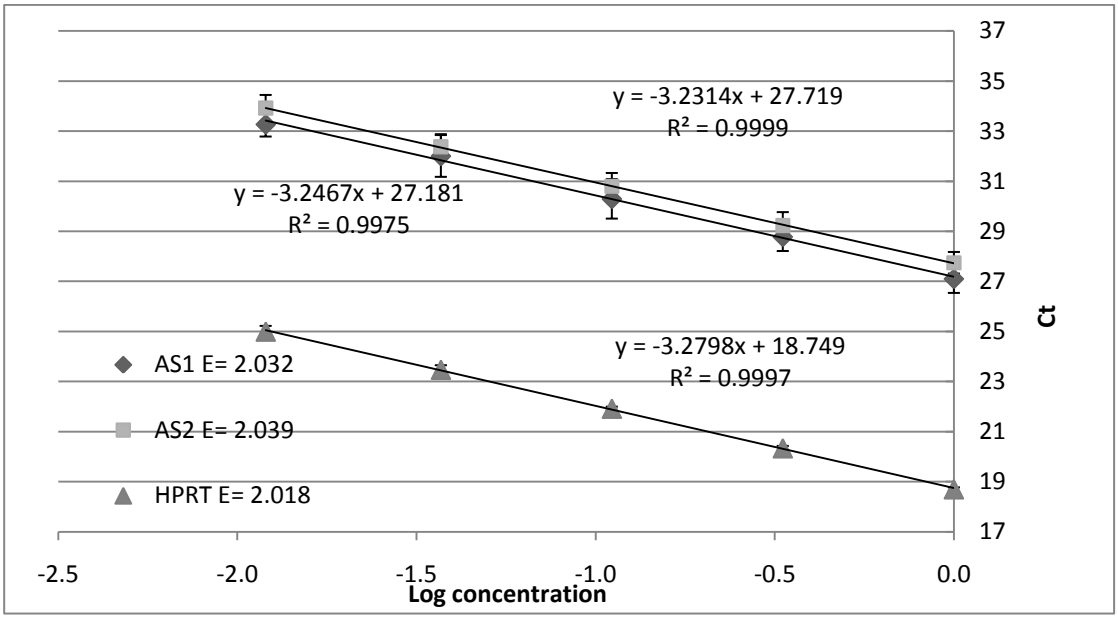

Figure 4.12: Constructed standard curves for the determination of the PCR amplification efficiencies.

Serially diluted 1:3 cDNA dilutions from the #1295 LCL. Each standard curve represents the pooled results of four runs. Amplifications in each individual experiment were conducted in triplicate. Housekeeping gene; HPPT (triangles), wild type *RYR*1; AS1 (diamonds) and mutant *RYR*1; AS2 (squares). The error bars show the standard deviation. The regression coefficient was ≥0.99 in all cases.

Table 4.12: Mean PCR amplification efficiencies (n=4)

LCL #	Amplification efficiencies and coefficient of correlation (E/R^2)		
	AS1	**AS2**	**HPRT**
1295	2.032/0.9975	2.039/0.9999	2.018/0.9997
1333	2.010/0.9993	2.014/0.9978	2.019/0.9997

4.3.3.4 Screening for the relative allele frequencies

After assessing the linearity of the reverse transcription reactions and determining the PCR amplification efficiencies, mRNA stability assays were conducted. LCLs were cultured in the absence or presence of actinomycin D for 0, 2, 7 or 24 hours, respectively. Subsequently, total RNA was extracted and used for first-strand cDNA synthesis. cDNA was generated each time from the same amount of RNA (1.5 µg). The

levels of all three targets (wild type *RYR*1; AS1, mutant *RYR*1; AS2 and *HPRT*) were then measured in real-time PCR assays. To confirm accuracy and reproducibility, all targets were measured in triplicate within each experiment (intra assay variability). Inter assay variability was addressed by conducting each individual experiment three times. To assess assay reproducibility the complete mRNA stability assays were repeated three times for both LCL #1295 and #1333. Table 4.13 shows the average real-time PCR results of the LCL #1295, of three independent mRNA stability assays. A clear increase in Ct values was detected with increasing actinomycin D incubations, indicating a considerable decrease in initial mRNA levels, due to the inhibition of the transcription.

Table 4.13: Average real-time PCR results of three independent mRNA stability assays for LCL #1295

Actinomycin D incubation time (h)	AS1			AS2			HPRT		
	Mean Ct	Stdev.	CV%	Mean Ct	Stdev.	CV%	Mean Ct	Stdev.	CV%
0	30.31	0.24	0.79	30.45	0.10	0.34	20.22	0.28	1.38
2	30.52	0.26	0.84	30.88	0.12	0.38	20.23	0.26	1.27
7	31.44	0.22	0.70	31.78	0.20	0.62	20.56	0.24	1.19
24	33.34	0.08	0.23	33.33	0.13	0.38	21.41	0.24	1.13

Stdev.= Standard deviation, CV%= coefficient of variance

In Figure 4.13, the differences between Ct values are represented as "percentages of the control", to give a more distinct view of the decreased mRNA expression levels due to incubation of the cells with actinomycin D. The percentages were calculated by setting the Ct values derived from the cells that weren't incubated with actinomycin D (t=0h) at 100%. Reproducibility between the three assays was high, as CVs for both LCL #1295 and #1333, were <3%. For both LCLs (#1295 and #1333) the *RYR*1 mRNA levels decreased by >86%. The mRNA levels of the housekeeping gene in each LCL, decreased by at least 57%. Note that, actinomycin D inhibits transcription by binding to the pre-melted DNA conformation present within the transcription complex. This immobilizes the complex, interfering with the elongation of the growing RNA chain [125]. Therefore, not only mRNA transcription is sensitive to actinomycin D.

Ribosomal RNA synthesis is particularly sensitive. In this study, the same amount of total RNA was isolated at each of the four time points (0, 2, 7 & 24h), and used for cDNA synthesis. As actinomycin D does not only inhibit mRNA synthesis, the depicted decreases in mRNA levels in Figure 4.13 are only estimates, since the levels of the three transcripts are compared with t=0h. The relative amount of mRNA in the t=24h sample however, can be expected to be much higher compared to the relative amount of mRNA in the t=0h sample. This is because the actinomycin D has a more pronounced effect on ribosomal RNA synthesis than it has on mRNA synthesis. The true decrease in mRNA transcript levels due to inhibition of transcription by actinomycin D can therefore be expected to be even more pronounced. Nevertheless, Figure 4.13 confirms a considerable inhibition of transcription occurs (>86% for *RYR*1). The observed decrease in mRNA transcripts was believed to be of an adequate range to allow for the detection of possible allele-specific differences between *RYR*1 mRNA stabilities.

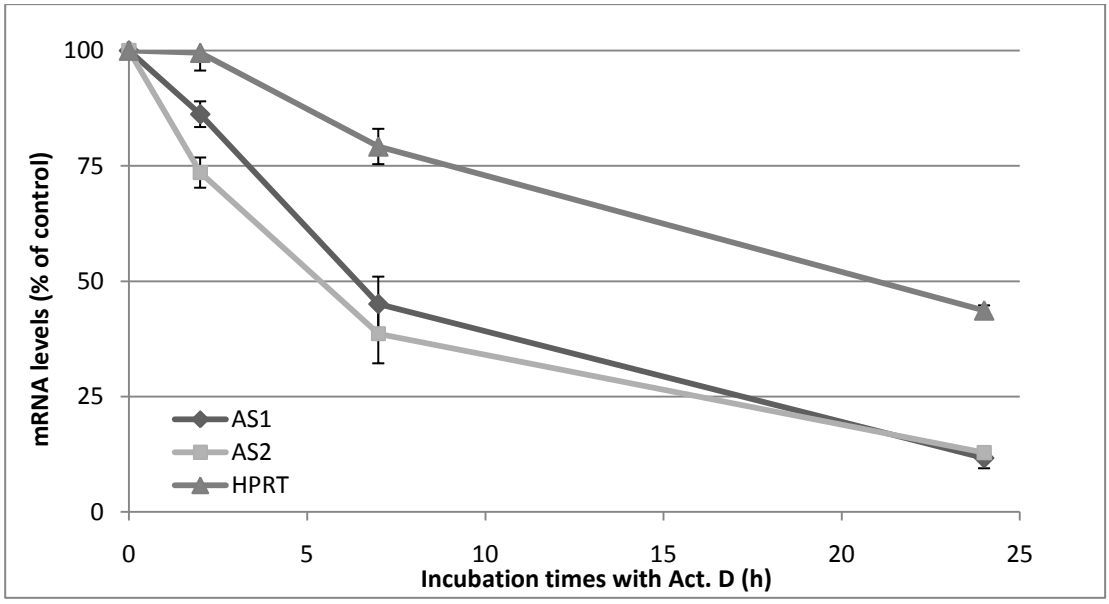

Figure 4.13: mRNA expression levels in LCL #1295 after actinomycin D incubations.

Initial mRNA expression levels were measured in real-time PCR after LCLs were incubated for different times with the transcriptional inhibitor actinomycin D. Each curve represents the pooled results of three independent mRNA stability assays. Housekeeping gene; HPRT (triangles), wild type *RYR*1; AS1 (diamonds) and mutant *RYR*1; AS2 (squares). The error bars show the standard deviation.

After confirming transcriptional inhibition, the normalized ratios of the two RyR1 alleles were calculated, using Equation 4.4. Table 4.14 and 4.15 depict the results for LCL #1295 and #1333, respectively. As in muscle, in both LCLs the wild type *RYR*1 transcript (AS1) was found to be more abundant than the mutant *RYR*1 transcript (AS2). For both LCLs the ratios between the wild type and mutant *RYR*1 alleles did not seem to change after different incubation times with actinomycin D.

Table 4.14: Relative *RYR*1 transcript abundance ratios of LCL #1295 after incubation with actinomycin D

Normalized ratios	**Actinomycin D incubation time (h)**			
mean ± stdev.	**0**	**7**	**7**	**24**
Wild type *RYR*1 (CV%)	1.22±0.25 (20.70%)	1.44± 0.24 (16.83%)	1.43± 0.22 (15.17%)	1.12± 0.07 (6.24%)
Mutant *RYR*1	1.00	1.00	1.00	1.00

Stdev.= Standard deviation, CV%= coefficient of variance.

Table 4.15: Relative *RYR*1 transcript abundance ratios of LCL #1333 after incubation with actinomycin D

`

Normalized ratios	**Actinomycin D incubation time (h)**			
mean ± stdev.	**0**	**7**	**7**	**24**
Wild type *RYR*1 (CV%)	1.86±0.28 (15.21%)	1.82±0.15 (8.14%)	1.86±0.43 (23.38%)	1.67±0.17 (10.05%)
Mutant *RYR*1	1.00	1.00	1.00	1.00

Stdev.= Standard deviation, CV%= coefficient of variance.

4.4 Discussion

In this study the aim was to determine if there are allelic-specific differences in RyR1 expression levels, in heterozygous MHS samples. Allelic variations in RyR1 expression levels might provide insight into the observed variable penetrance and variations in MH phenotypes between different individuals [92-94, 106]. An allele-specific PCR assay was designed that allowed for the relative quantification of the two *RYR*1 transcripts in

heterozygous samples. The presence/absence of the H4833Y mutation in the *RYR*1 transcripts provided a suitable marker that allowed discrimination between the two alleles. Plasmid constructs, representing the wild type and mutant 4833 *RYR*1 transcripts, were used for assay validation. Four MHS skeletal muscle tissues (#470, #835, #116 and #145) were screened to determine if there were allele-specific differences in mRNA expression levels between the wild type and mutant *RYR*1. In addition, two LCLs (#1295 and #1333), derived from blood of MHS individuals, were used in mRNA stability assays to determine possible allelic-specific differences in *RYR*1 mRNA stabilities.

In order to differentiate between the two *RYR*1 transcripts, two forward allele-specific primers (AS1 & AS2) and a third common reverse primer were designed to be used in separate reactions. Primer specificities were assessed by using engineered plasmid constructs and revealed a delay of at least 10 cycles upon non-specific binding (see Figure 4.5). To test the possibility of using the designed AS-PCR protocol for relative quantification, different ratios of the engineered wild type and mutant plasmid constructs were mixed together in order to simulate heterozygotes. Results revealed accurate quantifications were possible, as the observed allele frequencies deviated by <2% compared to the theoretical allele frequencies (see Table 4.2). Relative quantification of the *RYR*1 mRNA frequencies required amplification efficiency determinations. Thus, after confirmation of reverse transcription linearity, PCR amplification efficiencies were determined. The generated standard curves were both reliable and reproducible, as amplification efficiencies lay between 1.92 and 2.10, and regression coefficients of >0.99 were obtained.

Screening of the four MHS muscle samples revealed allele specific differences in *RYR*1 mRNA expression levels (see Table 4.7). In all four samples the wild type (H4833) transcript was found to be expressed at higher levels than the mutant *RYR*1 transcript (Y4833). In three (#470, #835 & # 145) out of four samples the H4833Y MH mutation could be traced back and was found to be inherited from the mother. Interestingly, Zhou *et al*. (2006) recently reported complete silencing of the maternal RyR1 allele in association with core myopathies [105]. Intra- and inter-assay Ct value variations were

low as CV% values were between 0.12% and 3% in all cases. The slightly higher CV% values were associated with the more dilute samples. Calculations were conducted by using sample-specific amplification efficiencies. The calculated averages of the relative RyR1 allelic ratios of three independent assays led to CV% values of <17%, in all cases. These CV% values are in agreement with the observed variation in other studies [126, 127]. The higher values are the result of the fact that the Ct values are exponentially related to initial mRNA concentrations. When the detected allelic ratios were compared with data from the IVCT (see Table 4.8) no clear trend was detected. This is not unexpected as the SR calcium release is a finely regulated process that involves not only RyR1s. Several genetic and environmental factors can contribute to the observed muscle contractions in the IVCT (metabolic processes, enzyme activation, muscle composition, differences in gene expression). Furthermore, the RyR1 is comprised of four identical subunits. In each tetramer, any of the individual RyR1 subunits can be defective and thus lead/contribute to the observed variations in MH phenotypes. Only every other RyR1 tetramer is associated with a DHPR tetrad.

To assess a possible cause for the detected allelic variation in *RYR*1 mRNA expression levels, mRNA stability assays were conducted on LCL (from MHS H4833Y individuals) incubated with the transcription inhibitor actinomycin D. No myoblasts containing the H4833Y mutation were available. LCLs are progressively being used to assess the role of RyR1 mutations in calcium release [44, 45]. Possible allelic variations in RyR1 expression levels in LCLs can therefore greatly affect the functional characterization of potentially causative MH mutations. Initial optimizations for the mRNA stability assays were conducted using LCL #1051. This cell line had been previously cultured, frozen, and reactivated from liquid nitrogen for an unknown number of times. Prolonged culturing of these cell lines resulted in loss of heterozygosity, due to loss of the mutant (Y4833) RyR1 allele at both the mRNA and gDNA level. Thus, the observed loss of heterozygosity could not be explained by alterations in methylation status or random monoallelic expression, as previously reported for LCLs [128-130]. These developments however, are common problems in cell culture. As LCL are rapidly proliferating immortal cells it is not unlikely that recombination events might have led to observed loss of heterozygosity. Mitotic

recombination between two sister chromatids can lead to a cell having both normal wild type alleles and another having both mutant alleles (homozygous mutant). The cell homozygous for the wild type alleles might have a growth advantage that can lead to clonal evolution after prolonged culturing. In light of this, care should be taken when using immortalized LCLs for functional analysis of RyR1 mutations. In addition it seems prudent to store samples from early subcultures.

Consequently, two newly and never before used immortalized LCLs (#1295 and #1333) were employed for the mRNA stability assays. Experiments using these two LCLs were conducted with short culture times in order to eliminate the effects of clonal evolution. Note however, that the effects of clonal evolution on these two never before used immortalized LCL cannot be excluded completely. As for the muscle samples, linearity of the reverse transcription reactions and PCR efficiencies were determined for all three targets. PCR amplification efficiencies lay between 2.01 and 2.04, and regression coefficients of >0.99 were obtained (see Table 4.12). Intra- and inter-assay Ct value variations were very low as CV% values were <3% in all cases. Subsequently, LCLs were subsequently cultured in the absence or presence of the actinomycin D for 0, 2, 7 or 24 hours, respectively. The mRNA levels of the housekeeping gene (*HPRT*) and the *RYR*1 were found to be decreased after actinomycin D incubation by at least 57% and 86%, respectively. This was believed to be sufficient to allow for the detection of possible allele-specific differences between RyR1 mRNA stability‟s. As for skeletal muscle tissue, in each of the two LCLs (#1295 and #1333) the wild type RyR1 transcript (AS1) was found to be more abundant then the mutant RyR1 transcript (AS2; see Tables 4.14 and 4.15). In all cases, CV% values of <24% were obtained based on the calculated averages of the relative *RYR*1 allelic ratios of three independent experiments. These slightly higher CV% values were to be expected and are the consequence of lower *RYR*1 mRNA expression levels in LCLs. For both LCLs, the ratios between the wild type and mutant *RYR*1 transcripts did not change after different incubation times with actinomycin D. This suggests that there are no allele-specific differences in RyR1 mRNA stability, at least in LCLs. Allelic variation however, has been reported to be tissue specific [96, 104]. Thus, the effect of allele-specific

differences in RyR1 mRNA stabilities in H4833Y MHS skeletal muscle tissues should not be ruled out.

The data presented in this study revealed for the first time allele-specific differences in RyR1 mRNA expression levels in heterozygous MHS. Allelic variations were observed not only in skeletal muscle biopsy tissues but also in LCLs that carried the H4833Y causative MH mutation. The detected allelic variations in RyR1 expression levels can at least in part contribute to the observed variation in MH phenotypes [92-94]. Additionally, loss of heterozygosity was observed after prolonged culturing of LCLs #1051. This can have major consequences for the use of LCLs in functional characterizations. The cause of the observed allelic variations is as yet unknown. Nevertheless, the mechanism seems to be distinct from the one reported by Zhou *et al*. (2006). In that study, the maternal RyR1 allele was found to be completely silenced only in skeletal muscle. Normal, biallelic expression was observed in LCLs and skin fibroblasts. This indicated that the detected monoallelic expression was tissue-specific [105]. Conversely, the mRNA stability assays conducted in this study, suggested that the observed allelic variations were not the results of allele-specific differences in RyR1 mRNA stabilities, at least in LCL. Alternatively, the allelic variation could be the result of variations in mRNA transcription levels or mRNA maturation. Note however, that it is not necessarily the mutant RyR1 allele that is down-regulated. It is possible that the cell compensates for the defective RyR1 allele by increasing transcript levels of the wild type RyR1 allele.

5. HIGH-THROUGHPUT AMPLICON SEQUENCING

5.1 Introduction

With the introduction of high-throughput DNA sequencing the characterization of nucleic acids has taken a giant leap forward. Three major high-throughput sequencing platforms are in use today: the Genome Sequencers from Roche/454 Life Sciences (GS20 or GS FLX), the 1G Analyzer from Illumina/Solexa and the SOLiD System from Applied Biosystems. Each platform allows the rapid production of vast amounts of DNA sequencing data but differs in the chemistry and the average sequence read length and the number of DNA molecules that can be sequenced [131]. Here the aim was to use the 454/Roche GS FLX System for the determination of allele-specific differences in RyR1 mRNA expression levels.

The GS FLX System is an update of the GS20 and was developed by 454 Life Sciences, a biotechnology company based in Branford, Connecticut, USA. Using standard reagents, the machine has the capacity to perform 400,000 sequencing reads in a single run. With potential sequencing reads of 200-300 bases, the GS FLX can sequence 100 million bases per 7.5 hours in one run. With specially developed reagents these read lengths can be extended to an average length of 400 bases. With the ability to perform over 1 million reads, the maximum sequencing throughput can be expanded to 400-600 million bases per 10 hours in one run. The GS FLX System offers a range of applications, including amplicon sequencing [132], whole genome sequencing (*de novo*- and resequencing) [133], differential gene expression [134] and transcriptome studies [135] .

The Roche Genome Sequencers work on the principle of pyrosequencing [136]. This sequencing technology is based on the detection of pyrophosphates which are released on the incorporation of nucleotides by DNA polymerase. DNA sequencing using the GS FLX involves the application of new and innovative technology. The principal steps are

listed below. The first step in the process is the preparation of a DNA library. Depending on the application DNA libraries are prepared by nebulation of genomic DNA followed by adaptor ligation, or alternatively by the amplification of specific regions of the genes of interest by fusion primers that contain the adaptor tags (for amplicon sequencing). The adaptor tags enable the single-stranded DNA fragments to bind to their own unique DNA capture bead. The adaptors are used for purification, amplification and sequencing steps. After binding of the DNA, the beads are emulsified with the amplification reagents in a water-in-oil mixture. The microreactors created facilitate the clonal amplification of the single DNA molecules. This emulsion PCR (emPCR) process amplifies each fragment to a copy number of several million per bead. After the emPCR the microreactors are disrupted, DNA is made single stranded, and the DNA bound capture beads are retrieved using a biotin-labelled primer that binds to the immobilized DNA strand on the bead. Streptavidin magnetic beads are used to separate beads with and without template.

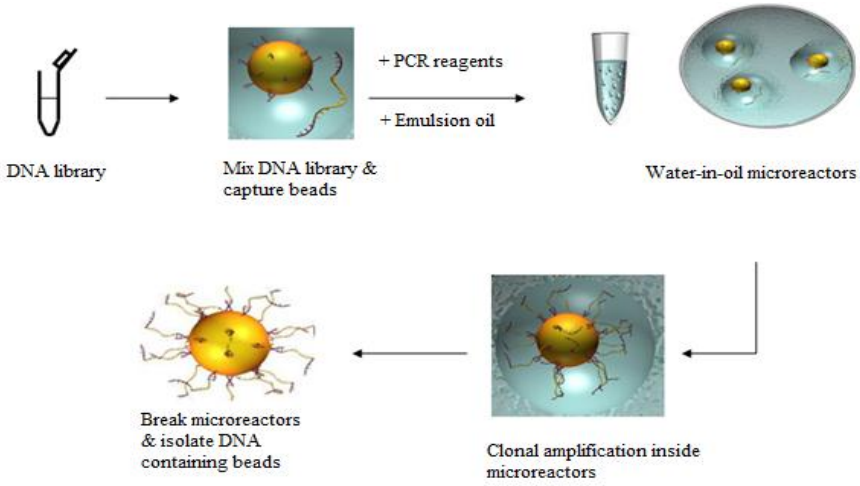

Figure 5.1: Clonal amplification of annealed DNA fragments.

After the preparation of a DNA library, adaptor tags enable single-stranded DNA fragments to bind to their own unique DNA capture bead. After binding of the DNA, the beads are emulsified with the amplification reagents in a water-in-oil mixture. The microreactors created, facilitate the clonal amplification of the single DNA molecules (emPCR). After the emPCR the microreactors are disrupted, DNA is made single-stranded, and the DNA-bound capture beads are retrieved using a biotin labelled primer that binds to the immobilized DNA strand on the bead. Streptavidin magnetic beads are used to separate beads with and without template. Figures were adapted from Margulies et al. (2005) [137].

The single strand template DNA (sstDNA) library beads are added to DNA Bead Incubation Mix (containing DNA polymerase) and are layered with enzyme beads (containing sulfurylase and luciferase) onto a PicoTiterPlate device. The device is centrifuged to deposit the beads into the wells. The layer of enzyme beads ensures that the DNA beads remain positioned in the wells during the sequencing reaction. Each well is large enough for just one bead.

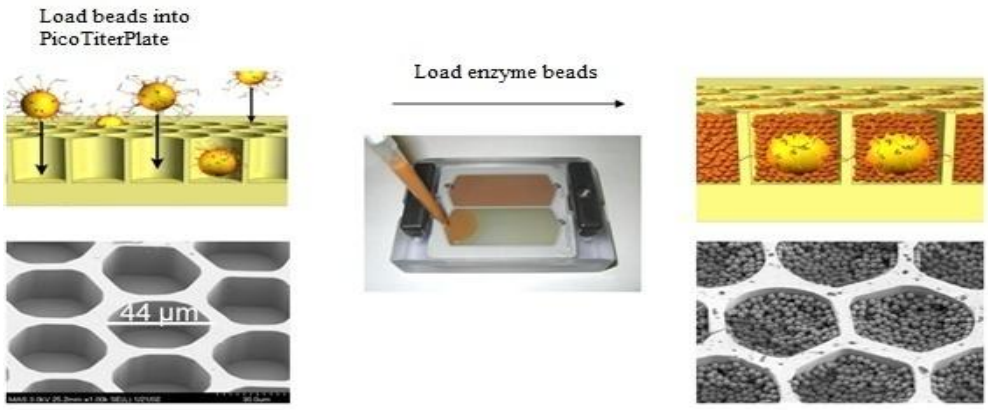

Figure 5.2: Bead deposition into PicoTiterPlate.

Beads carrying single-stranded DNA clones are deposited into wells of a fibre optic slide. Smaller beads carrying immobilized enzymes required for pyrophosphate sequencing are layered on top. Bottom left and right shows SEM photographs of portions of a picotiter sequencing plate prior to and after bead deposition into the wells, respectively. Figures were adapted from Margulies et al. (2005) [137].

The loaded PicoTiterPlate device is placed into the GS FLX Instrument. The GS FLX uses sequencing-by-synthesis. During the nucleotide flow, millions of copies of DNA bound to each of the beads are sequenced in parallel. When a nucleotide complementary to the template strand is added into a well, the polymerase extends the existing DNA strand by adding nucleotide(s). The incorporation of the correct dNTP releases pyrophosphate (PPi) in a quantity equimolar to the amount of incorporated nucleotide. ATP sulfurylase quantitatively converts PPi to ATP in the presence of adenosine 5′ phosphosulfate (APS). This ATP drives the luciferase-mediated conversion of luciferin to oxyluciferin that generates visible light (which is recorded by the CCD camera in the instrument) in amounts that are proportional to the amount of ATP. Thus the signal strength is proportional to the number of nucleotides. Deoxyadenosine alfa-thio

triphosphate is used as a substitute for the natural deoxyadenosine triphosphate since it is efficiently used by the DNA polymerase, but not recognized by the luciferase.

Post-sequencing GS FLX data processing comprises of several complete software packages, for mapping, assembly, and amplicon variation detection. These post sequencing data analysis applications are carried out separately and are supported via a graphical user interface (GUI) or at the command line level using a command line interface (CLI).

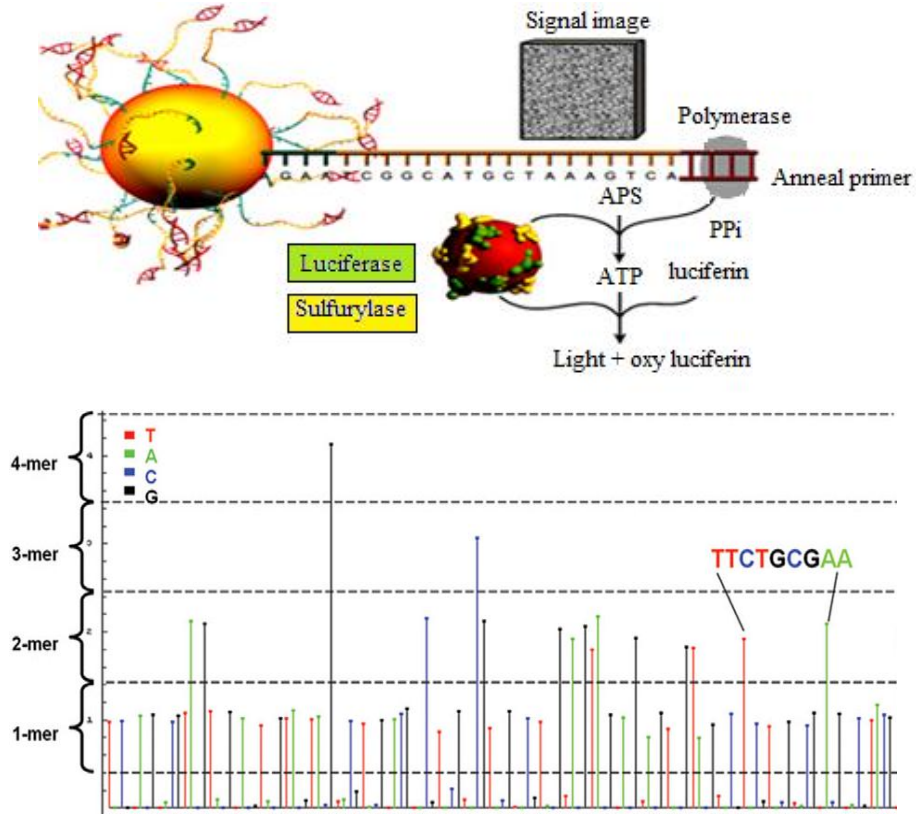

Figure 5.3: Sequencing-by-synthesis.

The top figure shows a schematic overview of the pyrosequencing principle as performed by the GS FLX. Each dNTP is repeatedly flowed across the growing DNA strand. When incorporation of the correct dNTP occurs, a cascade reaction is triggered resulting in the emission of light. The bottom graph depicts an example of a raw flowgram generated from an individual read. The relative luminescence signal (y-axis) is plotted against each sequentially flowed nucleotide (x-axis). Nucleotides are flowed in the order T, A,C, G. The signal strength is proportional to the number of nucleotides. Part of the detected sequence is shown in the inset. The first four bases (T, C, A, G) constitute the "key" sequence and is used for identifying wells and calibration. Figures were adapted from www.roche-applied-science.com.

Several studies have recently employed high-throughput amplicon sequencing as a tool for mutation detection as well as a technique that allows for quantitative SNP frequency determinations [138, 139]. Thus, in this study the aim was to use high-throughput amplicon sequencing for the accurate quantification of the T4826I and H4833Y transcripts in heterozygous MHS samples. The four H4833Y samples that were previously analysed by the allele-specific PCR assay described chapter four were also analysed by high-throughput amplicon sequencing. This allowed for comparisons between the two experimental strategies that were employed to determine the allele-specific RyR1 expression levels in heterozygous MHS samples that contained the causative H4833Y MH mutation.

A DNA bar coding system similar to the one described by Hoffmann *et al*. (2007) was designed to allow multiplex analysis of multiple samples [139]. Initially, a DNA library consisting of ten samples was analysed by high-throughput amplicon sequencing. This library was made up of four H4833Y samples (#835, #470, #116, and #145) and six T4826I samples (# 541, #289, #323, #255, #109, and #300). As the results generated from the four H4833Y samples did not match the results obtained from the designed allele-specific PCR assay, some discussion was prompted regarding correct sample preparation and assay reliability. Therefore, a second set of seven samples was prepared accordingly, and sequenced. This DNA library was made up of again four H4833Y samples (#835, #470, #116 and #145), two T4826I samples (#289 and #323) and one control. The control was included to validate the applicability and accuracy of the high-throughput amplicon sequencing approach for the determination of allele-specific differences in expression levels in heterozygous samples. Both DNA libraries were sequenced on a 1/16 region of a PicoTiterPlate, using the GS FLX. On average this should yield about 12,000 sequence reads.

5.2 Assay design

5.2.1 Bar coded fusion primers

In this study high-throughput amplicon sequencing was conducted on two DNA libraries that were constructed by pooling initially ten and then seven different purified cDNA PCR products. This was made possible by amplifying individual samples with unique bar coded fusion primer pairs. Figure 5.4 shows a schematic representation of an amplification product generated by the bar coded fusion primer amplification.

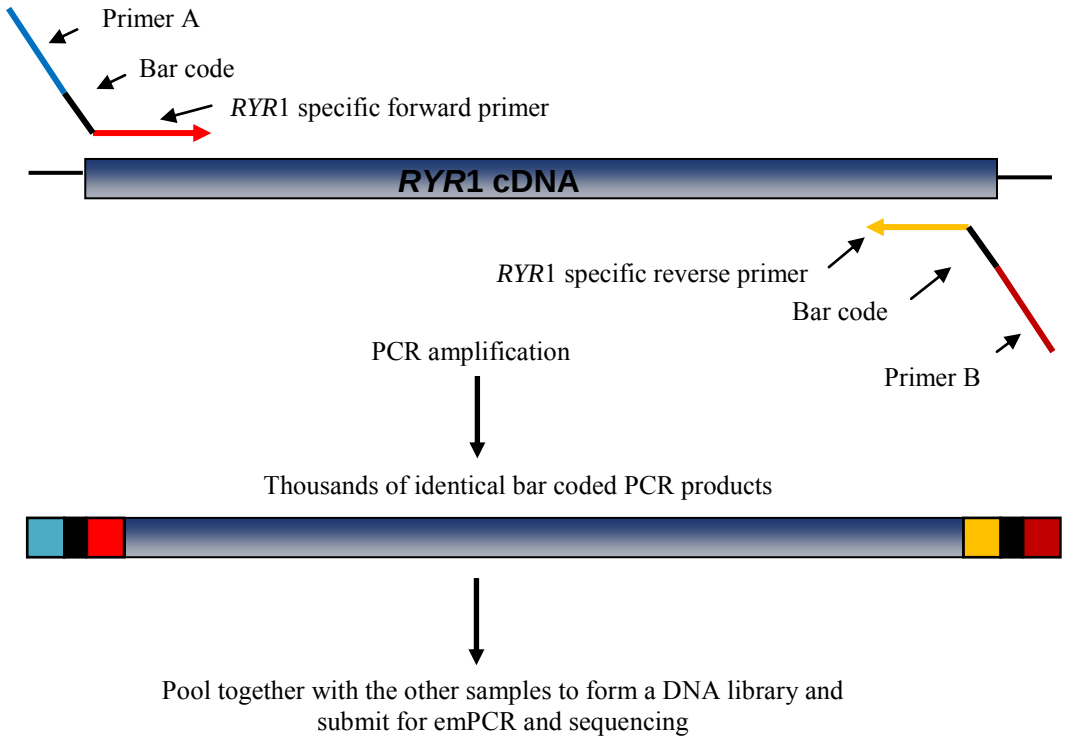

Figure 5.4: Schematic representation of a PCR product generated by the amplification using bar coded fusion primers.

The amplification with bar coded fusion primers allows pooling of multiple DNA samples for high-throughput amplicon sequencing as individual DNA sequences can be traced back to their source by the attached bar code.

The bar coded fusion primers were each 43 bp long and consist of: (i) a 19 bp 454 adaptor sequence on the 5‟-end (Primer A or Primer B) that match the other components of the Genome Sequencing System, (ii) a 4 bp barcode sequence that was used to trace

each DNA sequence back to its source, and (iii) a 20 bp *RYR1* specific sequence (3' end). Tables 5.1 and 5.2 list the bar coded fusion primer pairs used in this study, together with their individual amplification templates. Each bar coded fusion primer pair generates an amplicon of 240 bp in size. Barcodes containing adjacent identical nucleotides were avoided as the 454 sequencing method has an increased error rate at positions of adjacent nucleotides of the same type (homopolymers).

Table 5.1: Ten sample DNA library and the bar coded fusion primers used

Muscle sample # (mutation)	**Orientation**	**Sequence (5'-> 3')**
835	Fw.	**GCCTCCCTCGCGCCATCAG**ACTG*TTCTTCTTTGCTGCCCATCT*
(H4833Y)	Rev.	**GCCTTGCCAGCCCGCTCAG**ACTG*TCATCCTCATCCTCGCTCTT*
470	Fw.	**GCCTCCCTCGCGCCATCAG**CGAC*TTCTTCTTTGCTGCCCATCT*
(H4833Y)	Rev.	**GCCTTGCCAGCCCGCTCAG**CGAC*TCATCCTCATCCTCGCTCTT*
116	Fw.	**GCCTCCCTCGCGCCATCAG**CGTA*TTCTTCTTTGCTGCCCATCT*
(H4833Y)	Rev.	**GCCTTGCCAGCCCGCTCAG**CGTA*TCATCCTCATCCTCGCTCTT*
145	Fw.	**GCCTCCCTCGCGCCATCAG**TCAG*TTCTTCTTTGCTGCCCATCT*
(H4833Y)	Rev.	**GCCTTGCCAGCCCGCTCAG**TCAG*TCATCCTCATCCTCGCTCTT*
289	Fw.	**GCCTCCCTCGCGCCATCAG**CTGA*TTCTTCTTTGCTGCCCATCT*
(T4826I)	Rev.	**GCCTTGCCAGCCCGCTCAG**CTGA*TCATCCTCATCCTCGCTCTT*
323	Fw.	**GCCTCCCTCGCGCCATCAG**TACG*TTCTTCTTTGCTGCCCATCT*
(T4826I)	Rev.	**GCCTTGCCAGCCCGCTCAG**TACG*TCATCCTCATCCTCGCTCTT*
109	Fw.	**GCCTCCCTCGCGCCATCAG**ACGA*TTCTTCTTTGCTGCCCATCT*
(T4826I)	Rev.	**GCCTTGCCAGCCCGCTCAG**ACGA*TCATCCTCATCCTCGCTCTT*
541	Fw.	**GCCTCCCTCGCGCCATCAG**AGCA*TTCTTCTTTGCTGCCCATCT*
(T4826I)	Rev.	**GCCTTGCCAGCCCGCTCAG**AGCA*TCATCCTCATCCTCGCTCTT*
300	Fw.	**GCCTCCCTCGCGCCATCAG**TGCA*TTCTTCTTTGCTGCCCATCT*
(T4826I)	Rev.	**GCCTTGCCAGCCCGCTCAG**TGCA*TCATCCTCATCCTCGCTCTT*
255	Fw.	**GCCTCCCTCGCGCCATCAG**AGTC*TTCTTCTTTGCTGCCCATCT*
(T4826I)	Rev.	**GCCTTGCCAGCCCGCTCAG**AGTC*TCATCCTCATCCTCGCTCTT*

Primer A and B adaptor sequences are depicted in bold and attached to the 5''-ends of the forward and reverse primers, respectively. The 4 bp bar code sequences are underlined. *RYR1* specific forward and reverse primers are depicted in italics.

Table 5.2: Seven sample DNA library and the bar coded fusion primers used

Muscle sample # (mutation)	Orientation	Sequence (5'-> 3')
835 (H4833Y)	Fw.	**GCCTCCCTCGCGCCATCAG**ACTG*TTCTTCTTTGCTGCCCATCT*
	Rev.	**GCCTTGCCAGCCCGCTCAG**ACTG*TCATCCTCATCCTCGCTCTT*
470 (H4833Y)	Fw.	**GCCTCCCTCGCGCCATCAG**CGAC*TTCTTCTTTGCTGCCCATCT*
	Rev.	**GCCTTGCCAGCCCGCTCAG**CGAC*TCATCCTCATCCTCGCTCTT*
116 (H4833Y)	Fw.	**GCCTCCCTCGCGCCATCAG**CGTA*TTCTTCTTTGCTGCCCATCT*
	Rev.	**GCCTTGCCAGCCCGCTCAG**CGTA*TCATCCTCATCCTCGCTCTT*
145 (H4833Y)	Fw.	**GCCTCCCTCGCGCCATCAG**TCAG*TTCTTCTTTGCTGCCCATCT*
	Rev.	**GCCTTGCCAGCCCGCTCAG**TCAG*TCATCCTCATCCTCGCTCTT*
289 (T4826I)	Fw.	**GCCTCCCTCGCGCCATCAG**AGCA*TTCTTCTTTGCTGCCCATCT*
	Rev.	**GCCTTGCCAGCCCGCTCAG**AGCA*TCATCCTCATCCTCGCTCTT*
323 (T4826I)	Fw.	**GCCTCCCTCGCGCCATCAG**ACGA*TTCTTCTTTGCTGCCCATCT*
	Rev.	**GCCTTGCCAGCCCGCTCAG**ACGA*TCATCCTCATCCTCGCTCTT*
Control (H4833Y)	Fw.	**GCCTCCCTCGCGCCATCAG**AGTC*TTCTTCTTTGCTGCCCATCT*
	Rev.	**GCCTTGCCAGCCCGCTCAG**AGTC*TCATCCTCATCCTCGCTCTT*

Primer A and B adaptor sequences are depicted in bold and attached to the 5‟-ends of the forward and reverse primers, respectively. The 4 bp bar code sequences are underlined. *RYR1* specific forward and reverse primers are depicted in italics.

5.2.2 DNA samples

5.2.2.1 Ten sample DNA library

Initially amplicons prepared from cDNA for ten different muscle tissues were pooled together and screened. cDNA from each tissue sample was synthesised from DNase-treated total RNA, as described in 2.2.8-2.2.10. Four samples contained the H4833Y causative MH mutation (#835, #470, #116 and # 145) and six samples contained the the T4826I causative MH mutation (# 541, #289, #323, #255, #109, and #300). See Table 5.1.

5.2.2.2 Seven sample DNA library

A second DNA library was constructed and screened by pooling together amplicons prepared from cDNAs for six different muscle tissues, and one control. cDNA from each tissue sample was synthesised from DNase-treated total RNA, as described in 2.2.8-2.2.10. Four samples contained the SNP that causes the H4833Y amino acid mutation (#835, #470, #116 and # 145) and two samples contained the SNP that causes the T4826I amino acid mutation (#289 and #323). The control was included for assay validation and constructed by mixing purified *RYR1* wild type and mutant PCR products in a 3:1 ratio (see Table 5.2).

5.2.3 PCR conditions and sample preparation

5.2.3.1 Ten sample DNA library

PCRs were performed as described in chapter 2.2.2., except the annealing temperatures were 55ºC and the extension temperatures were 20 seconds. To ensure reproducible and specific amplification, 5 µL of each PCR product was visualized on 1% agarose gels stained with ethidium bromide. PCR products were purified directly and eluted in 25 µL MQ water using the Wizard® SV Gel and PCR Clean-Up System. The DNA concentrations were measured by absorbance at 260 nm using the Nanodrop spectrophotometer (Nanodrop Technologies). Subsequently, the DNA library was constructed by diluting and pooling the samples together in equimolar concentrations.

5.2.3.2 Seven sample DNA library

PCRs were performed as described in chapter 2.2.2., except the annealing temperatures were 55ºC and the extension temperatures were 20 seconds. To ensure PCR products were not over amplified, a three step 1:4 dilution series (1, 0.25 and 0.0625) of the seven templates for PCR was made. After amplification, 5 µL of the PCR products were visualized on 1% agarose gels stained with ethidium bromide. PCR products that yielded the lowest, but still detectable signals were excised from the gel using the Wizard® SV Gel and PCR Clean-Up System. Purified PCR products were eluted off the column in 30 µL MQ water. The DNA concentrations were measured using the Qubit™

fluorometer and the Quant-iT™ dsDNA HS Assay Kit. Subsequently, the DNA library was constructed by diluting and pooling the seven samples together in equimolar concentrations.

5.3 Results

The development of bar coded fusion primers allowed the pooling of multiple samples into a DNA library. The DNA libraries were then submitted for high-throughput amplicon sequencing for the quantification of the T4826I and H4833Y transcripts in heterozygous MHS samples. Bar coded fusion primers were designed for amplification of the cDNA C-terminal region of the RyR1. Primers were chosen so that all the H4833Y and T4826I transcripts could be amplified and sequenced at the same time. Each individual sample was amplified with its own unique bar coded fusion primer pair (see Tables 5.1 and 5.2). This allows for each DNA sequence to be traced back to its source.

5.3.1 Ten sample DNA library

5.3.1.1 Library preparation

Initially, a DNA library consisting of ten samples was submitted for high-throughput amplicon sequencing. The ten PCR products that made up the DNA library were generated by the amplification of the cDNA templates. After amplification 5 µL of the PCR products were visualized on 1% agarose gels stained with ethidium bromide. Figure 5.5 shows two specific 240 bp products generated by the amplification of samples #255 and #109 with their bar coded fusion primers, and is indicative of the amplicons produced for each template.

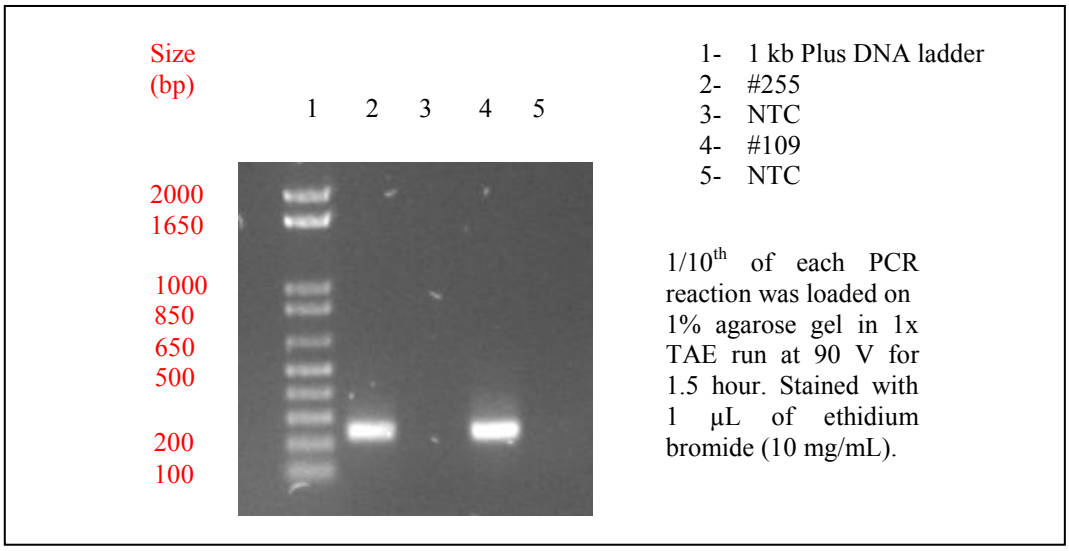

Figure 5.5: Visualizing the amplified products used for library preparation.

For all ten products, (four H4833Y samples: #835, #470, #116 and # 145 and six T4826I sampes: # 541, #289, #323, #255, #109, and #300) single bands of the correct size were present. The remaining PCR products were purified directly using the Wizard® SV Gel and PCR Clean-Up System and DNA concentrations were determined by A_{260} measurements using the Nanodrop spectrophotometer (Nanodrop Technologies). All ten purified samples had similar DNA concentrations of ~80 ng/µL. The DNA library was constructed by diluting and pooling the samples together in equimolar concentrations of 30 ng/µL. 20 µL of each sample was used to construct the DNA library. The constructed DNA library was send to the Department of Anatomy and Structural Biology, University of Otago, Dunedin, New Zealand for emPCR and amplicon sequencing. After sequencing, staff of Otago University resolved the generated reads into separated data bins according to their 4 bp barcode sequences, and placed the sequences on a server to allow data analysis at Massey University.

5.3.1.2 Data analysis

Data analysis was performed using the Amplicon Variant Analyser Command Line Interface (AVA-CLI). For more information see the Genome Sequences FLX Data Analysis Software Manual. The different steps necessary for data analysis using the AVA-CLI are described in detail in Appendix V.

5.3.1.3 Detected mutation frequencies

The T4826I and H4833Y cDNA allele frequencies were determined one by one as described in Appendix V, for all ten muscle samples that were in the DNA library. The output files of the ten samples are included in Appendix VI-A. In the output file the detected Variants are displayed in two ways: Consensus and Individual reads (see Appendix VI-A). The Consensus is a collapsed representation of multiple similar reads. Its intention is to simplify the data and eliminate noise. The Individual reads represents every sequence read that is directly extracted from the Read Data Set. Delving into the individual reads can be useful to search for a particular variation that may have been erroneously spread amongst several consensi and treated as noise in base calling, rather than being exposed as a separate variation. In this study the focus simply lay on the detection of the two defined variants (H4833Y and T4826I). Thus, no in depth analyses to detect rare sequence variants were conducted. Both Consensus and Individual reads reinforce one another, as they were in close agreement. Table 5.3 depicts a summary of the detected H4833Y and T4826I SNP frequencies as reported using the Individual Read Type. Allele frequencies were determined by dividing the number of reads with the detected mutation (Forward Hits) by the total number of reads (Forward Denom).

Table 5.3: Detected SNP frequencies of the ten sample DNA library

Muscle sample #	Mutation	Bar code	Reads with mutation	Total number of reads	% mutant	% wild type
835	H4833Y	ACTG	1788	3677	48.6	51.4
470	H4833Y	CGAC	762	1564	48.7	51.3
116	H4833Y	CGTA	0	0	-	-
145	H4833Y	TCAG	1059	2085	50.8	49.2
289	T4826I	CTGA	168	348	48.3	51.7
323	T4826I	TACG	525	1097	47.9	52.1
109	T4826I	ACGA	903	2166	41.7	58.3
541	T4826I	AGCA	593	1189	49.9	50.1
300	T4826I	TGCA	1024	2088	49.0	51.0
255	T4826I	AGTC	794	1732	45.8	54.2
Total number of reads included in the analysis				**15946**		

No sequences were obtained for sample #116. A total of 471 sequences could not be matched, due to incomplete bar codes. Due to the AGCA and ACGA bar codes, sample #541 and #109 were only fully analysed after the seven DNA sample library was sequenced (see Appendix VI-A).

In total 15,946 sequence reads were included in the analyses. As shown in Table 5.3, reliable bar coded sequences were obtained from nine out of the ten samples. No sequences were obtained for sample #116 (CGTA). 117 sequences (0.9%) could not be matched due to incomplete bar codes or sequences. The final results revealed a variation in the sequence distributions between the pooled PCR products (348 to 3677 sequences). The detected H4833Y and T4826I SNP frequencies of all samples were about 50%. Note that, due to the AGCA and ACGA bar codes (see Appendix VI-A), samples #541 and #109, respectively, could only be fully analysed after the seven DNA sample library was sequenced (see below). In sample #109 however, the I4826 mutation was detected in 41.7% of the sequences screened. Besides the defined variants (T4826I and H4833Y) up to five additional variants were also detected, at low frequencies (<1.5%). Analysis of sample #541 on the other hand, revealed the presence of 21 variants. Additionally, it was found that H4833Y samples also contained T4826I SNPs, and *vice versa*.

The relative amounts of the two RyR1 transcripts in H4833Y muscle samples listed in Table 5.3 were compared with the relative amounts that were observed using the designed AS PCR assay (see chapter 4). As depicted in Table 5.4, the two quantification strategies did not generate the same results. The AS PCR assays reported that the wild type allele (H4883) was more abundant than the mutant *RYR*1 transcript (Y4833). The data shown obtained by high-throughput amplicon sequencing revealed an even distribution of the two alleles. A possible explanation for the observed discordance may have been because the amplicons had been over amplified prior to the construction of the DNA library.

Table 5.4: Comparison of the detected RyR1 expression levels using high-throughput sequencing or allele-specific PCR

Muscle sample #	**High-throughput amplicon sequencing**		**Allele-specific PCR assay**	
	% mutant	**% wild type**	**% mutant**	**% wild type**
835	48.6	51.4	36.8	63.2
470	48.7	51.3	36.2	63.8
116	-	-	41.0	59.0
145	50.8	49.2	29.1	70.9

The WT:MT RyR1 ratios listed in chapter four were converted to percentages to enable clearer comparisons between the two strategies employed to determine allelic variations between RyR1 expression levels in heterozygous H4933Y MHS skeletal muscle samples.

The observed discrepancies led initially to the development of a H4833Y gDNA AS-PCR assay. As gDNA should produce a 1:1 ratio of wild type to mutant allele, this assay could be used as a control to test the AS-PCR assay. In order to do so only a common intronic reverse primer needed to be designed. Both allele-specific primers (AS1 & AS2; see chapter 4) were then to be used with the intronic reverse primer in separate PCR reactions. If this assay would show an equal distribution of the two *RYR*1 alleles in heterozygous gDNA samples, it would provide support for the results produced from the AS-PCR assay. Several reverse intronic primers were tested. However, all led to either secondary product formation or poor amplification efficiencies. As a result, a second set of samples was sent for high-throughput amplicon

sequencing. This time six muscle samples and one control were included in the DNA library. The control was included to validate the applicability and accuracy of the high-throughput amplicon sequencing approach for allele frequency determinations (see section 5.2.3).

5.3.2 Seven sample DNA library

5.3.2.1 Library preparation

A second set of seven samples was sequenced. The DNA library was made up of four H4833Y samples (#835, #470, #116 and #145), two T4826I samples (#289 and #323), and one control that was used for assay validation. In order to eliminate possible unreliable results due to over amplification during PCRs, a three step 1:4 dilution series (1, 0.25 and 0.0625) of the individual cDNA templates was made. All three PCRs were amplified simultaneously. Figure 5.6 shows the three 240 bp PCR products generated by the amplification of sample #289 with its bar coded fusion primers. A clear decrease in band intensity over the three step dilution series suggests that the products with the more dilute templates (0.25 and 0.0625) have not been over amplified. The PCR products that yielded the lowest but still detectable signals on gel were excised from gel, using the Wizard® SV Gel and PCR Clean-Up System. In total six purified PCR products were excised from gel: four H4833Y cDNA transcripts (#835, #470, #145 and #116), and two T4826I cDNA transcripts (#289 and #323). The 0.0625x product was gel purified for the #289 sample shown below.

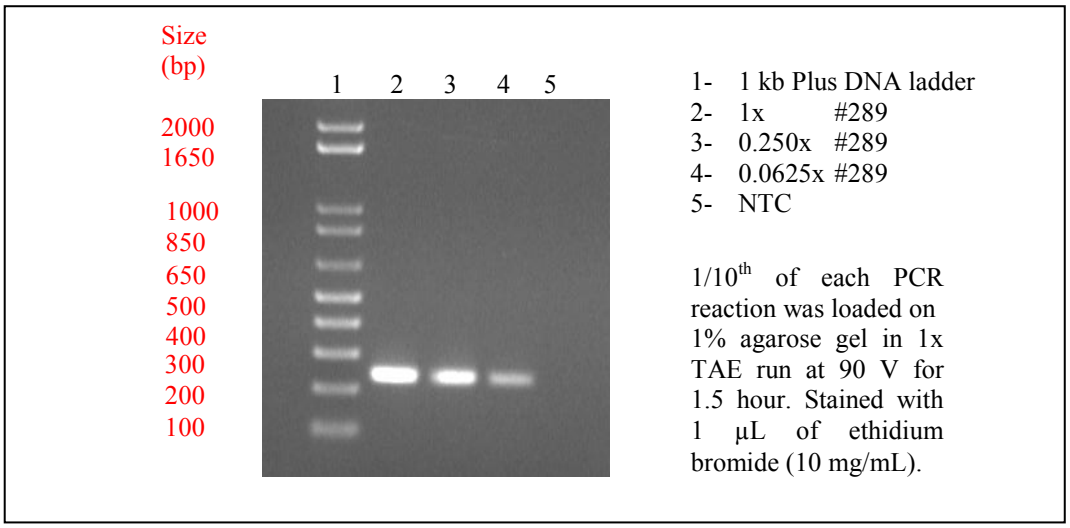

Figure 5.6: Visualizing the amplified products from serially diluted template used for library preparation.

The control was constructed by mixing purified *RYR1* wild type and mutant PCR products in a known ratio. These purified PCR products were generated by the amplification of small regions of the wild type (H4833) and mutant RyR1 (Y4833) cDNA sequences from engineered plasmid constructs (see chapter 4). Forward and reverse fusion bar coded primer sequences were used for these amplifications (see Table 5.2). After the amplification, 5 µL of the generated PCR products were analysed by electrophoresis on 1% agarose gel (see Figure 5.7). A single band of the expected size of 240 bp was visible. PCR products were purified directly using the Wizard® SV Gel and PCR Clean-Up System.

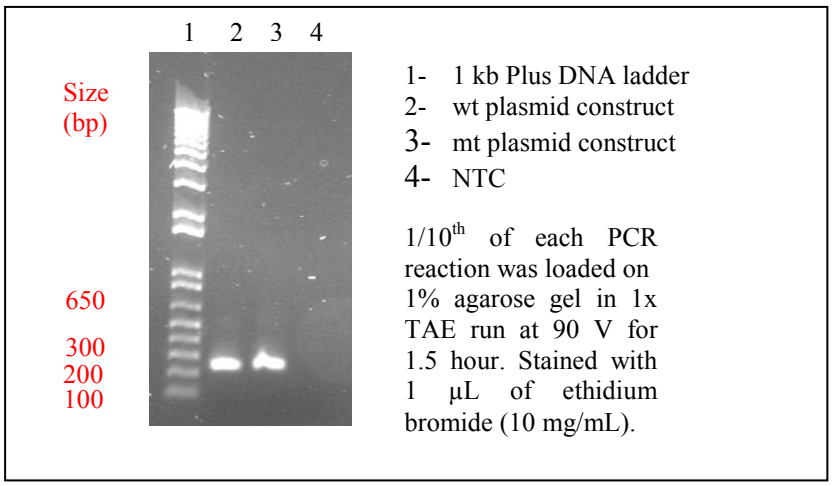

Figure 5.7: Visualizing cDNA PCR products generated for allele frequency determination control.

Concentrations of both wild type and mutant amplicons were determined using the Qubit fluorometer and the Quant-iT™ dsDNA HS Assay Kit. This was done because A_{260} measurements tend to be less reliable than fluorescence measurements at lower DNA concentrations. The DNA concentrations were found to be very similar at 19.62 ng/µL and 19.30 ng/µL for the wild type and mutant 4833 purified PCR products, respectively. The purified PCR products were mixed together in three different WT:MT ratios (1:1, 4:1 and 3:1), and subsequently verified using the designed AS-PCR assay described in chapter 4. The average of the three Ct values was used to calculate the allele frequencies of the wild type and mutant alleles by using Equation 5.1 (see below). To demonstrate the accuracy of the Qubit DNA measurements the 4:1 and 3:1 ratios weren"t corrected for by the 1:1 ratio as described previously (see chapter 4). As shown in Table 5.5 the observed percentages match the theoretical percentages with an error of less than 4%. The 1:1 ratio demonstrated that the percentages of the purified wild type and mutant PCR products were 46.6 and 53.4 %, respectively. This was in good agreement with the Qubit measurements which suggested DNA concentrations of both purified PCR products were alike. The theoretical wild type and mutant allele percentages should therefore both be 50%. After confirming the allele percentages in the three premixed samples, one sample (3:1) was prepared to be included in the DNA library and submitted for high-throughput amplicon sequencing. A three step 1:4 dilution series (1, 0.25 and 0.0625) of the 3:1 template was made to eliminate over amplification during PCR. All three PCRs were amplified simultaneously using the same unique bar coded fusion primers. The PCR product that yielded the lowest but still detectable signal on 1% agarose gel (as in Figure 5.6) was excised from gel using the Wizard® SV Gel and PCR Clean-Up System.

Table 5.5: Relative allele frequencies using purified PCR products

Ratio (WT:MT)		Ct values			Percentage (%)	
		Mean (n=3)	**Stdev.**	**ΔCt**	**Theor.**	**Obser.**
1:1	AS1	26.65	0.16	0.20	50.00	46.60
	AS2	26.45	0.23	-0.20	50.00	53.40
4:1	AS1	25.98	0.27	-2.06	80.00	80.62
	AS2	28.04	0.12	2.06	20.00	19.83
3:1	AS1	26.17	0.16	-1.38	75.00	72.29
	AS2	27.56	0.27	1.38	25.00	27.71

Stdev.= Standard deviation, Theor.= theorectical values, Obser.= experimentally observed values.

As the WT & MT purified PCR products concentrations were found to be alike, it can be assumed that the ΔCt values for the 1:1 ratio will be equal to zero. Any deviation is most likely to originate from differences in AS1 and AS2 primer amplification efficiencies.

Equation 5.1

$$\text{Frequency of allele}_1 = 1 / (2^{\Delta Ct} + 1)$$

$$\Delta Ct = (\text{Ct of allele}_1 \text{ specific PCR} - \text{Ct of allele}_2 \text{ specific PCR})$$

As a result of trying to eliminate over amplification during PCR, fewer amplicons were available for purification. As this might increase noise due to possible interferences from secondary products or primer-dimers during sequencing, gel purification was performed rather than the less laborious PCR clean ups. Note that, no unspecific products were visible on the agarose gel. As expected, significantly lower DNA concentrations were attained after gel purification. UV exposures could lead to sequence alterations, and were therefore were kept to a minimum. All seven purified samples had DNA concentrations of >8 ng/µL. Thus, the DNA concentrations of all samples (#835, #470, #116, #145, #289, #323) were measured using the Qubit™ fluorometer with the Quant-iT™ dsDNA HS Assay Kit. Accurate DNA concentrations for equimolar pooling are a key factor in obtaining an even distribution of the pooled products in the final sequencing results. The seven purified PCR products were pooled together in equimolar concentrations of 1.12 ng/µL. 17 µL of each sample was used to construct the DNA library. The constructed DNA library was send to the Department of Anatomy and

Structural Biology, University of Otago in Dunedin, New Zealand for emPCR and amplicon sequencing. After sequencing, staff of Otago University resolved the generated reads into separated data bins according to their 4 bp barcode sequences, and placed on the sequences on the server to allow data analysis.

5.3.2.2 Data analysis

Data analysis for the seven samples DNA library was performed one by one using the AVA-CLI, as described in Appendix V. The output files of the seven samples are included in Appendix VI-B. A summary of the results is listed in section 5.3.2.3.

5.3.2.3 Detected mutation frequencies

Table 5.6 depicts a summary of the detected H4833Y and T4826I SNP frequencies as reported using the Individual Read Type.

Table 5.6: Detected SNP frequencies of the seven sample DNA library

Muscle sample #	**Mutation**	**Bar code**	**Reads with mutation**	**Total number of reads**	**% mutant**	**% wild type**
835	H4833Y	ACGT	611	1302	46.9	53.1
470	H4833Y	CGAC	660	1389	47.5	52.5
116	H4833Y	CGTA	793	1608	49.3	50.7
145	H4833Y	TCAG	26	62	41.9	58.1
289	T4826I	AGCA	653	1345	48.6	51.4
323	T4826I	ACGA	602	1328	45.3	54.7
Control (3:1)	H4833Y	AGTC	1204	2671	45.1	54.9
Total number of reads included in the analysis				**9705**		

3584 sequences could not be matched, due to incomplete bar codes. Due to the AGCA and ACGA bar codes, samples #289 and 323 were analyzed in a slightly different way (see Appendix VI-B).

Reliable bar coded sequences were obtained for all seven samples. However, only 9705 (73%) sequence reads were included in the analysis. With the exception of sample #145, the results revealed a relatively even sequence distribution between the pooled products. Due to the AGCA and ACGA bar codes, samples #289 and 323 were analyzed in a

slightly different way, respectively (see Appendix VI-B). A total of 3584 sequences (~27%) could not be matched due to incomplete bar codes or sequences. Interestingly, the detected H4833Y and T4826I SNP frequencies of all samples were about 50%. This included the control, which was constructed and proven to have a 3:1 ratio of the wild type (H4833) versus the mutant (Y4833) *RYR*1 allele. This ratio was not detected after the samples were prepared, pooled together and submitted for high-throughput amplicon sequencing, despite the fact that care was taken not to over amplify the products during PCR. As before, both defined SNPs (T4826I and H4833Y) and additional low abundance variants (frequency ≤2.1%) were detected. Both samples #289 and the 3:1 control contained >10 additional variants (see Appendix VI-B). Additionally, it was found that H4833Y samples also contained T4826I SNPs, and *vice versa*.

5.4 Discussion

Ever since first being described by Margulies *et al*., 454-pyrosequencing has been used for a range of applications [137]. These include, amplicon sequencing [132], whole genome sequencing (*de novo*- and resequencing) [133], gene expression [134] and transcriptome studies [135]. Amplicon sequencing has been used in several studies as a tool that allows SNP detection as well as a technique that allows for quantitative SNP frequency determinations [138, 139]. More recently, amplicon sequencing has been used to measure allelic imbalances associated with heterozygous micro-RNA target sites [140].

This study aimed to use high-throughput amplicon sequencing for the accurate quantification of the T4826I and H4833Y causative MH mutations in heterozygous MHS samples. The design of a DNA bar coding system, similar to the one described by Hoffmann *et al*. (2007) was used to allow multiplex analysis of multiple samples [139]. Four H4833Y samples that were previously analysed by the designed allele-specific PCR assay were included (see chapter four). This allowed for comparisons between the two experimental strategies that were employed to determine the allele-specific *RYR*1 mRNA expression levels in heterozygous MHS samples that contained the causative H4833Y MH mutation.

Initially, a DNA library consisting of ten samples was submitted for high-throughput amplicon sequencing. This library was made up of four H4833Y samples (#835, #470, #116, and #145) and six T4826I samples (# 541, #289, #323, #255, #109, and #300). Reliable bar coded sequences were obtained from nine out of the ten samples. No sequences were obtained for sample #116 (CGTA). 117 sequences (0.9%) could not be matched due to incomplete bar codes or sequences. Missing or imperfect sequences may have been the result of incorrect primer syntheses, reverse transcriptions or amplification and sequencing errors. In total 15,946 sequence reads were included in the analyses (Table 5.3). Despite equimolar pooling, analysis of the 15,946 sequence reads revealed a variation in the sequence distribution between the pooled products. Some of this variation might be the results of inaccurate DNA concentrations measurements by A_{260}. Nevertheless, some sequence-specific differences in efficiency of fidelity of sequencing might also occur, as no sequence reads were obtained for sample #116. The H4833Y and T4826I mutation frequencies detected for all samples were about 50%. In sample #109 however, the I4826 mutation was detected in 41.7% of the sequences screened. Additional variants were also detected but only at very low frequencies (<1.5%). These were most likely due to the error rates of the polymerases used in the reverse transcription, PCR amplification and emPCR steps. Sample #541 contained markedly more of these low abundance variants compared to the other 8 samples (see Appendix V-A). It is hard to predict if these are the result of amplification errors, or alternatively possible contamination problems. Possible contamination problems were taken into consideration. All reverse transcription and PCR reactions were setup in a PCR cabinet. NO-RT controls were conducted for the four H4833Y samples, as they were previously used for AS PCR. As no contamination problems were ever observed, additional NO-RT controls were not conducted on the other samples. Additionally, NTC reactions were conducted each time a PCR was performed. The most important problem limitations of mutation detection using picotiter plate sequencing lies in its extreme sensitivity [132]. Therefore, any contamination with DNA from another sample, with PCR products or plasmid constructs carrying cDNAs of the gene that is being sequenced will be represented as a fraction of all alleles in the final analysis. This was illustrated by the fact that H4833Y samples also contained T4826I SNPs, and *vice versa*. Multiple mutations in the bar codes would have been needed for inter-sample

cross-over to occur. These results suggested that there might have been some minor contamination issues. Nevertheless, both the T4826I and H4833Y mutations greatly outnumber these low abundance variants. Thus, it is not likely that these variants will have major effects on the detected T4826I and H4833Y mutation frequencies.

The AS-PCR and the high-throughput amplicon sequencing strategies did not generate the same results (see Table 5.4). Staff of the Department of Anatomy and Structural Biology at the University of Otago suggested that this discrepancy might have been the results of the fact that the individual PCR products were over amplified prior to DNA library construction. Interestingly, none of the studies that have used amplicon sequencing for SNP frequency determination purposes had reported this to be an issue [138-140]. Kim and Bartel (2009) successfully employed and validated high-throughput sequencing for the measurements of allelic imbalances associated with heterozygous miRNA target sites [140]. In this study a gDNA was used for normalizations. The gDNA produced a target/non-target ratio that deviated only slightly from the expected target/non-target ratio of 1 (i.e. 0.96). Conversely, the target/non-target ratios of the mRNA alleles in either muscle or liver the mRNA samples were significantly different from 1, indicating miRNA mediated repression.

A second set of seven samples were pooled together into a DNA library, and submitted for high-throughput amplicon sequencing. This second DNA library was made up out of four H4833Y samples (#835, #470, #116 and #145), two T4826I samples (#289 and #323), and one control that was used for assay validation. Over amplifications were avoided by making a dilution series of each of the DNAs. Reliable bar coded sequences were obtained for all seven samples including sample #116 (CGTA). This suggests that previously the lack of sequence reads for sample #116 was not the results of incorrect primer syntheses. Only 9705 (73%) sequence reads could be included in the analysis. With the exception of sample #145, the results revealed a relatively even sequence distribution between the pooled products. This could have been a direct result of the more accurate DNA concentration measurements using the Qubit fluorometer. A total of 3584 sequences (~27%) could not be matched and analysed due to incomplete bar codes or sequences. It would be interesting to know whether these sequences contained an

even distribution between wild type and mutant H4833Y and T4826I *RYR*1 cDNA sequences. A biased distribution of more erroneous wild type sequences compared with mutant sequences might explain the observed discrepancies. The observed 3584 unmatched sequences is a significant increase compared to the 117 unmatched sequences for analysis of the ten sample DNA library. Possibly, this increased error rate is a direct result of the more dilute cDNAs used for the amplifications. The detected H4833Y and T4826I mutation frequencies of all samples were about 50%. This included the control, which was constructed and proven to have a 3:1 ratio of the wild type (H4833) versus the mutant (Y4833) *RYR*1 allele. This suggests that the high-throughput amplicon sequencing approach as used here, is not suitable for accurate quantification of the two RyR1 alleles in heterozygous H4833Y MHS samples. In addition, this would explain why discrepancies were found between the results that were obtained from the conducted AS PCR and the amplicon sequencing assays. Alternatively, the observed discrepancies can possibly be explained by slight differences in amplification efficiencies of the individual *RYR*1 wild type and mutant (H4833Y) cDNA sequences. This may result in a distortion of the initial library population over many rounds of PCR. Nevertheless, skewing of the true allelic *RYR*1 ratios by the high proportion of detected low abundance variants in some samples cannot be ruled out completely.

6. ALLELIC VARIATION AT THE PROTEIN LEVEL

6.1 Introduction

Until now the conducted studies have looked only at allele-specific differences in RyR1 mRNA expression levels and stabilities. Gene expression however, is not only modulated at the level of transcription, but also at the translational and post-translational level. Thus, allele-specific differences in mRNA expression levels do not necessarily translate through to the protein level. mRNA does not only consist of a coding sequence that encodes the protein that is being translated. It also contains untranslated regions which may play roles in regulating the processing and stability of mRNA translation into protein. In eukaryotes these untranslated regions include the 5‟ cap, 5‟ untranslated region (5‟ UTR), 3‟ untranslated region (3‟ UTR) and the poly-A tail. Alterations in any of these mRNA regions due to e.g. variations in post-transcriptional modifications, mutations or transcription errors can have significant effects on gene expression levels.

Examples of how the untranslated regions of the mRNA regulate translation are listed below. The 5‟UTRs influence and regulate translation by the formation of secondary structures. These structural elements can provide the framework for interactions with *trans*-acting proteins or reduce the efficiency of translation by impeding the progress of the scanning ribosome. Mutations leading to alterations in these secondary structures can thus have significant effects on translational regulation. The best studied example of a small structural element that affects translation is the iron-responsive element (IRE). Binding of the IRE-binding protein to this small structural element blocks the interaction of the 43S pre-initiation complex with the eukaryotic initiation factor 4E cap binding complex (eIF4E) [141]. The 5‟ cap of the mRNA also plays a major role in the initiation of translation. The 5‟ cap is also referred to as the 7 methylguanosine cap (m7G cap). Cap-dependent translation initiation is based on the promotion of ribosome binding to the m7G cap via an interaction with the eIF4E [142]. *In vivo* experiments confirmed a substantial reduction in translational efficiency (≥10-fold) when mRNAs

lack the m7G cap [143]. Other translational mechanisms localized within the 5‟-UTR are the upstream open reading frame (ORF) [144] and internal ribosome entry sites (IRES) [145]. Several studies have revealed that 3‟ UTR binding proteins can regulate the initiation of translation by direct physical interaction with the distant 5‟ region of the mRNA. These interactions lead to circular mRNA structures that can tightly regulate translation [146]. The poly(A) tail plays an important role in this process by recruiting the poly(A)-binding protein (PABP). PABP in turn promotes recruitment of the 40S ribosomal subunit via the scaffolding protein eukaryotic initiation factor 4G [147]. MicroRNA (miRNA) mediated mRNA silencing is another example of how mRNA translation can be regulated by the 3‟UTRs. Two general modes of miRNA-mediated down regulation of targets in metazoan cells have been identified: miRNA-mediated translational repression and miRNA-mediated RNA decay. Regulation by miRNAs is typically mediated by the formation of imperfect hybrids with 3‟ UTR sequences of target mRNAs [148].

The aim of this study was to determine possible allelic variations of RyR1 expression at the protein level, in a heterozygous H4833Y MHS sample. In order to do so, the RyR1 was isolated from microsomes prepared from H4833Y MHS frozen skeletal muscle tissue. Mass spectrometry was to be employed to determine quantities of the two RyR1 alleles. The microsomes were to be prepared from any of the four H4833Y MHS frozen skeletal muscle tissues that were used to determine the allele-specific differences in RyR1 mRNA expression levels. Consequently, this can reveal if the detected allelic variation is the result of transcriptional and/or translational regulation.

6.2 Assay design

In this study it was intended to use mass spectrometry to determine quantities of the two H4833Y RyR1 alleles. An online peptide cutter [http://ca.expasy.org] revealed that trypsin cleaves the RyR1 498 times (see appendix VII). One of the generated peptides includes the 4833 amino acid residue (see Figure 6.1). The peptides containing either the wild type (H4833) or mutant (Y4833) 4833 amino acids can thus, in theory, be used to distinguish and quantify expression of the two RyR1 alleles. After isolation the

protein was to be sent to the Australian Proteome Analysis Facility (APAF; Macquarie University, North Ryde, NSW, Australia) for quantification.

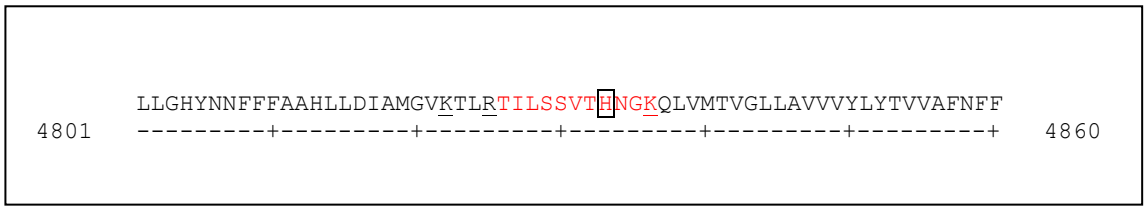

Figure 6.1: Trypsin cleavage sites around the 4833 amino acid.

Part of the RyR1 amino acid sequence and the corresponding trypsin cleavage sites (underlined), as detected by online peptide cutter software [http://ca.expasy.org]. Cleavage occurs at the right hand side of the marked amino acids. The generated peptide containing the 4833 amino acid is depicted in red. The 4833 amino acid is shown boxed.

RyR1 was isolated from H4833Y MHS frozen skeletal muscle tissue by the preparation of microsomal extracts. The RyR1 was separated from the other microsomal proteins by 1D SDS-polyacrylamide gel electrophoresis. After identification by immunoblotting the corresponding RyR1 band was to be excised from gel and submitted for mass spectrometric analysis. Whether the wild type and mutant 4833 peptides (TILSSVTHNGK and TILSSVTYNGK) could be detected in the mass spectrometer would depend on their ionization efficiencies. Thus, prior to quantification an initial MS/MS run would need to be carried out to ensure the targeted peptides could be detected. As different peptides rarely have identical ionization efficiencies two synthetic peptides must be used as references during the actual quantification experiments.

6.3 Results

6.3.1 Protocol optimizations using MHN skeletal muscle

To avoid unnecessary loss of valuable H4833Y MHS frozen skeletal muscle tissue, initial experiments were conducted using frozen MHN skeletal muscle tissue. Microsomes were prepared from the frozen MHN skeletal muscle tissue #1482 (biopsy date: 28-03-2008), as described in chapter 2.2.15. The RyR1 in the microsomes was separated from the other proteins by polyacryalmide gel electrophoresis under

denaturing conditions (see chapter 2.2.16). Figure 6.2A shows a representation of a typical 7.5% SDS-polyacrylamide gel. Here 32 µL of microsomal extract was mixed with 8 µL of 5x sample buffer. Half of the volume was incubated for 10 minutes at room temperature while the other 20 µL was boiled for 3 minutes. Four lanes, each with 8 µL boiled or unboiled microsomal extracts were loaded on gel. Gel electrophoresis was carried out for 1 h at 20 mA. After gel electrophoresis, two of the four lanes were analysed by immunoblotting (together with a third lane that contained a protein standard) while the other two lanes (plus protein standard) were stained with Coomassie-blue. The Coomassie-blue stained 7.5% SDS-polyacrylamide gel revealed several proteins larger than 250 kDa. in size. Western blot analysis was conducted on the other half of the gel to reveal if any of these proteins reacted with a ryanodine receptor specific antibody. Immunoblotting should detect an ~565 kDa. band. Thus, the separated proteins were transferred to a positively charged nylon membrane by overnight electro blotting at 4ºC for ~20 hours at 30 V. The membrane was incubated with the primary monoclonal anti-ryanodine receptor antibody (clone 34C, IgG1 isotype) and subsequently the secondary anti-mouse IgG antibody. The bands were detected using the BM Chemiluminescence Blotting Substrate. Results are shown in Figure 6.2B. After exposure, strong signals of >250 kDa in size were detected on X-ray film, indicating the presence of large amounts of RyR1. A weaker band at the top of the membrane revealed that some RyR1 remained in the well. Antibody-stained bands were also visible on the membrane after detection. The region on the SDS-polyacrylamide gel that corresponds to the bands on the X-ray film contained three protein bands which all lie closely together (two bands are scarcely visible on the gel photograph shown in Figure 6.2A). Although enough protein was transferred to the membrane to allow strong signals after detection, Coomassie-blue staining of the gel after western blot analysis revealed that not all of the >250 kDa proteins had been transferred.

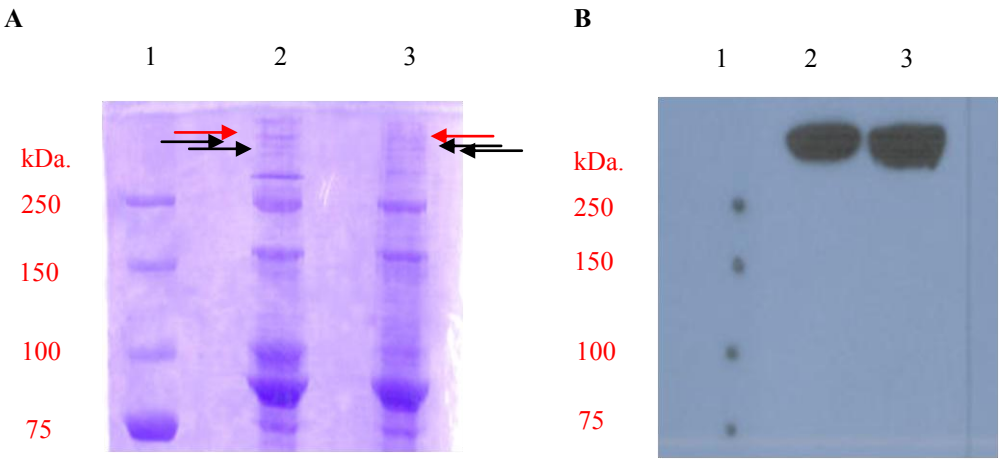

Figure 6.2: Separation of microsomal proteins prepared from a frozen MHN skeletal muscle tissue #1482.

(A) Coomassie-blue stained half of the 7.5% SDS-polyacrylamide gel. The proteins in the microsomal extracts were separated on a 7.5% SDS-polyacrylamide gel for 1 h at 20 mA. (B) The other half of the 7.5% SDS-polyacrylamide gel was loaded without spacing between the lanes and used for immunoblotting and later compared to the Coomassie-blue stained half to assign signals on the X-ray film to the protein bands. The separated proteins were transferred to a positively charged nylon membrane by overnight electro blotting at 4ºC for ~20 hours at 30 V. The bands were detected using the BM Chemiluminescence Blotting Substrate. The spots detected on the X-ray film in lane-1 were applied manually, according to the protein markers using a luminescent marker. For both figures: Lane 1- 5 µL precision Plus Protein Dual Color Standard; Lane 2- MHN microsomal extract mixed with sample buffer, incubated for 10 minutes at room temperature; Lane 3- MHN microsomal extract mixed with sample buffer and boiled for 3 minutes. Red arrows indicate the bands that correspond to the suspected full length size of the RyR1.

Due to overloading, it was not possible to detect any significant differences in signal intensities between the samples after the western and the individual protein bands on the Coomassie-blue stained gel in lanes 2 and 3 (Figure 6.2A and B). On the Coomassie-blue stained gel however, clear differences were visible in band intensities. In the sample that was incubated for 10 minutes at room temperature, the amount of protein in the band that was the largest in size (depicted by red arrows in Figure 6.2A) was about 2-3x stronger than the other two (assessed by visual observation). The amount of protein in the band of the largest size in the sample boiled for three minutes was decreased by comparison. These and previous data could suggest that the loss of protein

is the result of protein degradation due to boiling. Note that in this initial experiment no protease inhibitors had been added to the prepared microsomes.

A second microsome preparation was carried out from frozen MHN skeletal muscle tissue #1482 including protease inhibitors (Complete™ Mini Protease Inhibitor Mix). All samples were prepared for SDS-polyacrylamide gel electrophoresis by incubation at room temperature for 10 minutes. To better distinguish between the three bands, gel electrophoresis was carried out for 1.5 hours at 20 mA on a 7.5% SDS-polyacrylamide gel. Different amounts of the microsomal extracts were loaded onto the gel to eliminate possible differentiation problems due to overloading (Figure 6.3A). RyR1 was again detected by western blot analysis (Figure 6.3B). Again, three bands of similar size were visible after Coomassie-blue staining of the SDS-polyacrylamide gel. The largest (depicted by red arrows in Figures 6.3A and B) of the three bands however, clearly contained 8-10x (assessed by visual observation) more protein than the two smaller bands (depicted by black arrows in Figures 6.3A and B), which both contained similar amounts of protein (even when compared to Figure 6.2.). Western analysis revealed that of the three bands of similar mobility, at least the two larger bands bind the RyR1 antibody. The smaller of the two was most likely the result of degraded RyR1. As before, Coomassie-blue staining of the gel after western blot analysis revealed that not all of the >250 kDa proteins were transferred to the membrane.

In Figures 6.2 and 6.3 only 8 μL of a total of 150 μL of prepared microsomal extract was loaded onto gel. A visible protein band on a Coomassie-blue stained gel provides enough template for mass spectrometry. Even though some other proteins might be present in the identified band, gel excision of a 1.5 mm 7.5% SDS-polyacrylamide gel should yield enough RyR1 for quantification.

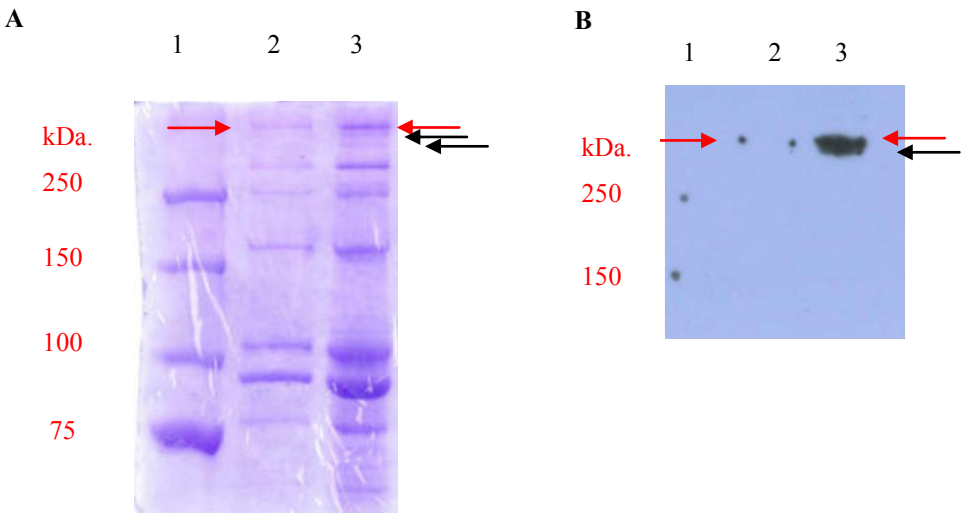

Figure 6.3: Separation of microsomal proteins prepared from a frozen MHN skeletal muscle tissue #1482.

(A) Coomassie-blue stained 7.5% SDS-polyacrylamide gel. The proteins in the microsomal extracts were separated on a 7.5% SDS-polyacrylamide gel for 1 h at 20 mA. (B) The separated proteins were transferred to a positively charged nylon membrane by overnight electro blotting at 4ºC for ~20 hours at 30 V. The bands were detected using the BM Chemiluminescence Blotting Substrate. The spots detected on the X-ray film were applied manually, according to the proteins marker using a luminescent marker. For both figures: Lane 1- 5 µL precision Plus Protein Dual Color Standard; Lane 2- MHN 2 µL microsomal extract mixed with 8 µL 5x sample buffer; Lane 3- 8 µL MHN microsomal extract mixed with 2 µL 5x sample buffer. Red arrows indicate the bands that correspond to the suspected full length size of the RyR1. Black arrows indicate the bands of similar apparent size.

6.3.2 Microsome preparation from MHS H4833Y skeletal muscle

After the establishment of a suitable protocol for RyR1 isolation, microsomes were prepared from frozen heterozygous H4833Y MHS skeletal muscle tissue #145 (biopsy date: 28-08-1992). This was the same muscle tissue that was used to determine the relative mRNA allele frequencies (see chapter 4). Figures 6.4A and B show the results from SDS-polyacrylamide gel electrophoresis and western blot analysis, respectively. The microsomes prepared from the frozen MHN skeletal muscle tissue #1482 was included as a positive control. Figure 6.4A revealed that the banding pattern is different in the #145 MHS sample compared to the #1482 MHN sample. In addition, the band that was believed to be the full length RyR1 is not present in the #145 MHS sample.

The two other closely located bands were present (depicted by black arrows in Figure 6.4A). But none of these bound the RyR1 specific antibody (Figure 6.4B).

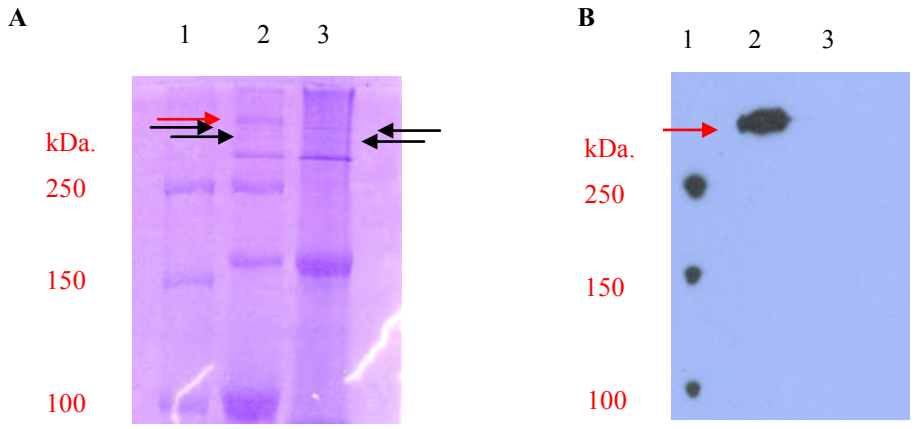

Figure 6.4: Separation of microsomal proteins prepared from a frozen skeletal muscle tissues #1482 (MHN) and #145 (MHS).

(A) Coomassie-blue stained 7.5% SDS-polyacrylamide gel. The proteins in the microsomal extracts were separated on a 7.5% SDS-polyacrylamide gel for 1 h at 20 mA. (B) The separated proteins were transferred to a positively charged nylon membrane by overnight electro blotting at 4ºC for ~20 hours at 30 V. The bands were detected using the BM Chemiluminescence Blotting Substrate. The spots detected on the X-ray film were applied manually, according to the proteins marker using a luminescent marker. For both figures: Lane 1- 5 µL precision Plus Protein Dual Color Standard; Lane 2- 5 µL #1482 MHN microsomal extract mixed with 5x sample buffer; Lane 3- 7 µL #145 MHS microsomal extract mixed with 5x sample buffer. Red arrows indicate the bands that correspond to the suspected full length size of the RyR1. Black arrows indicate the two additional bands of similar apparent size.

Three possible explanations may account for the apparent lack of RyR1 in the prepared MHS microsomes: (i) poor muscle quality, (ii) low RyR1 expression in MHS tissues or (iii) RyR1 tetramers that contain mutated 4833 monomers, are less anchored into the membrane and thus the RyR1 is "lost" (should therefore be present in either P1 or S1; see 2.2.15) during microsome preparation. To address these issues microsomes were initially prepared from two other frozen heterozygous H4833Y MHS skeletal muscle tissues (#116, biopsy date: 19-07-1991 and #835, biopsy date: 16-11-2001). Visual inspection suggests that of the two samples, #835 was of better quality than #116. For both samples, microsomes were prepared from the same muscle tissues used for the determination of the relative mRNA allele frequencies (see chapter 4). Figure 6.5A

shows the results of a 7.5 % SDS-polyacrylamide gel electrophoresis of sample #835. The #835 sample lacked the band that was believed to be the full length RyR1. Nevertheless, the banding pattern was similar to that of the #1482 MHN microsomes, suggesting the muscle might be of good quality although it has been stored for 8 years. The two other closely located bands were present, and had identical mobilities compared to the two smaller sized bands in sample # 1482 (depicted by black arrows). No western was conducted to confirm RyR1 presence/absence, as mass spectrometry required substantial amounts of RyR1 proteins levels for quantification.

Figure 6.5B shows the results of the 7.5 % SDS-polyacrylamide gel electrophoresis of sample #116. The banding pattern looks similar to that of sample #145 and different from that of the #1482 MHN sample (see Figure 6.5B lane 4). This sample also contained only two faint large sized protein bands (Figure 6.5B lane 4; depicted by black arrows) and lacked the band that was believed to be the full length RyR1. Aliquots of both the pellet (P1) and supernantant (S1) fractions, obtained during the microsome isolation protocol (see chapter 2.2.15), were also loaded onto the gel to check if the RyR1 was perhaps lost in any of the previous microsome isolation steps. Loading 12 & 13 µL of P1 (Figure 6.5B; lane-2) and S1 (Figure 6.5B; lane-3) respectively, was believed to suffice as RyR1 yields similar to those found from sample #1482 could be expected. The P1 and S1 fractions were 100 and 150 µL in total, respectively. However, no large sized bands that contained large amounts of protein were visible after Coomassie-blue staining. Therefore no westerns were conducted on these fractions.

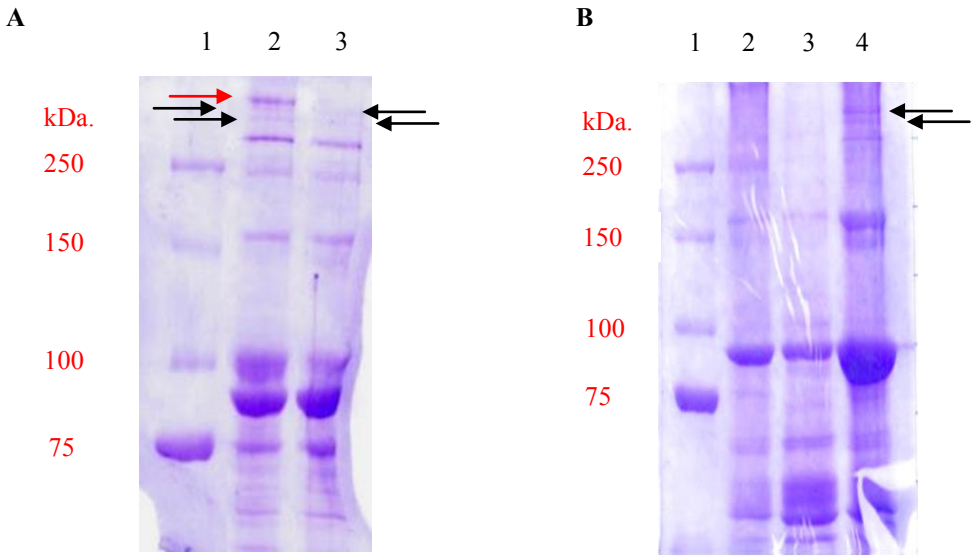

Figure 6.5: Separation of microsomal proteins prepared from a frozen MHS skeletal muscle tissues #835 and #116.

Coomassie-blue stained 7.5% SDS-polyacrylamide gels. The proteins in the microsomal extracts were separated on a 7.5% SDS-polyacrylamide gel for 1 h at 20 mA. (A) Lane 1- 5 µL precision Plus Protein Dual Color Standard; Lane 2- #1482 MHN 8 µL microsomal extract mixed with 2 µL 5x sample buffer; Lane 3- 8µL #835 MHS microsomal extract mixed with 2 µL 5x sample buffer. (B) Lane 1- 5 µL precision Plus Protein Dual Color Standard; Lane 2- #116 MHS 8 µL resuspended pellet (P1) mixed with 2 µL 5x sample buffer; Lane 3- 12 µL #116 MHS supernatant (S1) mixed with 3 µL 5x sample buffer. Lane 4- 12 µL #116 MHS microsomal extract mixed with 3 µL 5x sample buffer. Red arrows indicate the bands that correspond to the suspected full length size of the RyR1. Black arrows indicate the two additional bands of similar apparent size.

In addition microsomes were prepared from frozen MHN skeletal muscle tissue, #66 (biopsy date: 06-07-1989). Similar to the #145, #116 and #835 MHS samples, this sample had been stored for many years. Its appearance matched that of the #145, #116 samples and to a lesser extent that of the #835 sample. This was consistent with the biopsy dates of the samples, as sample #835 was from a biopsy carried out 9-13 years later than #66, #145 and #116. Figure 6.6 shows the results of the 7.5 % SDS-polyacrylamide gel electrophoresis of sample #116. The banding patterns looked identical those of sample #145 and #116 and different to that of the #1482 MHN sample. This strongly suggested that the lack of the strong band believed to be the full length RyR1 (as seen in #1482) was most likely due to poor muscle quality as a result of

long term storage. As a result of these observations no western blots were conducted on MHN sample #66.

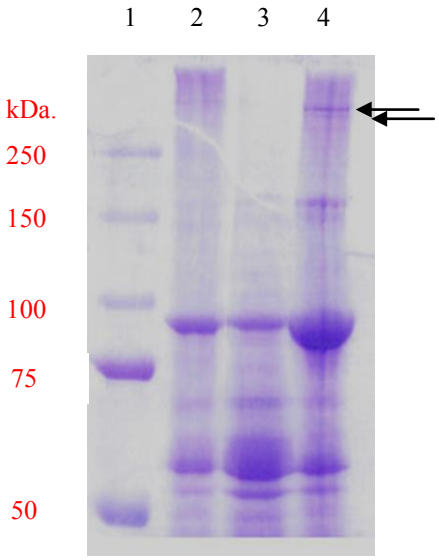

Figure 6.6: Separation of microsomal proteins prepared from a frozen MHN skeletal muscle tissue #66.

Coomassie-blue stained 7.5% SDS-polyacrylamide gel. The proteins were separated on a 7.5% SDS-polyacrylamide gel for 1 h at 20 mA. Lane 1- 5 µL precision Plus Protein Dual Color Standard; Lane 2- 8 µL resuspended pellet (P1) mixed with 2 µL 5x sample buffer; Lane 3- 12 µL supernatant (S1) mixed with 3 µL 5x sample buffer. Lane 4- 12 µL microsomal extract mixed with 3 µL 5x sample buffer. Black arrows indicate the two additional bands of similar apparent size closely located to the suspected full length size of the RyR1.

6.4 Discussion

In the previous chapters (chapters four and five) the conducted studies have focused on detecting possible allele specific differences in RyR1 mRNA expression levels and stabilities. Gene expression however, is not only modulated at the level of transcription. Thus, allele-specific differences in mRNA expression levels do not necessarily translate through to the protein level. Accordingly, this study focused on the determination of possible allelic variations of RyR1 expression at the protein level, in heterozygous H4833Y MHS samples. In order to do so, the RyR1 was to be isolated from microsomes prepared from a H4833Y MHS frozen skeletal muscle tissue. Microsomes were to be prepared from any of the four skeletal muscle tissues that were used to determine the

possible allele-specific differences in RyR1 mRNA expression levels. Subsequently, mass spectrometry was to be employed to determine quantities of the two RyR1 alleles.

To avoid unnecessary loss of H4833Y MHS frozen skeletal muscle tissue, initial protocol optimizations were conducted using frozen MHN skeletal muscle tissue #1482. 7.5% SDS-polyacrylamide gel electrophoresis of the microsomal extract revealed a strong band that was well over 250 KDa. in size. Immunoblotting revealed it contained significant amounts of RyR1. Thus, it is possible to readily detect the wild type RyR1 protein and the corresponding band should be able to be excised from the gel without any difficulties and provide enough template for mass spectrometry. The epitope of the monoclonal anti-ryanodine receptor antibody (clone 34C) lies between amino acids Asn2756 and Glu2803 and thus the H4833Y mutation should not disrupt antibody binding. Accordingly, after the establishment of a suitable protocol for RyR1 isolation, microsomes were prepared from frozen heterozygous H4833Y MHS skeletal muscle tissues. The same tissues were used for both microsome preparations and previously conducted mRNA isolations (chapters four and five). This would allow for comparisons between the two, and so might provide insight into the extent by which the two RyR1 alleles are differentially regulated. Microsomes were isolated from three different heterozygous H4833Y MHS skeletal muscle tissues (#145, 116 and #835). Unfortunately, none of these samples contained the band that was believed to be the full length RyR1.

Three possible explanations could account for the apparent lack of RyR1 in the prepared MHS microsomes: (i) poor muscle quality, (ii) low RyR1 expression in MHS tissues or (iii) RyR1 tetramers that contain mutated 4833 monomers, are less anchored into the membrane and thus the RyR1 is “lost” during microsome preparation. The apparent lack of the full length RyR1 in a second MHN frozen skeletal muscle sample (#66), suggested that poor muscle quality, due to long term storage was the main cause of RyR1 depletion, in at least samples #145, #116 & #66. Previously, the mutant RyR1 allele (Y4833) was found to have lower mRNA expression levels compared to the wild type RyR1 allele (H4833; see chapter 4). Nevertheless, severe depletion of especially the mutant RyR1 allele (Y4833) was not expected, as the mutation has been found to be

causative of MH by both genetic and biochemical studies [45]. Conversely, it is unknown what amount of dysfunctional RyR1 is required to provoke alterations in intracellular calcium release. Both visual inspection of the muscle tissue and banding patterns on the 7.5 % SDS-polyacrylamide gel suggested that sample #835 is of better quality than the #145, #116 and #66 samples. Nevertheless, this skeletal muscle tissue had been stored since November 2001. Therefore, RyR1 degradation during storage is not unlikely. Conversely, Lee *et al*. (2007) recently reported the involvement of C-terminus charged residues in RyR1 homo-dimerization [149]. Using rabbit RyR1 it was shown that amongst other residues, the positively charged H4832 RyR1 residue is involved in homo-tetramerization within and/or between RyR1 subunits. The rabbit H4832 RyR1 residue corresponds to the human H4833 RyR1 residue. Thus, it is not impossible that the H4833Y mutation causes RyR1 instability and loss during microsome preparations.

7. SUMMARY AND FUTURE DIRECTIONS

7.1 SNP detection using HRM

The need for more distinctive, faster and less expensive screening methodologies for the identification of genetic variants associated with MH, led to the development of high-throughput HRM assays to allow screening of the *RYR*1 gene for mutations associated with MH and/or CCD (see chapter 3). The designed assays required only two standard unlabelled primers that are commonly used in PCR. This significantly increased the robustness of the designed assays, as optimizations were normally not needed. In addition, all assays could be conducted using identical PCR and HRM conditions, making it ideal for high-throughput screening purposes. Conversely, only small amplicons could be used as they were found to improve discrimination between genotypes. This however does somewhat limit the usefulness of HRM for novel SNP discovery in large genes, such as the *RYR*1. As HRM has only recently become available, screening for a number of causative MH mutations is still being carried out using expensive labelled oligonucleotide probes. HRM however, has been proven to be a robust inexpensive method for *RYR*1 SNP screening/genotyping. Thus it should be considered for assay development in the future. Alternatively, several studies have described the use of inexpensive unlabelled oligonucleotide probes for HRM SNP detection and genotyping [117, 150]. Although the use of these unlabelled probes may somewhat limit the assay‟s robustness, as more optimizations are generally required, it can significantly improve SNP genotyping even in larger amplicons without being too costly.

7.2 Allele-specific ryanodine receptor 1 expression

7.2.1 Allele specific *RYR*1 mRNA expression

In the main project of this PhD the aim was to determine if there are allele-specific differences in RyR1 expression levels, in heterozygous MHS samples. Allele-specific

differences in RyR1 expression levels might provide insight into the observed variations in MH phenotypes and penetrance between different individuals with the same *RYR*1 mutation. Two different experimental strategies were designed to address possible allelic variation at the transcriptional level. Firstly an allele-specific PCR assay was designed that allowed the relative quantification of the two *RYR*1 mRNA transcripts in heterozygous MHS samples that contained the causative H4833Y MH mutation (see chapter 4). In both MHS skeletal muscle tissues and LCLs, the wild type (H4833) *RYR*1 allele was found to be more abundant than the mutant (Y4833) *RYR*1 allele. As H4833Y myoblasts were not available, LCLs were used for mRNA stability assays. Loss of heterozygosity was observed after prolonged culturing of LCL #1051, at both the mRNA and the gDNA level. This suggests that recombination events might have led to the observed loss of heterozygosity, which could be addressed by using polymorphic markers (such as microsatellites and SNPs) or karyotyping. The observed loss of heterozygosity can have major consequences for both the use of LCLs in functional characterization and in expression studies. The use of LCL have been suggested to be the system of choice for functional assays as they are RyR1 expressing cells which can be readily obtained from blood samples [45, 46]. Currently, more LCLs are being tested for loss of heterozygosity after prolonged culturing. It would have been valuable to examine more H4833Y skeletal muscle tissues, however no others were available. This was because the H4833Y mutation has been found causative of MH and as a result, muscle biopsies are no longer needed for MHS diagnosis. Alternatively, less invasive H4833Y genetic tests are employed. It would be interesting to examine other causative MH mutations in different regions of the RyR1, in additional MHS samples. Possible allele-specific differences in *RYR*1 mRNA expression levels in samples with causative MH mutations in putative pore- or regulatory-regions, such as the FKB12 binding pocket, might provide direct insights into the effect of allelic variations on different MH phenotypes [65].

Secondly, high-throughput amplicon sequencing was employed for the quantification of both the T4826I and H4833Y causative MH mutations in heterozygous MHS samples (see chapter 5). Four H4833Y samples that were previously analysed using the AS-PCR assay were also included. The two quantification strategies did not generate the same

results for the four H4833Y samples. The observed discrepancies led initially to the development of a H4833Y gDNA AS-PCR assay. Several reverse intronic primers were tested together with the previously used exonic allele-specific forward primers. However, all led to either secondary product formation or poor amplification efficiencies, which suggested this region of the gene was intractable for allele-specific PCR. Instead, a control was constructed and included in a second DNA library that was analysed by amplicon sequencing. Over-amplification was avoided by making a dilution series of the cDNAs. The control was proven to have a 3:1 ratio of the wild type (H4833) versus the mutant (Y4833) *RYR*1 allele. Nevertheless, the ratio was detected as 1:1 after data analysis. This strongly suggested that that the high-throughput amplicon sequencing approach as used here, was not suitable for accurate quantification of the two RyR1 alleles in heterozygous H4833Y MHS samples.

At the start of this project both the 1G Analyzer (Solexa/Illumina) and SOLiD (Applied Biosystems) systems did not allow quantification of allele-specific differences in mRNA expression levels, as required here. Since then, significant progress has been made to expand the capabilities of these systems. It might therefore be advantageous to re-examine the possible use of these alternative platforms for quantification of allele specific differences in *RYR*1 mRNA expression levels. If any future high-throughput amplicon sequencing experiments are to be conducted, additional controls (1:1, 4:1 and 1:3) need to be included in the DNA library to assess the validity of the earlier results. Additionally, is seems prudent to more rigorously address possible contamination problems. A high-fidelity polymerase can be used to ensure lower error rates as a result of extensive PCR amplification. Nevertheless, several other studies have used *Taq* polymerase for the amplification of PCR products for DNA library construction [138, 139]. As high-throughput DNA sequencing is costly it might be preferred to test the AS-PCR assay on gDNA using another mutation. Although different primers are necessary, an equal distribution of the two gDNA *RYR*1 alleles would indicate that the designed AS-PCR assay is a suitable method for the determination of allelic variation. Alternatively, using the Qubit™ fluorometer, DNA concentration could be measured accurately before mixing wild type and mutant *RYR*1 cDNA PCR products in a 1:1 ratio. Subsequently, PCR amplification efficiencies could be determined and the relative

allele frequencies can be calculated using Equation 4.4. Alternatively, methods such as MALDI-TOF, SnaPshot, Affymetrix HuSNP oligo arrays can be also be used for allele-specific measurements of *RYR*1 mRNA expression (see chapter 1) [95, 97, 100].

7.2.3 Allele-specific RyR1 expression

Given that an increase in mRNA levels does not necessarily lead to an increase in protein levels, a study also focussed on detecting possible variations in RyR1 alleles at the protein level (see chapter 6). In order to do so, the RyR1 was to be isolated from microsomes prepared from a H4833Y MHS frozen skeletal muscle tissue. Microsomes were prepared from three of the four skeletal muscle tissues that were used to determine the possible allele-specific differences in *RYR*1 mRNA expression levels. All H4833Y skeletal muscle samples investigated lacked the band that was believed to be the full length RyR1. The apparent lack of full-length RyR1 in a MHN frozen skeletal muscle sample suggested that poor muscle quality, due to long term storage, was the main cause of RyR1 depletion, in at least three of the four analysed samples. Microsomes isolated from a recently obtained MHN skeletal muscle biopsy, did contain significant amounts of RyR1. A recently biopsied H4833Y skeletal muscle tissue could be used to assess the lack of RyR1 in the previously isolated microsomes, although none were available for this study. If again no RyR1 was detected, it is likely that the loss may be the result of RyR1 instability due to the H4833Y mutation [149]. Alternatively, RyR1 presence could confirm that the previously observed RyR1 depletion was the result of long term storage. Alternatively, allele-specific RyR1 expression levels might be investigated using skeletal muscle tissues or myoblasts from other MHS samples. Myoblasts would need to be differentiated into myotubes prior to the analysis of allele-specific expression as RyR1 expression is extremely low in myoblasts.

In future experiments it would be interesting to more closely investigate RyR1 allelic variations, especially at the protein level. As yet, it is unknown how many RyR1 subunits in each tetramer are defective, or how many defective subunits are associated with each DHPR tetrad. Nevertheless, it might be possible to separately label the wild type and mutant RyR1 subunits in each tetramer in MHS samples, using epitope-specific antibodies or probes in consideration with very high resolution fluorescence or

electron microscopy. Allele specific differences in RyR1 expression levels can have a direct affect on the number of defective subunits per RyR1 tetramer, and consequently affect MH phenotype or penetrance. Furthermore, it would be interesting to look at the effect allelic variations can have on the function of the RyR1 tetramer. If possible, cells could be transformed with each of the two constructs, one representing the wild type and another representing the mutant RyR1 allele, respectively. The two constructs could be expressed differently in the cell using e.g. different promoters and as a result produce allelic imbalances. Alternatively it might be possible to skew allele-specific RyR1 expression levels in MHS cells using RNA interference [151].

REFERENCES

1. Denborough M, Lovell R: **Anaesthetics deaths in family.** *Lancet* 1960, **ii:**45.
2. Denborough M: **Malignant hyperpyrexia and sudden infant death.** *Aust N Z J Obstet Gynaecol* 1991, **31:**91.
3. Denborough M: **Malignant hyperthermia.** *Lancet* 1998, **352:**1131-1136.
4. Fruen BR, Mickelson JR, Louis CF: **Dantrolene inhibition of sarcoplasmic reticulum Ca2+ release by direct and specific action at skeletal muscle ryanodine receptors.** *J Biol Chem* 1997, **272:**26965-26971.
5. Stowell KM: **Malignant hyperthermia: a pharmacogenetic disorder.** *Pharmacogenomics* 2008, **9:**1657-1672.
6. Brown RL, Pollock AN, Couchman KG, Hodges M, Hutchinson DO, Waaka R, Lynch P, McCarthy TV, Stowell KM: **A novel ryanodine receptor mutation and genotype-phenotype correlation in a large malignant hyperthermia New Zealand Maori pedigree.** *Hum Mol Genet* 2000, **9:**1515-1524.
7. MacLennan DH: **The genetic basis of malignant hyperthermia.** *Trends Pharmacol Sci* 1992, **13:**330-334.
8. MacLennan DH, Phillips MS: **Malignant hyperthermia.** *Science* 1992, **256:**789-794.
9. Robinson RL, Brooks C, Brown SL, Ellis FR, Halsall PJ, Quinnell RJ, Shaw MA, Hopkins PM: **RYR1 mutations causing central core disease are associated with more severe malignant hyperthermia in vitro contracture test phenotypes.** *Hum Mutat* 2002, **20:**88-97.
10. Islander G, Rydenfelt K, Ranklev E, Bodelsson M: **Male preponderance of patients testing positive for malignant hyperthermia susceptibility.** *Acta Anaesthesiol Scand* 2007, **51:**614-620.
11. Robinson R, Carpenter D, Shaw MA, Halsall J, Hopkins P: **Mutations in RYR1 in malignant hyperthermia and central core disease.** *Hum Mutat* 2006, **27:**977-989.

12. Chu SH, Sutherland K, Beck J, Kowalski J, Goldspink P, Schwertz D: **Sex differences in expression of calcium-handling proteins and beta-adrenergic receptors in rat heart ventricle.** *Life Sci* 2005, **76:**2735-2749.
13. Johnson BD, Zheng W, Korach KS, Scheuer T, Catterall WA, Rubanyi GM: **Increased expression of the cardiac L-type calcium channel in estrogen receptor-deficient mice.** *J Gen Physiol* 1997, **110:**135-140.
14. Britt BA: **Malignant hyperthermia.** *Can Anaesth Soc J* 1985, **32:**S40-41.
15. Censier K, Urwyler A, Zorzato F, Treves S: **Intracellular calcium homeostasis in human primary muscle cells from malignant hyperthermia-susceptible and normal individuals. Effect Of overexpression of recombinant wild-type and Arg163Cys mutated ryanodine receptors.** *J Clin Invest* 1998, **101:**1233-1242.
16. Wappler F, Fiege M, Antz M, Schulte am Esch J: **Hemodynamic and metabolic alterations in response to graded exercise in a patient susceptible to malignant hyperthermia.** *Anesthesiology* 2000, **92:**268-272.
17. Bellinger AM, Reiken S, Dura M, Murphy PW, Deng SX, Landry DW, Nieman D, Lehnart SE, Samaru M, LaCampagne A, Marks AR: **Remodeling of ryanodine receptor complex causes "leaky" channels: a molecular mechanism for decreased exercise capacity.** *Proc Natl Acad Sci U S A* 2008, **105:**2198-2202.
18. Larach MG, Localio AR, Allen GC, Denborough MA, Ellis FR, Gronert GA, Kaplan RF, Muldoon SM, Nelson TE, Ording H, et al.: **A clinical grading scale to predict malignant hyperthermia susceptibility.** *Anesthesiology* 1994, **80:**771-779.
19. Mickelson JR, Gallant EM, Litterer LA, Johnson KM, Rempel WE, Louis CF: **Abnormal sarcoplasmic reticulum ryanodine receptor in malignant hyperthermia.** *J Biol Chem* 1988, **263:**9310-9315.
20. MacLennan DH, Duff C, Zorzato F, Fujii J, Phillips M, Korneluk RG, Frodis W, Britt BA, Worton RG: **Ryanodine receptor gene is a candidate for predisposition to malignant hyperthermia.** *Nature* 1990, **343:**559-561.
21. McCarthy TV, Healy JM, Heffron JJ, Lehane M, Deufel T, Lehmann-Horn F, Farrall M, Johnson K: **Localization of the malignant hyperthermia**

susceptibility locus to human chromosome 19q12-13.2. *Nature* 1990, **343:**562-564.

22. McCarthy TV, Quane KA, Lynch PJ: **Ryanodine receptor mutations in malignant hyperthermia and central core disease.** *Hum Mutat* 2000, **15:**410-417.
23. Lynch PJ, Krivosic-Horber R, Reyford H, Monnier N, Quane K, Adnet P, Haudecoeur G, Krivosic I, McCarthy T, Lunardi J: **Identification of heterozygous and homozygous individuals with the novel RYR1 mutation Cys35Arg in a large kindred.** *Anesthesiology* 1997, **86:**620-626.
24. Monnier N, Krivosic-Horber R, Payen JF, Kozak-Ribbens G, Nivoche Y, Adnet P, Reyford H, Lunardi J: **Presence of two different genetic traits in malignant hyperthermia families: implication for genetic analysis, diagnosis, and incidence of malignant hyperthermia susceptibility.** *Anesthesiology* 2002, **97:**1067-1074.
25. Monnier N, Procaccio V, Stieglitz P, Lunardi J: **Malignant-hyperthermia susceptibility is associated with a mutation of the alpha 1-subunit of the human dihydropyridine-sensitive L-type voltage-dependent calcium-channel receptor in skeletal muscle.** *Am J Hum Genet* 1997, **60:**1316-1325.
26. Quane KA, Healy JM, Keating KE, Manning BM, Couch FJ, Palmucci LM, Doriguzzi C, Fagerlund TH, Berg K, Ording H, et al.: **Mutations in the ryanodine receptor gene in central core disease and malignant hyperthermia.** *Nat Genet* 1993, **5:**51-55.
27. Romero NB, Monnier N, Viollet L, Cortey A, Chevallay M, Leroy JP, Lunardi J, Fardeau M: **Dominant and recessive central core disease associated with RYR1 mutations and fetal akinesia.** *Brain* 2003, **126:**2341-2349.
28. Treves S, Anderson AA, Ducreux S, Divet A, Bleunven C, Grasso C, Paesante S, Zorzato F: **Ryanodine receptor 1 mutations, dysregulation of calcium homeostasis and neuromuscular disorders.** *Neuromuscul Disord* 2005, **15:**577-587.
29. Ferreiro A, Quijano-Roy S, Pichereau C, Moghadaszadeh B, Goemans N, Bonnemann C, Jungbluth H, Straub V, Villanova M, Leroy JP, et al: **Mutations of the selenoprotein N gene, which is implicated in rigid spine muscular**

dystrophy, cause the classical phenotype of multiminicore disease: reassessing the nosology of early-onset myopathies. *Am J Hum Genet* 2002, **71:**739-749.

30. Dulhunty AF, Haarmann CS, Green D, Laver DR, Board PG, Casarotto MG: **Interactions between dihydropyridine receptors and ryanodine receptors in striated muscle.** *Prog Biophys Mol Biol* 2002, **79:**45-75.
31. Araya R, Liberona JL, Cardenas JC, Riveros N, Estrada M, Powell JA, Carrasco MA, Jaimovich E: **Dihydropyridine receptors as voltage sensors for a depolarization-evoked, IP3R-mediated, slow calcium signal in skeletal muscle cells.** *J Gen Physiol* 2003, **121:**3-16.
32. Carrasco MA, Riveros N, Rios J, Muller M, Torres F, Pineda J, Lantadilla S, Jaimovich E: **Depolarization-induced slow calcium transients activate early genes in skeletal muscle cells.** *Am J Physiol Cell Physiol* 2003, **284:**C1438-1447.
33. Kobayashi S, Bannister ML, Gangopadhyay JP, Hamada T, Parness J, Ikemoto N: **Dantrolene stabilizes domain interactions within the ryanodine receptor.** *J Biol Chem* 2005, **280:**6580-6587.
34. Avila G, Dirksen RT: **Functional effects of central core disease mutations in the cytoplasmic region of the skeletal muscle ryanodine receptor.** *J Gen Physiol* 2001, **118:**277-290.
35. Lopez JR, Linares N, Pessah IN, Allen PD: **Enhanced response to caffeine and 4-chloro-m-cresol in malignant hyperthermia-susceptible muscle is related in part to chronically elevated resting [Ca2+]i.** *Am J Physiol Cell Physiol* 2005, **288:**C606-612.
36. Fletcher JE, Rosenberg H, Aggarwal M: **Comparison of European and North American malignant hyperthermia diagnostic protocol outcomes for use in genetic studies.** *Anesthesiology* 1999, **90:**654-661.
37. Larach MG: **Standardization of the caffeine halothane muscle contracture test. North American Malignant Hyperthermia Group.** *Anesth Analg* 1989, **69:**511-515.
38. Deufel T, Sudbrak R, Feist Y, Rubsam B, Du Chesne I, Schafer KL, Roewer N, Grimm T, Lehmann-Horn F, Hartung EJ, et al.: **Discordance, in a malignant**

hyperthermia pedigree, between in vitro contracture-test phenotypes and haplotypes for the MHS1 region on chromosome 19q12-13.2, comprising the C1840T transition in the RYR1 gene. *Am J Hum Genet* 1995, **56:**1334-1342.

39. Fortunato G, Carsana A, Tinto N, Brancadoro V, Canfora G, Salvatore F: **A case of discordance between genotype and phenotype in a malignant hyperthermia family.** *Eur J Hum Genet* 1999, **7:**415-420.
40. Serfas KD, Bose D, Patel L, Wrogemann K, Phillips MS, MacLennan DH, Greenberg CR: **Comparison of the segregation of the RYR1 C1840T mutation with segregation of the caffeine/halothane contracture test results for malignant hyperthermia susceptibility in a large Manitoba Mennonite family.** *Anesthesiology* 1996, **84:**322-329.
41. Treves S, Larini F, Menegazzi P, Steinberg TH, Koval M, Vilsen B, Andersen JP, Zorzato F: **Alteration of intracellular Ca2+ transients in COS-7 cells transfected with the cDNA encoding skeletal-muscle ryanodine receptor carrying a mutation associated with malignant hyperthermia.** *Biochem J* 1994, **301 (Pt 3):**661-665.
42. Tong J, Oyamada H, Demaurex N, Grinstein S, McCarthy TV, MacLennan DH: **Caffeine and halothane sensitivity of intracellular Ca2+ release is altered by 15 calcium release channel (ryanodine receptor) mutations associated with malignant hyperthermia and/or central core disease.** *J Biol Chem* 1997, **272:**26332-26339.
43. Sei Y, Gallagher KL, Basile AS: **Skeletal muscle type ryanodine receptor is involved in calcium signaling in human B lymphocytes.** *J Biol Chem* 1999, **274:**5995-6002.
44. Sei Y, Brandom BW, Bina S, Hosoi E, Gallagher KL, Wyre HW, Pudimat PA, Holman SJ, Venzon DJ, Daly JW, Muldoon S: **Patients with malignant hyperthermia demonstrate an altered calcium control mechanism in B lymphocytes.** *Anesthesiology* 2002, **97:**1052-1058.
45. Anderson AA, Brown RL, Polster B, Pollock N, Stowell KM: **Identification and biochemical characterization of a novel ryanodine receptor gene**

mutation associated with malignant hyperthermia. *Anesthesiology* 2008, **108:**208-215.

46. Levano S, Vukcevic M, Singer M, Matter A, Treves S, Urwyler A, Girard T: **Increasing the number of diagnostic mutations in malignant hyperthermia.** *Hum Mutat* 2009, **30:**590-598.
47. Wehner M, Rueffert H, Koenig F, Neuhaus J, Olthoff D: **Increased sensitivity to 4-chloro-m-cresol and caffeine in primary myotubes from malignant hyperthermia susceptible individuals carrying the ryanodine receptor 1 Thr2206Met (C6617T) mutation.** *Clin Genet* 2002, **62:**135-146.
48. Yang T, Ta TA, Pessah IN, Allen PD: **Functional defects in six ryanodine receptor isoform-1 (RyR1) mutations associated with malignant hyperthermia and their impact on skeletal excitation-contraction coupling.** *J Biol Chem* 2003, **278:**25722-25730.
49. Samso M, Wagenknecht T, Allen PD: **Internal structure and visualization of transmembrane domains of the RyR1 calcium release channel by cryo-EM.** *Nat Struct Mol Biol* 2005, **12:**539-544.
50. Radermacher M, Rao V, Grassucci R, Frank J, Timerman AP, Fleischer S, Wagenknecht T: **Cryo-electron microscopy and three-dimensional reconstruction of the calcium release channel/ryanodine receptor from skeletal muscle.** *J Cell Biol* 1994, **127:**411-423.
51. Sharma MR, Penczek P, Grassucci R, Xin HB, Fleischer S, Wagenknecht T: **Cryoelectron microscopy and image analysis of the cardiac ryanodine receptor.** *J Biol Chem* 1998, **273:**18429-18434.
52. Sharma MR, Jeyakumar LH, Fleischer S, Wagenknecht T: **Three-dimensional structure of ryanodine receptor isoform three in two conformational states as visualized by cryo-electron microscopy.** *J Biol Chem* 2000, **275:**9485-9491.
53. Takeshima H, Nishimura S, Matsumoto T, Ishida H, Kangawa K, Minamino N, Matsuo H, Ueda M, Hanaoka M, Hirose T, et al.: **Primary structure and expression from complementary DNA of skeletal muscle ryanodine receptor.** *Nature* 1989, **339:**439-445.
54. Zorzato F, Fujii J, Otsu K, Phillips M, Green NM, Lai FA, Meissner G, MacLennan DH: **Molecular cloning of cDNA encoding human and rabbit**

forms of the Ca2+ release channel (ryanodine receptor) of skeletal muscle sarcoplasmic reticulum. *J Biol Chem* 1990, **265:**2244-2256.

55. Furuichi T, Furutama D, Hakamata Y, Nakai J, Takeshima H, Mikoshiba K: **Multiple types of ryanodine receptor/Ca2+ release channels are differentially expressed in rabbit brain.** *J Neurosci* 1994, **14:**4794-4805.
56. Otsu K, Willard HF, Khanna VK, Zorzato F, Green NM, MacLennan DH: **Molecular cloning of cDNA encoding the Ca2+ release channel (ryanodine receptor) of rabbit cardiac muscle sarcoplasmic reticulum.** *J Biol Chem* 1990, **265:**13472-13483.
57. Hakamata Y, Nakai J, Takeshima H, Imoto K: **Primary structure and distribution of a novel ryanodine receptor/calcium release channel from rabbit brain.** *FEBS Lett* 1992, **312:**229-235.
58. Takeshima H, Yamazawa T, Ikemoto T, Takekura H, Nishi M, Noda T, Iino M: **Ca(2+)-induced Ca2+ release in myocytes from dyspedic mice lacking the type-1 ryanodine receptor.** *Embo J* 1995, **14:**2999-3006.
59. Jeyakumar LH, Copello JA, O'Malley AM, Wu GM, Grassucci R, Wagenknecht T, Fleischer S: **Purification and characterization of ryanodine receptor 3 from mammalian tissue.** *J Biol Chem* 1998, **273:**16011-16020.
60. Sorrentino V, Volpe P: **Ryanodine receptors: how many, where and why?** *Trends Pharmacol Sci* 1993, **14:**98-103.
61. Sharma MR, Wagenknecht, T.: **Cryo-Electron Microscopy and 3D Reconstruction of Ryanodine Receptors and Their Interactions with E-C coupling Proteins.** *Basic Appl Myol* 2004, **14:**299-306.
62. Ludtke SJ, Serysheva, II, Hamilton SL, Chiu W: **The pore structure of the closed RyR1 channel.** *Structure* 2005, **13:**1203-1211.
63. Du GG, Sandhu B, Khanna VK, Guo XH, MacLennan DH: **Topology of the Ca2+ release channel of skeletal muscle sarcoplasmic reticulum (RyR1).** *Proc Natl Acad Sci U S A* 2002, **99:**16725-16730.
64. Dulhunty AF, Pouliquin P: **What we don't know about the structure of ryanodine receptor calcium release channels.** *Clin Exp Pharmacol Physiol* 2003, **30:**713-723.

65. Serysheva, II, Ludtke SJ, Baker ML, Cong Y, Topf M, Eramian D, Sali A, Hamilton SL, Chiu W: **Subnanometer-resolution electron cryomicroscopy-based domain models for the cytoplasmic region of skeletal muscle RyR channel.** *Proc Natl Acad Sci U S A* 2008, **105:**9610-9615.

66. Costello B, Chadwick C, Saito A, Chu A, Maurer A, Fleischer S: **Characterization of the junctional face membrane from terminal cisternae of sarcoplasmic reticulum.** *J Cell Biol* 1986, **103:**741-753.

67. Copello JA, Barg S, Onoue H, Fleischer S: **Heterogeneity of Ca2+ gating of skeletal muscle and cardiac ryanodine receptors.** *Biophys J* 1997, **73:**141-156.

68. Chen SR, Zhang L, MacLennan DH: **Characterization of a Ca2+ binding and regulatory site in the Ca2+ release channel (ryanodine receptor) of rabbit skeletal muscle sarcoplasmic reticulum.** *J Biol Chem* 1992, **267:**23318-23326.

69. Hayek SM, Zhao J, Bhat M, Xu X, Nagaraj R, Pan Z, Takeshima H, Ma J: **A negatively charged region of the skeletal muscle ryanodine receptor is involved in Ca(2+)-dependent regulation of the Ca(2+) release channel.** *FEBS Lett* 1999, **461:**157-164.

70. Laver DR, Baynes TM, Dulhunty AF: **Magnesium inhibition of ryanodine-receptor calcium channels: evidence for two independent mechanisms.** *J Membr Biol* 1997, **156:**213-229.

71. Meissner G, Darling E, Eveleth J: **Kinetics of rapid Ca2+ release by sarcoplasmic reticulum. Effects of Ca2+, Mg2+, and adenine nucleotides.** *Biochemistry* 1986, **25:**236-244.

72. Zucchi R, Ronca-Testoni S: **The sarcoplasmic reticulum Ca2+ channel/ryanodine receptor: modulation by endogenous effectors, drugs and disease states.** *Pharmacol Rev* 1997, **49:**1-51.

73. Rossi AE, Dirksen RT: **Sarcoplasmic reticulum: the dynamic calcium governor of muscle.** *Muscle Nerve* 2006, **33:**715-731.

74. Beard NA, Sakowska MM, Dulhunty AF, Laver DR: **Calsequestrin is an inhibitor of skeletal muscle ryanodine receptor calcium release channels.** *Biophys J* 2002, **82:**310-320.

75. Beard NA, Casarotto MG, Wei L, Varsanyi M, Laver DR, Dulhunty AF: **Regulation of ryanodine receptors by calsequestrin: effect of high luminal Ca2+ and phosphorylation.** *Biophys J* 2005, **88:**3444-3454.

76. Paolini C, Quarta M, Nori A, Boncompagni S, Canato M, Volpe P, Allen PD, Reggiani C, Protasi F: **Reorganized stores and impaired calcium handling in skeletal muscle of mice lacking calsequestrin-1.** *J Physiol* 2007, **583:**767-784.

77. Treves S, Feriotto G, Moccagatta L, Gambari R, Zorzato F: **Molecular cloning, expression, functional characterization, chromosomal localization, and gene structure of junctate, a novel integral calcium binding protein of sarco(endo)plasmic reticulum membrane.** *J Biol Chem* 2000, **275:**39555-39568.

78. Suk JY, Kim YS, Park WJ: **HRC (histidine-rich Ca2+ binding protein) resides in the lumen of sarcoplasmic reticulum as a multimer.** *Biochem Biophys Res Commun* 1999, **263:**667-671.

79. Tanabe T, Beam KG, Adams BA, Niidome T, Numa S: **Regions of the skeletal muscle dihydropyridine receptor critical for excitation-contraction coupling.** *Nature* 1990, **346:**567-569.

80. Arikkath J, Campbell KP: **Auxiliary subunits: essential components of the voltage-gated calcium channel complex.** *Curr Opin Neurobiol* 2003, **13:**298-307.

81. Tripathy A, Xu L, Mann G, Meissner G: **Calmodulin activation and inhibition of skeletal muscle Ca2+ release channel (ryanodine receptor).** *Biophys J* 1995, **69:**106-119.

82. Samso M, Wagenknecht T: **Apocalmodulin and Ca2+-calmodulin bind to neighboring locations on the ryanodine receptor.** *J Biol Chem* 2002, **277:**1349-1353.

83. Sencer S, Papineni RV, Halling DB, Pate P, Krol J, Zhang JZ, Hamilton SL: **Coupling of RYR1 and L-type calcium channels via calmodulin binding domains.** *J Biol Chem* 2001, **276:**38237-38241.

84. Wagenknecht T, Radermacher M, Grassucci R, Berkowitz J, Xin HB, Fleischer S: **Locations of calmodulin and FK506-binding protein on the three-**

dimensional architecture of the skeletal muscle ryanodine receptor. *J Biol Chem* 1997, **272:**32463-32471.

85. Timerman AP, Ogunbumni E, Freund E, Wiederrecht G, Marks AR, Fleischer S: **The calcium release channel of sarcoplasmic reticulum is modulated by FK-506-binding protein. Dissociation and reconstitution of FKBP-12 to the calcium release channel of skeletal muscle sarcoplasmic reticulum.** *J Biol Chem* 1993, **268:**22992-22999.
86. Ahern GP, Junankar PR, Dulhunty AF: **Subconductance states in single-channel activity of skeletal muscle ryanodine receptors after removal of FKBP12.** *Biophys J* 1997, **72:**146-162.
87. Lamb GD, Stephenson DG: **Effects of FK506 and rapamycin on excitation-contraction coupling in skeletal muscle fibres of the rat.** *J Physiol* 1996, **494 (Pt 2):**569-576.
88. Anderson AA, Altafaj X, Zheng Z, Wang ZM, Delbono O, Ronjat M, Treves S, Zorzato F: **The junctional SR protein JP-45 affects the functional expression of the voltage-dependent Ca2+ channel Cav1.1.** *J Cell Sci* 2006, **119:**2145-2155.
89. Feng W, Tu J, Yang T, Vernon PS, Allen PD, Worley PF, Pessah IN: **Homer regulates gain of ryanodine receptor type 1 channel complex.** *J Biol Chem* 2002, **277:**44722-44730.
90. Weigl L, Zidar A, Gscheidlinger R, Karel A, Hohenegger M: **Store operated Ca2+ influx by selective depletion of ryanodine sensitive Ca2+ pools in primary human skeletal muscle cells.** *Naunyn Schmiedebergs Arch Pharmacol* 2003, **367:**353-363.
91. Cherednichenko G, Hurne AM, Fessenden JD, Lee EH, Allen PD, Beam KG, Pessah IN: **Conformational activation of Ca2+ entry by depolarization of skeletal myotubes.** *Proc Natl Acad Sci U S A* 2004, **101:**15793-15798.
92. Girard T, Urwyler A, Censier K, Mueller CR, Zorzato F, Treves S: **Genotype-phenotype comparison of the Swiss malignant hyperthermia population.** *Hum Mutat* 2001, **18:**357-358.
93. Girard T, Treves S, Censier K, Mueller CR, Zorzato F, Urwyler A: **Phenotyping malignant hyperthermia susceptibility by measuring halothane-induced**

changes in myoplasmic calcium concentration in cultured human skeletal muscle cells. *Br J Anaesth* 2002, **89:**571-579.

94. Fiege M, Wappler F, Weisshorn R, Ulrich Gerbershagen M, Steinfath M, Schulte Am Esch J: **Results of contracture tests with halothane, caffeine, and ryanodine depend on different malignant hyperthermia-associated ryanodine receptor gene mutations.** *Anesthesiology* 2002, **97:**345-350.
95. Ding C, Maier E, Roscher AA, Braun A, Cantor CR: **Simultaneous quantitative and allele-specific expression analysis with real competitive PCR.** *BMC Genet* 2004, **5:**8.
96. Cowles CR, Hirschhorn JN, Altshuler D, Lander ES: **Detection of regulatory variation in mouse genes.** *Nat Genet* 2002, **32:**432-437.
97. Lo HS, Wang Z, Hu Y, Yang HH, Gere S, Buetow KH, Lee MP: **Allelic variation in gene expression is common in the human genome.** *Genome Res* 2003, **13:**1855-1862.
98. Johnson AD, Wang D, Sadee W: **Polymorphisms affecting gene regulation and mRNA processing: broad implications for pharmacogenetics.** *Pharmacol Ther* 2005, **106:**19-38.
99. Yan H, Yuan W, Velculescu VE, Vogelstein B, Kinzler KW: **Allelic variation in human gene expression.** *Science* 2002, **297:**1143.
100. Zhang Y, Wang D, Johnson AD, Papp AC, Sadee W: **Allelic expression imbalance of human mu opioid receptor (OPRM1) caused by variant A118G.** *J Biol Chem* 2005, **280:**32618-32624.
101. Freeman JL, Perry GH, Feuk L, Redon R, McCarroll SA, Altshuler DM, Aburatani H, Jones KW, Tyler-Smith C, Hurles ME, et al: **Copy number variation: new insights in genome diversity.** *Genome Res* 2006, **16:**949-961.
102. Monnier N, Ferreiro A, Marty I, Labarre-Vila A, Mezin P, Lunardi J: **A homozygous splicing mutation causing a depletion of skeletal muscle RYR1 is associated with multi-minicore disease congenital myopathy with ophthalmoplegia.** *Hum Mol Genet* 2003, **12:**1171-1178.
103. Zhou H, Jungbluth H, Sewry CA, Feng L, Bertini E, Bushby K, Straub V, Roper H, Rose MR, Brockington M, et al: **Molecular mechanisms and phenotypic**

variation in RYR1-related congenital myopathies. *Brain* 2007, **130:**2024-2036.

104. Zhou H, Yamaguchi N, Xu L, Wang Y, Sewry C, Jungbluth H, Zorzato F, Bertini E, Muntoni F, Meissner G, Treves S: **Characterization of recessive RYR1 mutations in core myopathies.** *Hum Mol Genet* 2006, **15:**2791-2803.
105. Zhou H, Brockington M, Jungbluth H, Monk D, Stanier P, Sewry CA, Moore GE, Muntoni F: **Epigenetic allele silencing unveils recessive RYR1 mutations in core myopathies.** *Am J Hum Genet* 2006, **79:**859-868.
106. Robinson RL, Carpenter D, Halsall PJ, Iles DE, Booms P, Steele D, Hopkins PM, Shaw MA: **Epigenetic allele silencing and variable penetrance of malignant hyperthermia susceptibility.** *Br J Anaesth* 2009.
107. Neitzel H: **A routine method for the establishment of permanent growing lymphoblastoid cell lines.** *Hum Genet* 1986, **73:**320-326.
108. Saito A, Seiler S, Chu A, Fleischer S: **Preparation and morphology of sarcoplasmic reticulum terminal cisternae from rabbit skeletal muscle.** *J Cell Biol* 1984, **99:**875-885.
109. Orita M, Iwahana H, Kanazawa H, Hayashi K, Sekiya T: **Detection of polymorphisms of human DNA by gel electrophoresis as single-strand conformation polymorphisms.** *Proc Natl Acad Sci U S A* 1989, **86:**2766-2770.
110. Fischer SG, Lerman LS: **DNA fragments differing by single base-pair substitutions are separated in denaturing gradient gels: correspondence with melting theory.** *Proc Natl Acad Sci U S A* 1983, **80:**1579-1583.
111. Papp AC, Pinsonneault JK, Cooke G, Sadee W: **Single nucleotide polymorphism genotyping using allele-specific PCR and fluorescence melting curves.** *Biotechniques* 2003, **34:**1068-1072.
112. Okimoto R, Dodgson JB: **Improved PCR amplification of multiple specific alleles (PAMSA) using internally mismatched primers.** *Biotechniques* 1996, **21:**20-26.
113. Bernard PS, Ajioka RS, Kushner JP, Wittwer CT: **Homogeneous multiplex genotyping of hemochromatosis mutations with fluorescent hybridization probes.** *Am J Pathol* 1998, **153:**1055-1061.

114. Crockett AO, Wittwer CT: **Fluorescein-labeled oligonucleotides for real-time pcr: using the inherent quenching of deoxyguanosine nucleotides.** *Anal Biochem* 2001, **290:**89-97.

115. Gundry CN, Vandersteen JG, Reed GH, Pryor RJ, Chen J, Wittwer CT: **Amplicon melting analysis with labeled primers: a closed-tube method for differentiating homozygotes and heterozygotes.** *Clin Chem* 2003, **49:**396-406.

116. Wittwer CT, Reed GH, Gundry CN, Vandersteen JG, Pryor RJ: **High-resolution genotyping by amplicon melting analysis using LCGreen.** *Clin Chem* 2003, **49:**853-860.

117. Zhou L, Wang L, Palais R, Pryor R, Wittwer CT: **High-resolution DNA melting analysis for simultaneous mutation scanning and genotyping in solution.** *Clin Chem* 2005, **51:**1770-1777.

118. Liew M, Pryor R, Palais R, Meadows C, Erali M, Lyon E, Wittwer C: **Genotyping of single-nucleotide polymorphisms by high-resolution melting of small amplicons.** *Clin Chem* 2004, **50:**1156-1164.

119. Reed GH, Wittwer CT: **Sensitivity and specificity of single-nucleotide polymorphism scanning by high-resolution melting analysis.** *Clin Chem* 2004, **50:**1748-1754.

120. Krypuy M, Newnham GM, Thomas DM, Conron M, Dobrovic A: **High resolution melting analysis for the rapid and sensitive detection of mutations in clinical samples: KRAS codon 12 and 13 mutations in non-small cell lung cancer.** *BMC Cancer* 2006, **6:**295.

121. Pastinen T, Ge B, Hudson TJ: **Influence of human genome polymorphism on gene expression.** *Hum Mol Genet* 2006, **15 Spec No 1:**R9-16.

122. Rollinson S, Allan JM, Law GR, Roddam PL, Smith MT, Skibola C, Smith AG, Forrest MS, Sibley K, Higuchi R, et al: **High-throughput association testing on DNA pools to identify genetic variants that confer susceptibility to acute myeloid leukemia.** *Cancer Epidemiol Biomarkers Prev* 2004, **13:**795-800.

123. Germer S, Holland MJ, Higuchi R: **High-throughput SNP allele-frequency determination in pooled DNA samples by kinetic PCR.** *Genome Res* 2000, **10:**258-266.

124. Pfaffl MW: **A new mathematical model for relative quantification in real-time RT-PCR.** *Nucleic Acids Res* 2001, **29:**e45.

125. Sobell HM: **Actinomycin and DNA transcription.** *Proc Natl Acad Sci U S A* 1985, **82:**5328-5331.

126. Ovstebo R, Haug KB, Lande K, Kierulf P: **PCR-based calibration curves for studies of quantitative gene expression in human monocytes: development and evaluation.** *Clin Chem* 2003, **49:**425-432.

127. Kuhne BS, Oschmann P: **Quantitative real-time RT-PCR using hybridization probes and imported standard curves for cytokine gene expression analysis.** *Biotechniques* 2002, **33:**1078, 1080-1072, 1084 passim.

128. Hannula K, Lipsanen-Nyman M, Scherer SW, Holmberg C, Hoglund P, Kere J: **Maternal and paternal chromosomes 7 show differential methylation of many genes in lymphoblast DNA.** *Genomics* 2001, **73:**1-9.

129. Migeon BR, Axelman J, Stetten G: **Clonal evolution in human lymphoblast cultures.** *Am J Hum Genet* 1988, **42:**742-747.

130. Pastinen T, Sladek R, Gurd S, Sammak A, Ge B, Lepage P, Lavergne K, Villeneuve A, Gaudin T, Brandstrom H, et al: **A survey of genetic and epigenetic variation affecting human gene expression.** *Physiol Genomics* 2004, **16:**184-193.

131. Mardis ER: **The impact of next-generation sequencing technology on genetics.** *Trends Genet* 2008, **24:**133-141.

132. Thomas RK, Nickerson E, Simons JF, Janne PA, Tengs T, Yuza Y, Garraway LA, LaFramboise T, Lee JC, Shah K, et al: **Sensitive mutation detection in heterogeneous cancer specimens by massively parallel picoliter reactor sequencing.** *Nat Med* 2006, **12:**852-855.

133. Green RE, Malaspinas AS, Krause J, Briggs AW, Johnson PL, Uhler C, Meyer M, Good JM, Maricic T, Stenzel U, et al: **A complete Neandertal mitochondrial genome sequence determined by high-throughput sequencing.** *Cell* 2008, **134:**416-426.

134. Axtell MJ, Jan C, Rajagopalan R, Bartel DP: **A two-hit trigger for siRNA biogenesis in plants.** *Cell* 2006, **127:**565-577.

135. Gowda M, Li H, Alessi J, Chen F, Pratt R, Wang GL: **Robust analysis of 5'-transcript ends (5'-RATE): a novel technique for transcriptome analysis and genome annotation.** *Nucleic Acids Res* 2006, **34:**e126.

136. Ronaghi M, Karamohamed S, Pettersson B, Uhlen M, Nyren P: **Real-time DNA sequencing using detection of pyrophosphate release.** *Anal Biochem* 1996, **242:**84-89.

137. Margulies M, Egholm M, Altman WE, Attiya S, Bader JS, Bemben LA, Berka J, Braverman MS, Chen YJ, Chen Z, et al: **Genome sequencing in microfabricated high-density picolitre reactors.** *Nature* 2005, **437:**376-380.

138. Binladen J, Gilbert MT, Bollback JP, Panitz F, Bendixen C, Nielsen R, Willerslev E: **The use of coded PCR primers enables high-throughput sequencing of multiple homolog amplification products by 454 parallel sequencing.** *PLoS ONE* 2007, **2:**e197.

139. Hoffmann C, Minkah N, Leipzig J, Wang G, Arens MQ, Tebas P, Bushman FD: **DNA bar coding and pyrosequencing to identify rare HIV drug resistance mutations.** *Nucleic Acids Res* 2007, **35:**e91.

140. Kim J, Bartel DP: **Allelic imbalance sequencing reveals that single-nucleotide polymorphisms frequently alter microRNA-directed repression.** *Nat Biotechnol* 2009, **27:**472-477.

141. Muckenthaler M, Gray NK, Hentze MW: **IRP-1 binding to ferritin mRNA prevents the recruitment of the small ribosomal subunit by the cap-binding complex eIF4F.** *Mol Cell* 1998, **2:**383-388.

142. Pickering BM, Willis AE: **The implications of structured 5' untranslated regions on translation and disease.** *Semin Cell Dev Biol* 2005, **16:**39-47.

143. Lo HJ, Huang HK, Donahue TF: **RNA polymerase I-promoted HIS4 expression yields uncapped, polyadenylated mRNA that is unstable and inefficiently translated in Saccharomyces cerevisiae.** *Mol Cell Biol* 1998, **18:**665-675.

144. Morris DR, Geballe AP: **Upstream open reading frames as regulators of mRNA translation.** *Mol Cell Biol* 2000, **20:**8635-8642.

145. Hellen CU, Sarnow P: **Internal ribosome entry sites in eukaryotic mRNA molecules.** *Genes Dev* 2001, **15:**1593-1612.

146. Mazumder B, Seshadri V, Fox PL: **Translational control by the 3'-UTR: the ends specify the means.** *Trends Biochem Sci* 2003, **28:**91-98.

147. Tarun SZ, Jr., Sachs AB: **A common function for mRNA 5' and 3' ends in translation initiation in yeast.** *Genes Dev* 1995, **9:**2997-3007.

148. Shyu AB, Wilkinson MF, van Hoof A: **Messenger RNA regulation: to translate or to degrade.** *EMBO J* 2008, **27:**471-481.

149. Lee EH, Allen PD: **Homo-dimerization of RyR1 C-terminus via charged residues in random coils or in an alpha-helix.** *Exp Mol Med* 2007, **39:**594-602.

150. Zhou L, Myers AN, Vandersteen JG, Wang L, Wittwer CT: **Closed-tube genotyping with unlabeled oligonucleotide probes and a saturating DNA dye.** *Clin Chem* 2004, **50:**1328-1335.

151. Fire A, Xu S, Montgomery MK, Kostas SA, Driver SE, Mello CC: **Potent and specific genetic interference by double-stranded RNA in Caenorhabditis elegans.** *Nature* 1998, **391:**806-811.

APPENDICES

Appendix I: PGEM®-T Easy Vector map and sequence reference points.

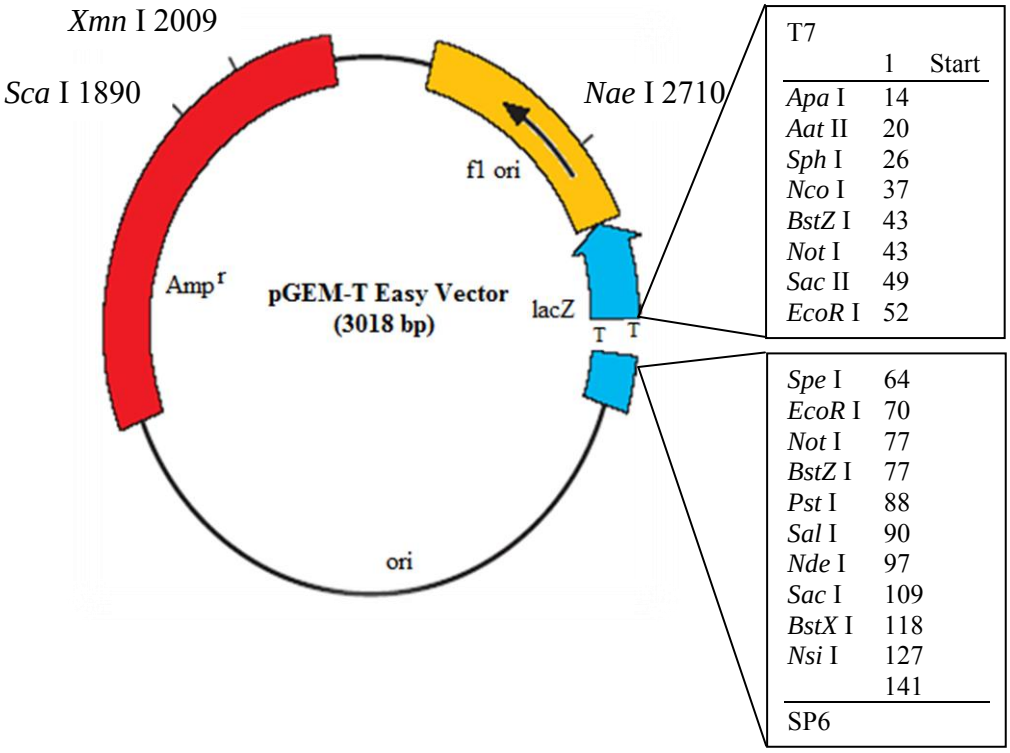

Picture was adapted from www.promega.com

Appendix II: Sequence results of the engineered 4861 HRM templates

A- Sequencing results of the wild type 4861 insert. The codon (CGC) that encodes the R4861 amino acid is highlighted in grey.

GTGGGTGGTGAAGGGATAAGGGCCGGGCAGCTGGGCTGAGGAGGGGCAAG
GCCAGGTGCGCTGAGCCGGGGGTGTGTGGGGCAGCAAGGTAGAGCCACAG
GGACTGAACCGGGGCCAGGACCCAGCATGGGCAGGGTGGGGGGAGGGCAA
GCCCAGGGCGGAGCTGACCTGGCCCCATCCTGCCCCCAGCTGGTGATGACC
GTGGGCCTTCTGGCGGTGGTCGTCTACCTGTACACCGTGGTGGCCTTCAACT
TCTTCCGCAAGTTCTACAACAAGAGCGAGGATGAGGATGAACCTGACATGA
AGTGTGATGACATGATGACGGTGAGCCCCTCCCCTAGCACTCTGGGACCCTT
CCTTCTCGCATCTGTTGAAGGAGTTAATAATGGTACCTCCAGGCCGGGCGTG
GTGCCTCCAGCCTGCAATCCCAGTGCGTCGGGAGGCCGAGGCGGGACGATT
ACTTGAGTCCAGGAGTTGGAAACCAG

B- Sequencing results of the mutated 4861 insert. Underlined is the introduced mutation that causes the R4861H amino acid change (CGC->CAC). The codon that encodes the 4861 amino acid is highlighted in grey

GTGGGTGGTGAAGGGATAAGGGCCGGGCAGCTGGGCTGAGGAGGGGCAAG
GCCAGGTGCGCTGAGCCGGGGGTGTGTGGGGCAGCAAGGTAGAGCCACAG
GGACTGAACCGGGGCCAGGACCCAGCATGGGCAGGGTGGGGGGAGGGCAA
GCCCAGGGCGGAGCTGACCTGGCCCCATCCTGCCCCCAGCTGGTGATGACC
GTGGGCCTTCTGGCGGTGGTCGTCTACCTGTACACCGTGGTGGCCTTCAACT
TCTTCCACAAGTTCTACAACAAGAGCGAGGATGAGGATGAACCTGACATGA
AGTGTGATGACATGATGACGGTGAGCCCCTCCCCTAGCACTCTGGGACCCTT
CCTTCTCGCATCTGTTGAAGGAGTTAATAATGGTACCTCCAGGCCGGGCGTG
GTGCCTCCAGCCTGCAATCCCAGTGCGTCGGGAGGCCGAGGCGGGACGATT
ACTTGAGTCCAGGAGTTGGAAACCAG

C- Sequencing results of the mutated 4861 insert. Underlined is the introduced mutation that causes the R4861P amino acid change (CGC->CCC). The codon that encodes the 4861 amino acid is highlighted in grey

GTGGGTGGTGAAGGGATAAGGGCCGGGCAGCTGGGCTGAGGAGGGGCAAG
GCCAGGTGCGCTGAGCCGGGGGTGTGTGGGGCAGCAAGGTAGAGCCACAG
GGACTGAACCGGGGCCAGGACCCAGCATGGGCAGGGTGGGGGGAGGGCAA
GCCCAGGGCGGAGCTGACCTGGCCCCATCCTGCCCCCAGCTGGTGATGACC
GTGGGCCTTCTGGCGGTGGTCGTCTACCTGTACACCGTGGTGGCCTTCAACT
TCTTCCCCAAGTTCTACAACAAGAGCGAGGATGAGGATGAACCTGACATGA
AGTGTGATGACATGATGACGGTGAGCCCCTCCCCTAGCACTCTGGGACCCTT
CCTTCTCGCATCTGTTGAAGGAGTTAATAATGGTACCTCCAGGCCGGGCGTG
GTGCCTCCAGCCTGCAATCCCAGTGCGTCGGGAGGCCGAGGCGGGACGATT
ACTTGAGTCCAGGAGTTGGAAACCAG

D- Sequencing results of the mutated 4861 insert. Underlined is the introduced mutation that causes the R4861L amino acid change (CGC->CTC). The codon that encodes the 4861 amino acid is highlighted in grey

GTGGGTGGTGAAGGGATAAGGGCCGGGCAGCTGGGCTGAGGAGGGGCAAG
GCCAGGTGCGCTGAGCCGGGGGTGTGTGGGGCAGCAAGGTAGAGCCACAG
GGACTGAACCGGGGCCAGGACCCAGCATGGGCAGGGTGGGGGGAGGGCAA
GCCCAGGGCGGAGCTGACCTGGCCCCATCCTGCCCCCAGCTGGTGATGACC
GTGGGCCTTCTGGCGGTGGTCGTCTACCTGTACACCGTGGTGGCCTTCAACT
TCTTCCTCAAGTTCTACAACAAGAGCGAGGATGAGGATGAACCTGACATGA
AGTGTGATGACATGATGACGGTGAGCCCCTCCCCTAGCACTCTGGGACCCTT
CCTTCTCGCATCTGTTGAAGGAGTTAATAATGGTACCTCCAGGCCGGGCGTG
GTGCCTCCAGCCTGCAATCCCAGTGCGTCGGGAGGCCGAGGCGGGACGATT
ACTTGAGTCCAGGAGTTGGAAACCAG

Appendix III: Partial C-terminal amino acid and cDNA sequence of the *RYR*1

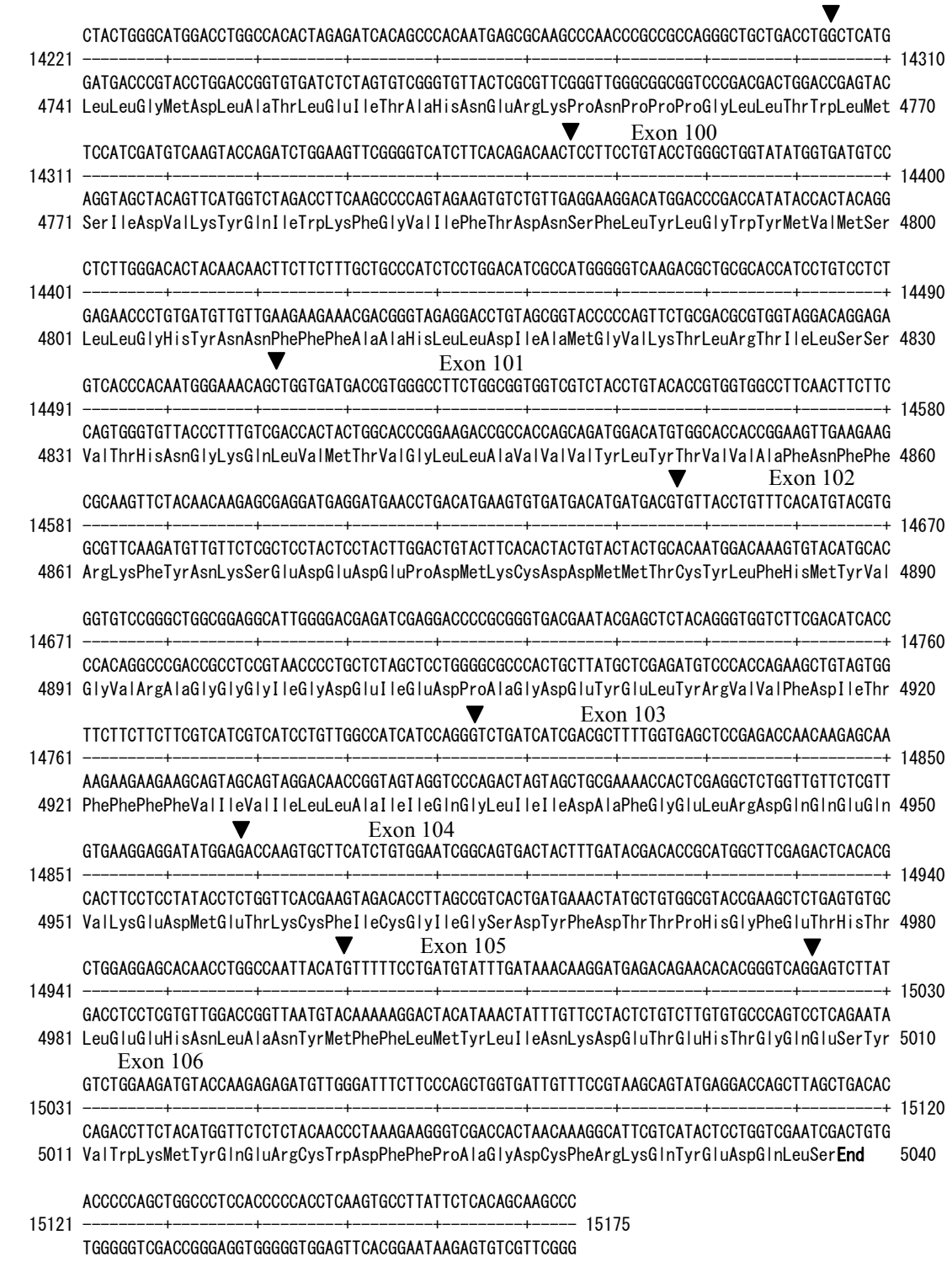

Appendix IV: Sequence results of the engineered 4833 plasmid contructs

A- Sequencing results of the wild type 4833 insert. The codon (CAC) that encodes the H4833 amino acid is highlighted in grey.

ACCTGGGCTGGTATATGGTGATGTCCCTCTTGGGACACTACAACAACTTCTT
CTTTGCTGCCCATCTCCTGGACATCGCCATGGGGGTCAAGACGCTGCGCACC
ATCCTGTCCTCTGTCACCCACAATGGGAAACAGCTGGTGATGACCGTGGGC
CTTCTGGCGGTGGTCGTCTACCTGTACACCGTGGTGGCCTTCAACTTCTTCC
GCAAGTTCTACAACAAGAGCGAGGATGAGGATGAACCTGACATGAAGTGTG
ATGACATGATGACGTGTTACCTGTTTCACATGTACGTGGGTGTCCGGGCTGG
CGGAGGCATTGGGG

B- Sequencing results of the mutant Y4833 insert. Underlined is the introduced mutation that causes the H4833Y amino acid change (CAC->TAC). The codon that encodes the 4833 amino acid is highlighted in grey.

ACCTGGGCTGGTATATGGTGATGTCCCTCTTGGGACACTACAACAACTTCTT
CTTTGCTGCCCATCTCCTGGACATCGCCATGGGGGTCAAGACGCTGCGCACC
ATCCTGTCCTCTGTCACCTACAATGGGAAACAGCTGGTGATGACCGTGGGCC
TTCTGGCGGTGGTCGTCTACCTGTACACCGTGGTGGCCTTCAACTTCTTCCG
CAAGTTCTACAACAAGAGCGAGGATGAGGATGAACCTGACATGAAGTGTGA
TGACATGATGACGTGTTACCTGTTTCACATGTACGTGGGTGTCCGGGCTGGC
GGAGGCATTGGGG

Appendix V: Workflow for using the Amplicon Variant Analyser Command Line Interface

Creating a new Project

After logging on to the server the AVA-CLI is accessed via the command "doAmplicon". The first step in creating a Project is setting up the project directory structure that will store the Project configuration, data, and results. This was done using the "create project" command. The project creation command used here was:

create project Hilbert

To continue the set up or work on a previously created Project, one uses the "open" command. To open an existing Project, the Project path must be entered after the open command, as follows:

open Hilbert

Creating References

The next step is to add a Reference Sequence. Its definition is simply a string of A, T, G, C (or N) characters representing a DNA sequence against which the sequencing reads will be aligned and compared so variations can be identified and reported. Shorter Reference Sequences are more efficient for computation in the AVA-CLI software. Thus the bar code and adaptor sequences are not included. The reference is created by using the "create reference" command. In this Project a table containing the Reference Sequence was saved to a file and that file was subsequently used as input. As for all files used in this project, the file containing the reference features was created in tab-separated value (tsv) format. By saving the table to a file, all the parameters for the "create reference" command are in fact provided from the supplied file. This reduces the chance of error that might occur when manually creating a Table. In this Project only one Reference Sequence was necessary, since both the 4826 and 4833 sequences were

amplified with identical RYR1 specific forward and reverse primers, respectively (see Table 5.1). Multiple Reference Sequences can, however, be created by saving to a file, a table containing all specific Reference Sequences. A screen shot of the file containing the Reference Sequence in tsv-format shown in Figure V.1.

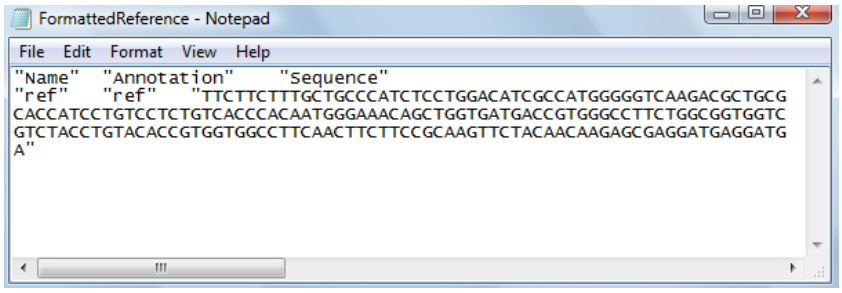

Figure V.1: Screen shot of the file that contains the Reference sequence in tsv-format.

The header of the table shows the name of the parameters that need to be supplied to the "create reference" command. In order to use the table to create the Reference Sequence in the Project, it was saved as a file (FormattedReference.txt) in the directory from which the script was run (i.e. the directory: Hilbert). Subsequently the file is cited as argument under –file option of the "create reference" command:

create reference –file Hilbert/FormattedReference.txt

Creating Amplicons

Once Reference Sequences are in the system, Amplicons can be completely specified for the project. The term Amplicon in the AVA software is used to represent essentially the same sequence as in the preparation of the DNA library except that it doesn"t include the bar code and adaptor parts of the bar coded fusion primers. The table containing the Amplicon was saved as a file (Amplicon.txt; see Figure V.2) in the directory from which the script was run. The part of the Amplicon that lies between the primers is called the Target. This is the sequence that is actually aligned to the Reference Sequence during the computations.

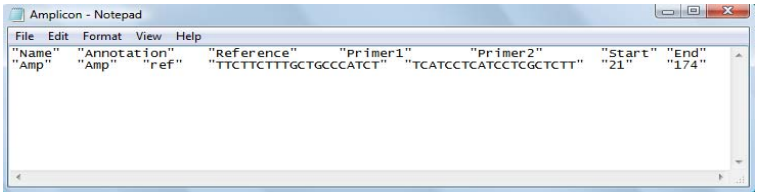

Figure V.2: Screen shot of the file that contains the specified Amplicon in tsv-format.

As mentioned previously, both the sequences surrounding the 4826 and 4833 mutations were amplified with identical *RYR*1 specific forward and reverse primers, respectively. Thus, there is only one Amplicon that needs to be specified in this project. The "create amplicon" command is listed below:

create amplicon –file Hilbert/Amplicon.txt

Creating Variants

A Variant is a sequence difference relative to the Reference Sequence. In this project the known variants causing the T4826I and H4833Y amino acid mutations were investigated. If known Variants exist, they can be added to the project using the "create variant" command. The table containing the Variants was saved as a file (Variants.txt) in the directory from which the script was run. Figure V.3 shows a screen shot of the file that contains the defined Variants in tsv-format.

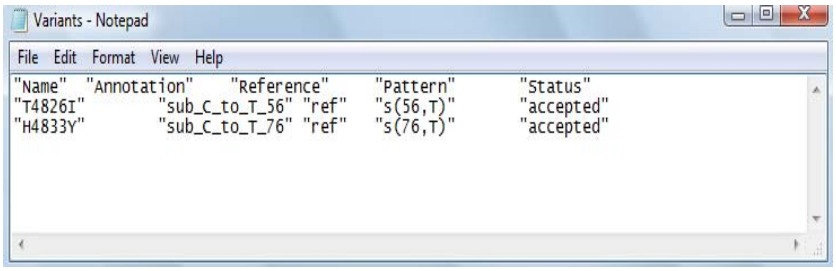

Figure V.3: Screen shot of the file that contains the specified Variants in tsv-format.

Subsequently the file was cited as argument under –file option of the "create reference" command:

create variant –file Hilbert/Variants.txt

The “create variant” command verifies the “pattern” set for each Variant in three different ways. The pattern is first checked to make sure that is it syntactically correct. Secondly, the coordinates of the “pattern” are checked to make sure that they actually exist within the Reference Sequence. Thirdly, any substitution must actually create a difference at the specified position (e.g. an error occurs when position 56 is already a T in the Reference Sequence).

Creating Samples

The term Sample, in the context of the AVA software, can be defined very generically as a virtual container specified only as a name (and an optional annotation), and used to group reads for analysis and reporting. The “Samples” thus represent the organizational foundation for the analysis, whose primary output is the Variants tab, such that the frequency of any or all defined Variants can be compared between the different “Samples” defined in the Project. In this project 10 muscle samples were investigated. Each of them was analysed one at the time and thus the table listed below was used for all 10. The table containing the Sample was saved as a file (Samples.txt) in the directory from which the script was run (see Figure V.4).

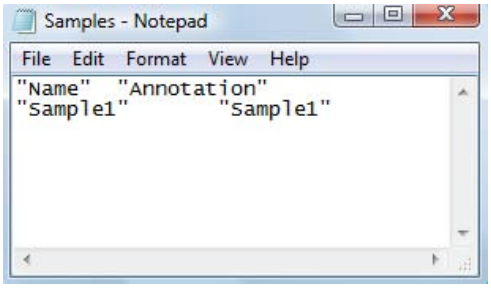

Figure V.4: Screen shot of the file that contains the specified Sample in tsv-format.

The file is cited as argument under –file option of the “create sample” command:

create sample –file Hilbert/Samples.txt

Associating Samples with Amplicons

With the Amplicons and Samples defined it was now possible to associate them according to the requirements of the experiment. The experiment performed here was quite straightforward. There was only one Amplicon and one Reference Sequence since both mutations under investigation were amplified with the sample *RYR*1 specific primers. The association was made using the table listed below (see Figure V.5). The table was saved as a file (Associate.txt) in the directory from which the script was run.

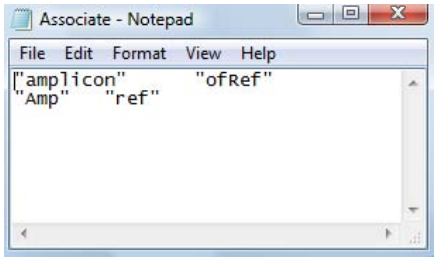

Figure V.5: Screen shot of the file that was used to associate the Amplicons with Samples in tsv-format.

The file is cited as argument under –file option of the "associate" command:

assoc –sample Sample1 –file Hilbert/Associate.txt

Loading Read Data Sets

A Read Data Set is a group of sequencing reads derived from the DNA library. In the current release of the AVA software, a Read Data Set is equivalent to an SFF file. The Read Data Sets are imported into the Project using the "load" command. In this project the sequences were resolved in bins according to their 4 bp bar code sequences. Every bin was therefore loaded into the Project and analysed separately. Figure V.6 lists the table that was saved to the file Readgr_TACG.txt, and used to load the TACG bar coded sequences into the Project.

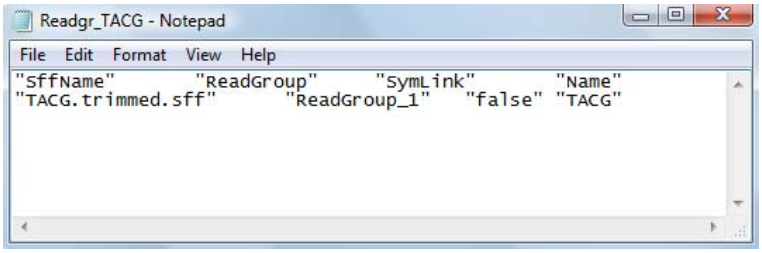

Figure V.6: Screen shot of the file that contains the table (in tsv-format) that was used to upload the ACGA bar coded sequences.

The exact way to load the Read Data Sets into the Project depends on how the data is organized on the disk. Depicted below is the "load" command used for the TACG.trimmed.sff Read Data Set. The file is located in the directory called "AVA":

load –sffDir AVA –file Hilbert/Readgr_TACG.txt

Associating Read Data Sets with Samples

With the Sample-Amplicon associations made and the Read Data Sets loaded into the Project, the Samples with their associated Amplicons can be associated with the Read Data Sets. This also uses the "associate" command described above. The "associate" command used to associate Sample1, and its associated Amplicon, with ReadGroup_1 is listed below.

assoc –readGroup ReadGroup_1 –sample Sample1

This set of commands and operations completes the project setup and should preferably be saved before computation. This is simply done by typing in the "save" command.

Computing

Once a Project has been set up properly the CLI can also be used to trigger the computation. There are two utility commands that can be used to validate a Project before computation:

The "utility validateNames" command is used to detect and correct naming problems in Projects. If any problem names are encountered (irresolvable duplicates or empty names) an error will be reported. The command does nothing if there are no errors to report.

Even if the names are correct, there can be other problems with a Project that might impact its computation. The command "utility validateForComputation" checks for these problems. If any of the criteria listed below are not met, warnings are reported and the command throws an error; otherwise it does nothing. Specifically, the command verifies: (a) that all Reference Sequences contain a sequence that is at least 1 base in length; (b) all Amplicons are associated with valid Reference Sequences and have target start and end coordinates that are contained within the Reference Sequence; (c) all Read Data files that are associated with at least one Sample and one or more valid Amplicons are available; and (d) if Variants are defined in the project that are associated with valid Reference Sequences, they have non-empty patterns that are valid with respect to that Reference Sequence.

If no errors are reported the computation can be triggered by the command:

computation start

The Variants that were part of the Project will have their frequency statistics updated after the computation. The application also attempts to automatically detect any other potential variations in the data. The pool of automatically detected variants is imported in the CLI by using the command:

computation loadDetectedVariants

Reporting

To report the measured SNP frequencies to a tab-delimited output file the following command was used:

report variantHits –outputFile TACG_variantHits.txt

In the example listed here the mutation frequencies of muscle tissue #323 were determined. The report output file was called “TACG_variantHits”. The SNP frequencies of the all samples were determined one by one. The AVA-CLI output files Appendix VI-A & B.

Appendix VI: Amplicon Variant Analyser Command Line Interface output files

A- Detected SNPs for each individual sample in the ten sample DNA library as compared to the imported Reference sequence. The report outputs files were generated using the AVA-CLI.

Reference sequence (NM_000540)

1	TTCTTCTTTG	CTGCCCATCT	CCTGGACATC
31	GCCATGGGGG	TCAAGACGCT	GCGCACCATC
61	CTGTCCTCTG	TCACCCACAA	TGGGAAACAG
91	CTGGTGATGA	CCGTGGGCCT	TCTGGCGGTG
121	GTCGTCTACC	TGTACACCGT	GGTGGCCTTC
151	AACTTCTTCC	GCAAGTTCTA	CAACAAGAGC
181	GAGGATGAGG	ATGA	

TACG #323 (T4826I)

"Reference Name" "Variant Name" "Variant Status" "Variant Pattern" "Sample Name" "Forward Hits" "Forward Denom" "Reverse Hits" "Reverse Denom" "Read Type"

"ref" "38:G/A" "putative" "s(38,A)" "Sample1" "19" "1097" "0" "0" "Individual"

"ref" "38:G/A" "putative" "s(38,A)" "Sample1" "19" "1097" "0" "0" "Consensus"

"ref" "101:C/T" "putative" "s(101,T)" "Sample1" "7" "1070" "0" "0" "Individual"

"ref" "101:C/T" "putative" "s(101,T)" "Sample1" "7" "1097" "0" "0" "Consensus"

"ref" "T4826I" "accepted" "s(56,T)" "Sample1" "525" "1094" "0" "0" "Individual"
"ref" "T4826I" "accepted" "s(56,T)" "Sample1" "525" "1097" "0" "0" "Consensus"

CTGA #289 (T4826I)

"Reference Name" "Variant Name" "Variant Status" "Variant Pattern" "Sample Name" "Forward Hits" "Forward Denom" "Reverse Hits" "Reverse Denom" "Read Type"
"ref" " T4826I " "putative" "s(56,T)" "Sample1" "168" "348" "0" "0" "Individual"
"ref" " T4826I " "putative" "s(56,T)" "Sample1" "168" "347" "0" "0" "Consensus"

ACTG #835 (H4833Y)

"Reference Name" "Variant Name" "Variant Status" "Variant Pattern" "Sample Name" "Forward Hits" "Forward Denom" "Reverse Hits" "Reverse Denom" "Read Type"
"ref" "160:C/T" "putative" "s(160,T)" "Sample1" "45" "3514" "0" "0" "Individual"
"ref" "160:C/T" "putative" "s(160,T)" "Sample1" "45" "3676" "0" "0" "Consensus"
"ref" "H4833Y" "accepted" "s(76,T)" "Sample1" "1788" "3619" "0" "0" "Individual"
"ref" "H4833Y" "accepted" "s(76,T)" "Sample1" "1788" "3677" "0" "0" "Consensus"
"ref" "T4826I" "accepted" "s(56,T)" "Sample1" "1" "3663" "0" "0" "Individual"
"ref" "T4826I" "accepted" "s(56,T)" "Sample1" "0" "3677" "0" "0" "Consensus"

AGTC #255 (T4826I)

"Reference Name" "Variant Name" "Variant Status" "Variant Pattern" "Sample Name" "Forward Hits" "Forward Denom" "Reverse Hits" "Reverse Denom" "Read Type"
"ref" "119:T/C" "putative" "s(119,C)" "Sample1" "8" "1557" "0" "0" "Individual"
"ref" "119:T/C" "putative" "s(119,C)" "Sample1" "8" "1738" "0" "0" "Consensus"
"ref" "H4833Y" "accepted" "s(76,T)" "Sample1" "1" "1608" "0" "0" "Individual"
"ref" "H4833Y" "accepted" "s(76,T)" "Sample1" "0" "1739" "0" "0" "Consensus"
"ref" "T4826I" "accepted" "s(56,T)" "Sample1" "794" "1732" "0" "0" "Individual"
"ref" "T4826I" "accepted" "s(56,T)" "Sample1" "794" "1749" "0" "0" "Consensus"

CGAC #470 (H4833Y)

"Reference Name" "Variant Name" "Variant Status" "Variant Pattern" "Sample Name" "Forward Hits" "Forward Denom" "Reverse Hits" "Reverse Denom" "Read Type"
"ref" "H4833Y" "accepted" "s(76,T)" "Sample1" "762" "1543" "0" "0" "Individual"
"ref" "H4833Y" "accepted" "s(76,T)" "Sample1" "762" "1564" "0" "0" "Consensus"
"ref" "T4826I" "accepted" "s(56,T)" "Sample1" "2" "1561" "0" "0" "Individual"
"ref" "T4826I" "accepted" "s(56,T)" "Sample1" "0" "1564" "0" "0" "Consensus"

TCAG #145 (H4833Y)

"Reference Name" "Variant Name" "Variant Status" "Variant Pattern" "Sample Name" "Forward Hits" "Forward Denom" "Reverse Hits" "Reverse Denom" "Read Type"
"ref" "H4833Y" "accepted" "s(76,T)" "Sample1" "1059" "2059" "0" "0" "Individual"
"ref" "H4833Y" "accepted" "s(76,T)" "Sample1" "1059" "2085" "0" "0" "Consensus"
"ref" "T4826I" "accepted" "s(80,G)" "Sample1" "12" "2054" "0" "0" "Individual"
"ref" "T4826I" "accepted" "s(80,G)" "Sample1" "12" "2085" "0" "0" "Consensus"
"ref" "26:A/G " "accepted" "s(26,G)" "Sample1" "13" "2085" "0" "0" "Individual"
"ref" "26:A/G " "accepted" "s(26,G)" "Sample1" "13" "2085" "0" "0" "Consensus"

TGAC #300 (T4826I)

"Reference Name" "Variant Name" "Variant Status" "Variant Pattern" "Sample Name" "Forward Hits" "Forward Denom" "Reverse Hits" "Reverse Denom" "Read Type"
"ref" "H4833Y" "accepted" "s(76,T)" "Sample1" "1" "1971" "0" "0" "Individual"
"ref" "H4833Y" "accepted" "s(76,T)" "Sample1" "0" "2107" "0" "0" "Consensus"
"ref" "T4826I" "accepted" "s(56,T)" "Sample1" "1024" "2088" "0" "0" "Individual"
"ref" "T4826I" "accepted" "s(56,T)" "Sample1" "1024" "2111" "0" "0" "Consensus"

Samples with the ACGA and AGCA barcodes could only be analyzed after adjustments of the primer and reference sequences, respectively. ACGA and AGCA are the first 4 bases for a number of MID-sequences used by Roche. During the demultiplexing phase of the variant analysis computation, the software looks for sequences that it believes to be contaminants and removes these from the data population. The two barcodes, in conjunction with the bases immediately following them were enough to cause them to be flagged as contamination and discarded. This problem was avoided by adding 4 bases (ACGA and/or AGCA) to the beginning of the forward primer and reference sequences. As a result all SNPs that are depicted below were shifted by 4 bases. Thus, the SNP leading to the H4833Y and T4826I amino acid mutations were now located at positions 80 and 60 of the reference gene instead of positions 76 and 56, respectively (see below).

ACGA #109 (T4826I)

"Reference Name" "Variant Name" "Variant Status" "Variant Pattern" "Sample Name" "Forward Hits" "Forward Denom" "Reverse Hits" "Reverse Denom" "Read Type"
"ref" "63:T/C" "putative" "s(63,C)" "Sample1" "15" "2042" "0" "0" "Individual"
"ref" "63:T/C" "putative" "s(63,C)" "Sample1" "15" "2187" "0" "0" "Consensus"
"ref" "89:A/G" "putative" "s(89,G)" "Sample1" "10" "1971" "0" "0" "Individual"
"ref" "89:A/G" "putative" "s(89,G)" "Sample1" "10" "2181" "0" "0" "Consensus"
"ref" "91:A/G" "putative" "s(91,G)" "Sample1" "26" "1969" "0" "0" "Individual"
"ref" "91:A/G" "putative" "s(91,G)" "Sample1" "26" "2181" "0" "0" "Consensus"
"ref" "104:A/G" "putative" "s(104,G)" "Sample1" "12" "1934" "0" "0" "Individual"

"ref" "104:A/G" "putative" "s(104,G)" "Sample1" "12" "2178" "0" "0" "Consensus"
"ref" "153:T/C" "putative" "s(153,C)" "Sample1" "10" "1889" "0" "0" "Individual"
"ref" "153:T/C" "putative" "s(153,C)" "Sample1" "10" "2178" "0" "0" "Consensus"
"ref" "H4833Y" "accepted" "s(80,T)" "Sample1" "34" "1989" "0" "0" "Individual"
"ref" "H4833Y" "accepted" "s(80,T)" "Sample1" "34" "2181" "0" "0" "Consensus"
"ref" "T4826I" "accepted" "s(60,T)" "Sample1" "903" "2166" "0" "0" "Individual"
"ref" "T4826I" "accepted" "s(60,T)" "Sample1" "903" "2187" "0" "0" "Consensus"

AGCA #541 (T4826I)

"Reference Name" "Variant Name" "Variant Status" "Variant Pattern" "Sample Name" "Forward Hits" "Forward Denom" "Reverse Hits" "Reverse Denom" "Read Type"
"ref" "25:C/T" "putative" "s(25,T)" "Sample1" "10" "1196" "0" "0" "Individual"
"ref" "25:C/T" "putative" "s(25,T)" "Sample1" "10" "1199" "0" "0" "Consensus"
"ref" "83:A/G" "putative" "s(83,G)" "Sample1" "6" "1166" "0" "0" "Individual"
"ref" "83:A/G" "putative" "s(83,G)" "Sample1" "6" "1199" "0" "0" "Consensus"
"ref" "95:C/G" "putative" "s(95,G)" "Sample1" "8" "1156" "0" "0" "Individual"
"ref" "95:C/G" "putative" "s(95,G)" "Sample1" "8" "1199" "0" "0" "Consensus"

"ref" "98:G/T" "putative" "s(98,T)" "Sample1" "8" "1154" "0" "0" "Individual"
"ref" "98:G/T" "putative" "s(98,T)" "Sample1" "8" "1199" "0" "0" "Consensus"
"ref" "99:T/G" "putative" "s(99,G)" "Sample1" "8" "1154" "0" "0" "Individual"
"ref" "99:T/G" "putative" "s(99,G)" "Sample1" "8" "1199" "0" "0" "Consensus"
"ref" "101:A/G" "putative" "s(101,G)" "Sample1" "6" "1154" "0" "0" "Individual"
"ref" "101:A/G" "putative" "s(101,G)" "Sample1" "6" "1199" "0" "0" "Consensus"
"ref" "102:T/G" "putative" "s(102,G)" "Sample1" "8" "1154" "0" "0" "Individual"
"ref" "102:T/G" "putative" "s(102,G)" "Sample1" "8" "1199" "0" "0" "Consensus"
"ref" "103:G/A" "putative" "s(103,A)" "Sample1" "7" "1153" "0" "0" "Individual"
"ref" "103:G/A" "putative" "s(103,A)" "Sample1" "7" "1199" "0" "0" "Consensus"
"ref" "104:A/G" "putative" "s(104,G)" "Sample1" "11" "1153" "0" "0" "Individual"
"ref" "104:A/G" "putative" "s(104,G)" "Sample1" "11" "1199" "0" "0" "Consensus"
"ref" "108:T/C" "putative" "s(108,C)" "Sample1" "7" "1150" "0" "0" "Individual"
"ref" "108:T/C" "putative" "s(108,C)" "Sample1" "7" "1199" "0" "0" "Consensus"
"ref" "114:T/G" "putative" "s(114,G)" "Sample1" "6" "1148" "0" "0" "Individual"
"ref" "114:T/G" "putative" "s(114,G)" "Sample1" "6" "1199" "0" "0" "Consensus"

"ref" "115:T/C" "putative" "s(115,C)" "Sample1" "7" "1148" "0" "0" "Individual"
"ref" "115:T/C" "putative" "s(115,C)" "Sample1" "7" "1199" "0" "0" "Consensus"
"ref" "117:T/G" "putative" "s(117,G)" "Sample1" "7" "1145" "0" "0" "Individual"
"ref" "117:T/G" "putative" "s(117,G)" "Sample1" "7" "1199" "0" "0" "Consensus"
"ref" "126:T/C" "putative" "s(126,C)" "Sample1" "7" "1142" "0" "0" "Individual"
"ref" "126:T/C" "putative" "s(126,C)" "Sample1" "7" "1198" "0" "0" "Consensus"
"ref" "128:G/A" "putative" "s(128,A)" "Sample1" "7" "1142" "0" "0" "Individual"
"ref" "128:G/A" "putative" "s(128,A)" "Sample1" "7" "1198" "0" "0" "Consensus"
"ref" "132:A/G" "putative" "s(132,G)" "Sample1" "7" "1142" "0" "0" "Individual"
"ref" "132:A/G" "putative" "s(132,G)" "Sample1" "7" "1198" "0" "0" "Consensus"
"ref" "140:A/G" "putative" "s(140,G)" "Sample1" "8" "1142" "0" "0" "Individual"
"ref" "140:A/G" "putative" "s(140,G)" "Sample1" "8" "1198" "0" "0" "Consensus"
"ref" "155:A/G" "putative" "s(155,G)" "Sample1" "8" "1133" "0" "0" "Individual"
"ref" "155:A/G" "putative" "s(155,G)" "Sample1" "8" "1198" "0" "0" "Consensus"
"ref" "156:A/G" "putative" "s(156,G)" "Sample1" "7" "1133" "0" "0" "Individual"
"ref" "156:A/G" "putative" "s(156,G)" "Sample1" "7" "1198" "0" "0" "Consensus"

"ref" "157:C/G" "putative" "s(157,G)" "Sample1" "7" "1133" "0" "0" "Individual"
"ref" "157:C/G" "putative" "s(157,G)" "Sample1" "7" "1198" "0" "0" "Consensus"
"ref" "161:T/C" "putative" "s(161,C)" "Sample1" "6" "1130" "0" "0" "Individual"
"ref" "161:T/C" "putative" "s(161,C)" "Sample1" "6" "1197" "0" "0" "Consensus"
"ref" "H4833Y" "accepted" "s(80,T)" "Sample1" "6" "1170" "0" "0" "Individual"
"ref" "H4833Y" "accepted" "s(80,T)" "Sample1" "6" "1199" "0" "0" "Consensus"
"ref" "T4826I" "accepted" "s(60,T)" "Sample1" "593" "1189" "0" "0" "Individual"
"ref" "T4826I" "accepted" "s(60,T)" "Sample1" "593" "1199" "0" "0" "Consensus"

B- Detected SNPs for each individual sample in the seven sample DNA library as compared to the reference sequence. The report outputs files were generated using the AVA-CLI.

ACTG #835 (H4833Y)

"Reference Name" "Variant Name" "Variant Status" "Variant Pattern" "Sample Name" "Forward Hits" "Forward Denom" "Reverse Hits" "Reverse Denom" "Read Type"
"ref" "46:A/G" "putative" "s(46,G)" "Sample1" "7" "1302" "0" "0" "Individual"
"ref" "46:A/G" "putative" "s(46,G)" "Sample1" "7" "1302" "0" "0" "Consensus"

"ref" "80:A/G" "putative" "s(80,G)" "Sample1" "7" "1300" "0" "0" "Individual"
"ref" "80:A/G" "putative" "s(80,G)" "Sample1" "7" "1302" "0" "0" "Consensus"
"ref" "H4833Y" "accepted" "s(76,T)" "Sample1" "611" "1300" "0" "0" "Individual"
"ref" "H4833Y" "accepted" "s(76,T)" "Sample1" "611" "1302" "0" "0" "Consensus"
"ref" "T4826I" "accepted" "s(56,T)" "Sample1" "3" "1302" "0" "0" "Individual"
"ref" "T4826I" "accepted" "s(56,T)" "Sample1" "0" "1302" "0" "0" "Consensus"

AGTC 3:1 control (H4833Y)

"Reference Name" "Variant Name" "Variant Status" "Variant Pattern" "Sample Name" "Forward Hits" "Forward Denom" "Reverse Hits" "Reverse Denom" "Read Type"
"ref" "44:A/G" "putative" "s(44,G)" "Sample1" "16" "2670" "0" "0" "Individual"
"ref" "44:A/G" "putative" "s(44,G)" "Sample1" "16" "2671" "0" "0" "Consensus"
"ref" "46:A/G" "putative" "s(46,G)" "Sample1" "24" "2670" "0" "0" "Individual"
"ref" "46:A/G" "putative" "s(46,G)" "Sample1" "24" "2671" "0" "0" "Consensus"
"ref" "55:A/G" "putative" "s(55,G)" "Sample1" "15" "2667" "0" "0" "Individual"
"ref" "55:A/G" "putative" "s(55,G)" "Sample1" "15" "2671" "0" "0" "Consensus"
"ref" "85:A/G" "putative" "s(85,G)" "Sample1" "14" "2660" "0" "0" "Individual"

"ref" "85:A/G" "putative" "s(85,G)" "Sample1" "14" "2671" "0" "0" "Consensus"
"ref" "86:A/G" "putative" "s(86,G)" "Sample1" "14" "2660" "0" "0" "Individual"
"ref" "86:A/G" "putative" "s(86,G)" "Sample1" "14" "2671" "0" "0" "Consensus"
"ref" "87:A/G" "putative" "s(87,G)" "Sample1" "15" "2660" "0" "0" "Individual"
"ref" "87:A/G" "putative" "s(87,G)" "Sample1" "15" "2671" "0" "0" "Consensus"
"ref" "89:A/G" "putative" "s(89,G)" "Sample1" "15" "2659" "0" "0" "Individual"
"ref" "89:A/G" "putative" "s(89,G)" "Sample1" "15" "2671" "0" "0" "Consensus"
"ref" "125:T/C" "putative" "s(125,C)" "Sample1" "20" "2654" "0" "0" "Individual"
"ref" "125:T/C" "putative" "s(125,C)" "Sample1" "20" "2671" "0" "0" "Consensus"
"ref" "163:A/G" "putative" "s(163,G)" "Sample1" "15" "2649" "0" "0" "Individual"
"ref" "163:A/G" "putative" "s(163,G)" "Sample1" "15" "2671" "0" "0" "Consensus"
"ref" "164:A/G" "putative" "s(164,G)" "Sample1" "19" "2648" "0" "0" "Individual"
"ref" "164:A/G" "putative" "s(164,G)" "Sample1" "19" "2671" "0" "0" "Consensus"
"ref" "167:T/C" "putative" "s(167,C)" "Sample1" "14" "2648" "0" "0" "Individual"
"ref" "167:T/C" "putative" "s(167,C)" "Sample1" "14" "2671" "0" "0" "Consensus"
"ref" "172:A/G" "putative" "s(172,G)" "Sample1" "16" "2647" "0" "0" "Individual"

"ref" "172:A/G" "putative" "s(172,G)" "Sample1" "16" "2671" "0" "0" "Consensus"
"ref" "173:A/G" "putative" "s(173,G)" "Sample1" "27" "2647" "0" "0" "Individual"
"ref" "173:A/G" "putative" "s(173,G)" "Sample1" "27" "2671" "0" "0" "Consensus"
"ref" "H4833Y" "accepted" "s(76,T)" "Sample1" "1204" "2662" "0" "0" "Individual"
"ref" "H4833Y" "accepted" "s(76,T)" "Sample1" "1204" "2671" "0" "0" "Consensus"
"ref" "T4826I" "accepted" "s(56,T)" "Sample1" "19" "2667" "0" "0" "Individual"
"ref" "T4826I" "accepted" "s(56,T)" "Sample1" "19" "2671" "0" "0" "Consensus"

CGAC #470 (H4833Y)

"Reference Name" "Variant Name" "Variant Status" "Variant Pattern" "Sample Name" "Forward Hits" "Forward Denom" "Reverse Hits" "Reverse Denom" "Read Type"
"ref" "26:A/G" "putative" "s(26,G)" "Sample1" "7" "1389" "0" "0" "Individual"
"ref" "26:A/G" "putative" "s(26,G)" "Sample1" "7" "1389" "0" "0" "Consensus"
"ref" "167:T/C" "putative" "s(167,C)" "Sample1" "7" "1371" "0" "0" "Individual"
"ref" "167:T/C" "putative" "s(167,C)" "Sample1" "7" "1389" "0" "0" "Consensus"
"ref" "172:A/G" "putative" "s(172,G)" "Sample1" "8" "1371" "0" "0" "Individual"
"ref" "172:A/G" "putative" "s(172,G)" "Sample1" "8" "1389" "0" "0" "Consensus"

"ref" "H4833Y" "accepted" "s(76,T)" "Sample1" "660" "1377" "0" "0" "Individual"
"ref" "H4833Y" "accepted" "s(76,T)" "Sample1" "660" "1389" "0" "0" "Consensus"
"ref" "T4826I" "accepted" "s(56,T)" "Sample1" "2" "1383" "0" "0" "Individual"
"ref" "T4826I" "accepted" "s(56,T)" "Sample1" "0" "1389" "0" "0" "Consensus"

CGTA #116 (H4833Y)

"Reference Name" "Variant Name" "Variant Status" "Variant Pattern" "Sample Name" "Forward Hits" "Forward Denom" "Reverse Hits" "Reverse Denom" "Read Type"
"ref" "23:T/C" "putative" "s(23,C)" "Sample1" "10" "1608" "0" "0" "Individual"
"ref" "23:T/C" "putative" "s(23,C)" "Sample1" "10" "1608" "0" "0" "Consensus"
"ref" "44:A/G" "putative" "s(44,G)" "Sample1" "9" "1607" "0" "0" "Individual"
"ref" "44:A/G" "putative" "s(44,G)" "Sample1" "9" "1608" "0" "0" "Consensus"
"ref" "55:A/G" "putative" "s(55,G)" "Sample1" "12" "1606" "0" "0" "Individual"
"ref" "55:A/G" "putative" "s(55,G)" "Sample1" "12" "1608" "0" "0" "Consensus"
"ref" "62:T/C" "putative" "s(62,C)" "Sample1" "9" "1605" "0" "0" "Individual"
"ref" "62:T/C" "putative" "s(62,C)" "Sample1" "9" "1608" "0" "0" "Consensus"
"ref" "100:A/G" "putative" "s(100,G)" "Sample1" "8" "1586" "0" "0" "Individual"

"ref" "100:A/G" "putative" "s(100,G)" "Sample1" "8" "1607" "0" "0" "Consensus"
"ref" "122:T/C" "putative" "s(122,C)" "Sample1" "11" "1585" "0" "0" "Individual"
"ref" "122:T/C" "putative" "s(122,C)" "Sample1" "11" "1607" "0" "0" "Consensus"
"ref" "136:A/G" "putative" "s(136,G)" "Sample1" "8" "1583" "0" "0" "Individual"
"ref" "136:A/G" "putative" "s(136,G)" "Sample1" "8" "1607" "0" "0" "Consensus"
"ref" "149:T/C" "putative" "s(149,C)" "Sample1" "9" "1583" "0" "0" "Individual"
"ref" "149:T/C" "putative" "s(149,C)" "Sample1" "9" "1607" "0" "0" "Consensus"
"ref" "157:T/C" "putative" "s(157,C)" "Sample1" "11" "1583" "0" "0" "Individual"
"ref" "157:T/C" "putative" "s(157,C)" "Sample1" "11" "1607" "0" "0" "Consensus"
"ref" "H4833Y" "accepted" "s(76,T)" "Sample1" "793" "1600" "0" "0" "Individual"
"ref" "H4833Y" "accepted" "s(76,T)" "Sample1" "793" "1608" "0" "0" "Consensus"

TCAG #145 (H4833Y)

"Reference Name" "Variant Name" "Variant Status" "Variant Pattern" "Sample Name" "Forward Hits" "Forward Denom" "Reverse Hits" "Reverse Denom" "Read Type"
"ref" "H4833Y" "accepted" "s(76,T)" "Sample1" "26" "56" "0" "0" "Individual"
"ref" "H4833Y" "accepted" "s(76,T)" "Sample1" "26" "62" "0" "0" "Consensus"

Samples with the ACGA and AGCA barcodes could only be analyzed after adjustments of the primer and reference sequences, respectively (see Appendix V-A).

ACGA #323 (T4826I)

"Reference Name" "Variant Name" "Variant Status" "Variant Pattern" "Sample Name" "Forward Hits" "Forward Denom" "Reverse Hits" "Reverse Denom" "Read Type"
"ref" "63:T/C" "putative" "s(63,C)" "Sample1" "27" "1303" "0" "0" "Individual"
"ref" "63:T/C" "putative" "s(63,C)" "Sample1" "27" "1336" "0" "0" "Consensus"
"ref" "64:C/T" "putative" "s(64,T)" "Sample1" "24" "1303" "0" "0" "Individual"
"ref" "64:C/T" "putative" "s(64,T)" "Sample1" "24" "1336" "0" "0" "Consensus"
"ref" "66-67:TG/--" "putative" "d(66-67)" "Sample1" "8" "1302" "0" "0" "Individual"
"ref" "66-67:TG/--" "putative" "d(66-67)" "Sample1" "8" "1336" "0" "0" "Consensus"
"ref" "67:G/C" "putative" "s(67,C)" "Sample1" "24" "1302" "0" "0" "Individual"
"ref" "67:G/C" "putative" "s(67,C)" "Sample1" "24" "1336" "0" "0" "Consensus"
"ref" "71:T/C" "putative" "s(71,C)" "Sample1" "7" "1289" "0" "0" "Individual"
"ref" "71:T/C" "putative" "s(71,C)" "Sample1" "7" "1336" "0" "0" "Consensus"
"ref" "75:T/C" "putative" "s(75,C)" "Sample1" "7" "1267" "0" "0" "Individual"
"ref" "75:T/C" "putative" "s(75,C)" "Sample1" "7" "1310" "0" "0" "Consensus"

"ref" "H4833Y" "accepted" "s(80,T)" "Sample1" "5" "1265" "0" "0" "Individual"
"ref" "H4833Y" "accepted" "s(80,T)" "Sample1" "5" "1303" "0" "0" "Consensus"
"ref" "T4826I" "accepted" "s(60,T)" "Sample1" "602" "1328" "0" "0" "Individual"
"ref" "T4826I" "accepted" "s(60,T)" "Sample1" "602" "1336" "0" "0" "Consensus"

AGCA #289 (T4826I)

"Reference Name" "Variant Name" "Variant Status" "Variant Pattern" "Sample Name" "Forward Hits" "Forward Denom" "Reverse Hits" "Reverse Denom" "Read Type"
"ref" "25:C/T" "putative" "s(25,T)" "Sample1" "10" "1359" "0" "0" "Individual"
"ref" "25:C/T" "putative" "s(25,T)" "Sample1" "10" "1360" "0" "0" "Consensus"
"ref" "47:A/G" "putative" "s(47,G)" "Sample1" "12" "1358" "0" "0" "Individual"
"ref" "47:A/G" "putative" "s(47,G)" "Sample1" "12" "1360" "0" "0" "Consensus"
"ref" "48:A/G" "putative" "s(48,G)" "Sample1" "7" "1357" "0" "0" "Individual"
"ref" "48:A/G" "putative" "s(48,G)" "Sample1" "7" "1360" "0" "0" "Consensus"
"ref" "63:T/C" "putative" "s(63,C)" "Sample1" "13" "1333" "0" "0" "Individual"
"ref" "63:T/C" "putative" "s(63,C)" "Sample1" "13" "1359" "0" "0" "Consensus"
"ref" "64:C/T" "putative" "s(64,T)" "Sample1" "8" "1333" "0" "0" "Individual"

"ref" "64:C/T" "putative" "s(64,T)" "Sample1" "8" "1359" "0" "0" "Consensus"
"ref" "67:G/C" "putative" "s(67,C)" "Sample1" "14" "1333" "0" "0" "Individual"
"ref" "67:G/C" "putative" "s(67,C)" "Sample1" "14" "1359" "0" "0" "Consensus"
"ref" "75:T/C" "putative" "s(75,C)" "Sample1" "7" "1314" "0" "0" "Individual"
"ref" "75:T/C" "putative" "s(75,C)" "Sample1" "7" "1345" "0" "0" "Consensus"
"ref" "81:A/G" "putative" "s(81,G)" "Sample1" "8" "1313" "0" "0" "Individual"
"ref" "81:A/G" "putative" "s(81,G)" "Sample1" "8" "1345" "0" "0" "Consensus"
"ref" "89:A/G" "putative" "s(89,G)" "Sample1" "15" "1312" "0" "0" "Individual"
"ref" "89:A/G" "putative" "s(89,G)" "Sample1" "15" "1345" "0" "0" "Consensus"
"ref" "90:A/G" "putative" "s(90,G)" "Sample1" "8" "1312" "0" "0" "Individual"
"ref" "90:A/G" "putative" "s(90,G)" "Sample1" "8" "1345" "0" "0" "Consensus"
"ref" "91:A/G" "putative" "s(91,G)" "Sample1" "8" "1310" "0" "0" "Individual"
"ref" "91:A/G" "putative" "s(91,G)" "Sample1" "8" "1345" "0" "0" "Consensus"
"ref" "99:T/C" "putative" "s(99,C)" "Sample1" "9" "1308" "0" "0" "Individual"
"ref" "99:T/C" "putative" "s(99,C)" "Sample1" "9" "1345" "0" "0" "Consensus"
"ref" "101:A/T" "putative" "s(101,T)" "Sample1" "7" "1307" "0" "0" "Individual"

"ref" "101:A/T" "putative" "s(101,T)" "Sample1" "7" "1345" "0" "0" "Consensus"
"ref" "102:T/C" "putative" "s(102,C)" "Sample1" "7" "1307" "0" "0" "Individual"
"ref" "102:T/C" "putative" "s(102,C)" "Sample1" "7" "1345" "0" "0" "Consensus"
"ref" "104:A/G" "putative" "s(104,G)" "Sample1" "8" "1307" "0" "0" "Individual"
"ref" "104:A/G" "putative" "s(104,G)" "Sample1" "8" "1345" "0" "0" "Consensus"
"ref" "114:T/C" "putative" "s(114,C)" "Sample1" "9" "1307" "0" "0" "Individual"
"ref" "114:T/C" "putative" "s(114,C)" "Sample1" "9" "1345" "0" "0" "Consensus"
"ref" "153:T/C" "putative" "s(153,C)" "Sample1" "11" "1304" "0" "0" "Individual"
"ref" "153:T/C" "putative" "s(153,C)" "Sample1" "11" "1345" "0" "0" "Consensus"
"ref" "161:T/C" "putative" "s(161,C)" "Sample1" "9" "1304" "0" "0" "Individual"
"ref" "161:T/C" "putative" "s(161,C)" "Sample1" "9" "1345" "0" "0" "Consensus"
"ref" "168:A/G" "putative" "s(168,G)" "Sample1" "7" "1304" "0" "0" "Individual"
"ref" "168:A/G" "putative" "s(168,G)" "Sample1" "7" "1345" "0" "0" "Consensus"
"ref" "173:T/C" "putative" "s(173,C)" "Sample1" "9" "1304" "0" "0" "Individual"
"ref" "173:T/C" "putative" "s(173,C)" "Sample1" "9" "1345" "0" "0" "Consensus"
"ref" "H4833Y" "accepted" "s(80,T)" "Sample1" "12" "1313" "0" "0" "Individual"

"ref" "H4833Y" "accepted" "s(80,T)" "Sample1" "12" "1345" "0" "0" "Consensus"
"ref" "T4826I" "accepted" "s(60,T)" "Sample1" "653" "1348" "0" "0" "Individual"
"ref" "T4826I" "accepted" "s(60,T)" "Sample1" "653" "1359" "0" "0" "Consensus"

Appendix VII: Results of RyR1 trypsin cleavage

Name enzyme	Number of cleavages	Amino acid positions of cleavage sites
Trypsin	498	14 29 33 44 75 98 109 114 124 129 154 156 161 163 177 207 220 241 242 256 260 265 274 280 282 305 309 316 319 321 327 328 339 364 367 372 373 374 391 401 415 425 463 466 468 471 473 492 515 530 533 549 552 583 591 594 597 614 628 651 660 682 757 787 789 795 800 817 819 826 829 830 834 843 868 870 872 885 896 900 901 917 929 944 950 951 953 956 975 986 997 999 1015 1016 1019 1024 1031 1032 1035 1043 1067 1070 1072 1075 1078 1086 1100 1127 1130 1179 1211 1239 1258 1270 1274 1289 1301 1323 1335 1336 1348 1353 1371 1376 1382 1384 1385 1386 1391 1393 1394 1409 1420 1437 1467 1469 1487 1507 1533 1546 1567 1569 1583 1584 1593 1606 1617 1618 1622 1645 1655 1660 1667 1670 1679 1707 1724 1726 1727 1742 1751 1759 1797 1808 1810 1813 1820 1827 1843 1860 1864 1892 1903 1908 1918 1930 1936 1954 1964 1968 1974 1976 1982 1993 1994 1996 1999 2013 2028 2062 2069 2071 2074 2075 2076 2084 2092 2104 2118 2126 2136 2140 2163 2189 2199 2221 2224 2227 2234 2241 2244 2248 2297 2316 2330 2336 2355 2359 2369 2385 2392 2398 2399 2401 2403 2415 2435 2447 2452 2454 2458 2481 2489 2499 2508 2531 2552 2564 2575 2588 2591 2593 2597 2600 2612 2624 2625 2638 2642 2650 2653 2676 2677 2689 2690 2697 2722 2725 2726 2750 2757 2765 2770 2786 2795 2800 2802 2806 2810 2814 2825 2827 2833 2836 2837 2838 2840 2841 2852 2869 2888 2889 2890 2891 2897 2914 2916 2918 2920 2922 2928 2939 2942 2953 2954 2965 2985 2988 2996 3000 3023 3034 3036 3045 3051 3053 3073 3078 3082 3089 3093 3105 3111 3114 3119 3123 3167 3179 3185 3196 3222 3225 3227 3248 3262 3283 3287 3321 3336 3337 3348 3364 3366 3367 3368 3371 3380 3384 3395 3403 3414 3420 3436 3447 3452 3453 3475 3477 3480 3493 3495 3496 3497 3498 3499 3502 3515 3516 3537 3539 3543 3550 3562 3570 3577 3582 3591 3594 3595 3614 3616 3617 3622 3626 3628 3630 3637 3648 3658 3672 3679 3693 3707 3713 3715 3731 3755 3759 3761 3768 3772 3786 3798 3814 3820 3822 3823 3848 3851 3867 3872 3885 3903 3924 3939 3947 3948 3952 3958 3983 4001 4013 4020 4041 4059 4066 4068 4084 4089 4090 4094 4100 4130 4136 4158 4179 4187 4188 4191 4201 4210 4213 4214 4229 4296 4303 4306 4311 4314 4316 4318 4319 4321 4322 4326 4342 4372 4373 4475 4476 4477 4503 4511 4523 4524 4533 4534 4549 4551 4558 4564 4582 4645 4666 4673 4674 4676 4680 4681 4699 4704 4719 4722 4723 4724 4728 4735 4737 4757 4775 4780 4822 4825 4836 4861 4862 4866 4876 4893 4914 4945 4952 4958 4999 5013 5018 5030 5031